NASA Innovative Advanced Concepts (NIAC) Phase I
Grant Number 80NSSC 20K1022

AQUA FACTOREM:
ULTRA LOW ENERGY LUNAR WATER EXTRACTION

FINAL REPORT

Philip T. Metzger, PhD (PI),[1] Dhaka Sapkota, PhD,[1]
Jack Fox[2], Nicholas Bennett[3]

[1]University of Central Florida, Florida Space Institute,
12354 Research Parkway,
Partnership 1 Building, Suite 214, Orlando, FL 32826

[2]Fox Technical Associates (consultant)

[3]UNSW Australian Centre for Space Engineering Research (ACSER),
Australia (collaborator)

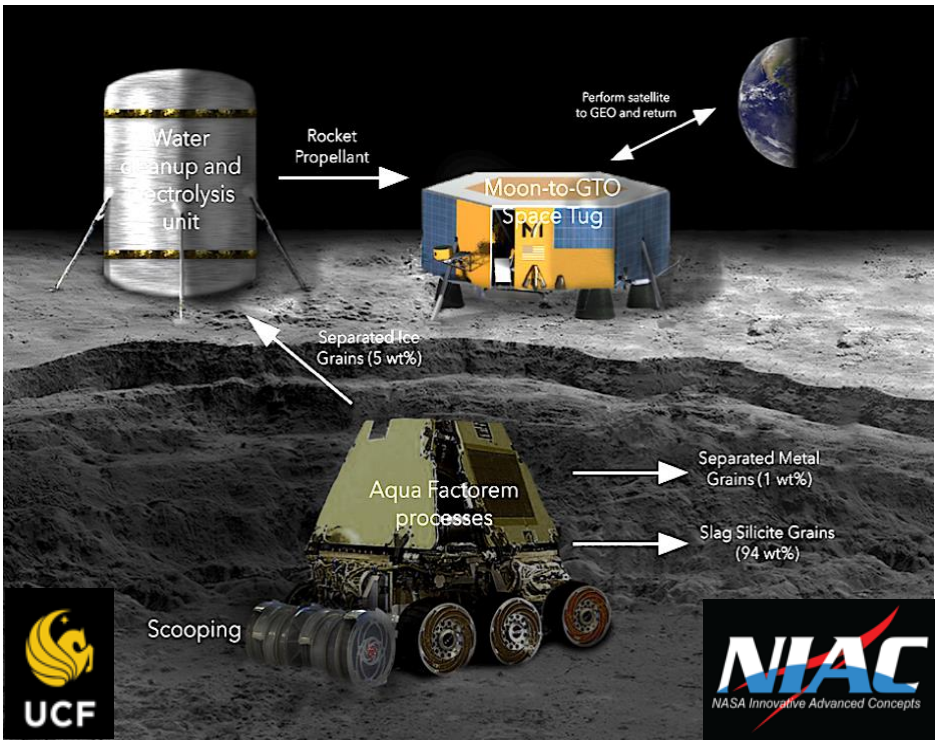

March 15, 2021

.

TABLE OF CONTENTS:

1.0 Overview of the Concept and Architecture 1
1.1 The Innovation 1
1.2 Overview of the Architecture 3
1.3 Physical State of the Resource 5
1.4 Ice Extraction Method 9
1.4.1 Excavation Subsystem 10
1.4.2 Rock Rejection 11
1.4.3 Gravel Separation Technology 11
1.4.4 Grinding and Fracture Subsystem 12
1.4.5 Beneficiation System 13
1.4.6 Pneumatic Separation 14
1.4.7 Magnetic Separation 14
1.4.8 Tribocharging and Electrostatic Separation 15
2.0 Viability of the Critical Function 15
2.1 Simulants 16
2.2 Lunar Soil and Ice Models 19
2.3 Grinding 21
2.4 De-Dusting and Pneumatic Separation 22
2.5 In-line Magnetic Separation 26
2.6 In-line Electrostatic Separation 28
2.7 Granular Magnetic Separation 30
2.8 Pneumatic Size Sorting 36
2.9 Granular Electrostatic Separation 39
2.9.1 Electrostatic Experiments with Actual Ice 40
2.10 Vibrational Separation 41
2.11 Summary of Beneficiation Processes 43
3.0 Architecture Analysis 43
3.1 Overview 43
3.2 Transportation and Utilization of Mined Propellant 44
3.2.1 Overview of Transportation Architecture 44
3.2.2 Vehicle Model Methodology 48
3.2.3 Astrodynamics Model Methodology 48
3.2.4 Baseline Results 49
3.2.5 GTO-GEO Variant Results 50
3.2.6 LEO-GEO Variant Results 51
3.2.7 Dependence on Vehicle Mass 52
3.2.8 Service Landers to Set Up the Mine 54

3.3 Surface Power System....55
3.4 Water Cleanup and Electrolysis....55
3.5 Mining (Extraction and Beneficiation)....59
3.6 Site Preparation....59
3.7 Mass and Power Estimates....60
3.8 Other Business Opportunities in the Architecture....61
4.0 Other Products from Lunar Beneficiation....62
5.0 Bringing the Concept to the Aerospace Market....62
6.0 Outreach and Public Engagement....62
7.0 Conclusion....63
8.0 Appendices....1
8.1 Appendix A. Lunar Soil and Ice Particle Size Distributions....1
8.2 Appendix B. Data Tables....6

1.0 Overview of the Concept and Architecture

1.1 The Innovation

The key problem in lunar propellant manufacture is how to bring the energy and the volatiles together. Most lunar ice mining concepts depend on thermal extraction based on the assumption that it will be easier than strip mining with robots in the dust. The problem with thermal extraction is two-fold. First, the energy budget is gigantic. Most of the energy is wasted heating the lithic fraction of the regolith. The high energy requires either nuclear fission or significant infrastructure to bring solar energy into the Permanently Shadowed Regions (PSRs), with associated increase in both risk and cost for infrastructure maturation and lunar deployment. Second, water vapor in lunar regolith is driven away from a heat source, not toward it, as both experiments[1] and modeling[2,3] show, so most of the vaporized ice will re-freeze elsewhere in the soil rather than being extracted. (PI Metzger was a member of two of the most recent ice mining architecture studies that demonstrated these challenges[4-9].) Driving the vapor in the correct direction requires either additional heating of the subsurface to create thermal gradients to overcome pressure gradients (if that is possible) or containment such as by physically drilling a

[1] Zacny, Kris, Phil Metzger, Kathryn Luczek, James Mantovani, Robert P. Mueller, and Justin Spring. "The world is not enough (WINE): harvesting local resources for eternal exploration of space." In *AIAA SPACE 2016*, p. 5279. 2016.
[2] Brisset, Julie, Thomas Miletich, and Philip Metzger, "Thermal Extraction of Water Ice from the Lunar Surface - A 3D Numerical Model," accepted for publication at *Planetary and Space Science* (Feb. 2020).
[3] Metzger, Philip T., Kris Zacny, and Phillip Morrison. "Thermal Extraction of Volatiles from Lunar and Asteroid Regolith in Axisymmetric Crank–Nicolson Modeling." *Journal of Aerospace Engineering* 33, no. 6 (2020): 04020075.
[4] Austin, Alex, Brent Sherwood, John Elliott, Anthony Colaprete, Kris Zacny, Philip Metzger, Michael Sims et al. "Robotic Lunar Surface Operations 2." *Acta Astronautica* 176 (2020): 424-437.
[5] Austin, Alex, Brent Sherwood, John Elliott, Anthony Colaprete, Kris Zacny, Philip Metzger, Michael Sims, Harrison Schmitt, Sandra Magnus, Terry Fong, Miles Smith, Raul Polit Casillas, A. Scott Howe, Gerald Voecks, Aaron Parness, Mar Vaquero, Vincent Vendiola, "Robotic Lunar Surface Operations 2," paper no. IAC-19.A3.1.6x49646, *70th International Astronautical Congress (IAC)*, Washington D.C., United States, 21-25 October 2019.
[6] Elliott, J.O., A. Austin, P.T. Metzger, B. Sherwood, and M. Smith, "Operations Modeling of Lunar Base Architectures," poster, *Lunar ISRU 2019 - Developing a New Space Economy through Lunar Resources and Their Utilization*, Columbia, MD, July 15-17, 2019.
[7] Howe, A. Scott, Raul Polit-Casillas, Alex Austin, John Elliott, Aaron Parness, Brent Sherwood, Miles Smith, Gerald Voecks, Anthony Colaprete, Terry Fong, Sandra Magnus, Philip T. Metzger, Harrison H. Schmitt, Michael Sims, Kris Zacny, "Planetary Autonomous Construction System (P@X)," paper no. IAC-19-D3.2A.4x50071, *70th International Astronautical Congress*, Washington, D.C., Oct. 21-24, 2019.
[8] Kornuta, David, Angel Abbud-Madrid, Jared Atkinson, Jonathan Barr, Gary Barnhard, Dallas Bienhoff, Brad Blair, Vanessa Clark,, Justin Cyrus, Blair DeWitt, Chris Dreyer, Barry Finger, Jonathan Goff, Koki Ho, Laura Kelsey, Jim Keravala, Bernard Kutter, Philip Metzger, Laura Montgomery, Phillip Morrison, Clive Neal, Erica Otto, Gordon Roesler, Jim Schier, Brandon Seifert, George Sowers, Paul Spudis, Mark Sundahl, Kris Zacny, Guangdong Zhu. *Commercial Lunar Propellant Architecture: A Collaborative Study of Lunar Propellant Production*. United Launch Alliance, 2018.
[9] Kornuta, David, Angel Abbud-Madrid, Jared Atkinson, Jonathan Barr, Gary Barnhard, Dallas Bienhoff, Brad Blair, Vanessa Clark,, Justin Cyrus, Blair DeWitt, Chris Dreyer, Barry Finger, Jonathan Goff, Koki Ho, Laura Kelsey, Jim Keravala, Bernard Kutter, Philip Metzger, Laura Montgomery, Phillip Morrison, Clive Neal, Erica Otto, Gordon Roesler, Jim Schier, Brandon Seifert, George Sowers, Paul Spudis, Mark Sundahl, Kris Zacny, Guangdong Zhu, "Commercial lunar propellant architecture: A collaborative study of lunar propellant production." *Reach* 13 (2019): 100026.

core tube into the subsurface. There is also large risk to investors deriving from our inadequate experience in the lunar environment. Mining architectures will be more attractive to investors if they can begin operations and buy down risks from a minimum infrastructure starting point and have smooth scale-up to larger operations when the risks have been retired. For startup commercial operations capable of supporting NASA's Sustainable Exploration concept and the Artemis program, what is needed is the "Minimum Viable Product" (MVP) space mining method that starts at *small size* while still producing commercial revenue,[10] yet can incrementally scale-up to *large size* as the risks are progressively bought-down so that the initial technology is not a dead-end. The larger scale infrastructure to operate deeper in PSRs may be more easily funded after the MVP mining operation has proven successful. Aqua Factorem was conceived to be exactly this: the MVP architecture that will grow smoothly to large scale.

The design philosophy behind the Aqua Factorem architecture takes advantage of the natural lunar environment rather than treating it as a foe to be defeated. Rather than transport energy into a PSR, we use the energy that nature has already transported into the PSRs, which has already done most of the work. Billions of years of (micro-)meteoroid bombardment has finely broken all the crystalline solids within a well-understood depth of the regolith's surface, everywhere on the Moon. The ice that was deposited hundreds of millions to billions of years ago in the lunar cold traps will have frozen as hard as granite,[11] so it is just another mineral. Just like all minerals and rocks on the Moon, it has been broken into fine grains and mixed with the other lithic fragments in the soil.[12] Note that the difference between "mineral" and "ice" is purely human-centric and not a real distinction in physics. They are both molecules arranged in solid crystalline form that are liberated from their lattice when heated above a certain temperature. The only difference is that one (the "ice") sublimates *below* our body temperature so it feels cold to the touch and cannot exist in the Earth's mid-latitude, summer environment, while the other (the "mineral" or "rock") remains solid above the human body temperature. In the temperatures of lunar PSRs, they are both extremely stable solids and share the same fracture behaviors when exposed to the lunar impact environment for hundreds of millions to billions of years. Thus, ice is really just another mineral and can be treated like any other mineral. We would not vaporize ilmenite to extract it from soil, and we do not need to vaporize the ice, either. The modeling of lunar geology by Dana Hurley et al.[12] demonstrated how lunar ice has been broken apart into individual ice grains and mixed into the lunar regolith like the grains of the other minerals. This modeling agrees with the observational evidence. Therefore, it is not reasonable to believe large lenses of solid ice exist within this upper churn-zone of lunar regolith. Grains of crystalline ice are most likely in the ~10-100 μm size range[13] based on M^3 Near Infrared (NIR) reflectance

[10] Bennet, N.J., "An Existing Market for Lunar Propellant - GTO Orbit Raising as a Service", In: *Lunar ISRU 2019: Developing a New Space Economy Through Lunar Resources and Their Utilization*, LPI #2152. July 15-17, 2019, Columbia, Maryland. (2019).
[11] Gertsch, Leslie, Richard Gertsch, and Robert Gustafson. "Excavatability of Lunar and Martian Regolith: Initial Laboratory Tests on JSC-1 Simulants." In *Golden Rocks 2006, The 41st US Symposium on Rock Mechanics (USRMS)*. American Rock Mechanics Association, 2006.
[12] Hurley, Dana M., David J. Lawrence, D. Benjamin J. Bussey, Richard R. Vondrak, Richard C. Elphic, and G. Randall Gladstone. "Two-dimensional distribution of volatiles in the lunar regolith from space weathering simulations." *Geophysical Research Letters* 39, no. 9 (2012).
[13] Anthony Colaprete (NASA, LCROSS PI), personal communication, Aug. 18, 2020.

spectra[14] indicating ~70 µm ice grains on the surface vapor deposition and NIR spectral band width and position of LCROSS ejecta[15] indicating the ice from depth were crystallized particles ~8 µm mean size. This is a gigantic advantage to lunar mining. Not only has nature already provided a gigantic quantity of energy into the PSRs to break the ice into fine pieces, but it has done so at a very low flux spread over a very long period of time so much of the ice remained solid and still exists in the soil. If we can sort the different crystalline phases from one another without phase change, then we can transport just the volatiles out of the PSRs to process in the sunlight where energy is available, avoiding most of the infrastructure and cost. To perform this, we have innovated Aqua Factorem, a combination of pneumatic separation, magnetic separation, and electrostatic separation that operates with low power and low equipment mass in a PSR.

1.2 Overview of the Architecture

The simplest version of the architecture would put the entire power system outside the PSR. The mining/beneficiating rover drives in and out of the PSR to bring ore back to the water processing plant. While it is at the plant it will recharge its onboard power systems to support the next mining cycle. The onboard power system can be batteries or regenerable fuel cells. A small fraction of the hydrogen and oxygen made for rocket propellant will be transferred into the rover's fuel cells, and the water produced by those fuel cells will be recycled back into the water processing plant. Power will be obtained outside the PSRs by vertical arrays of solar PV cells that have sun-tracking. The processing site will be located on a high terrain feature where the lunar nights are very short, on the order of 9 Earth-days. Keepalive power can be provided by fuel cells to last through these nights.

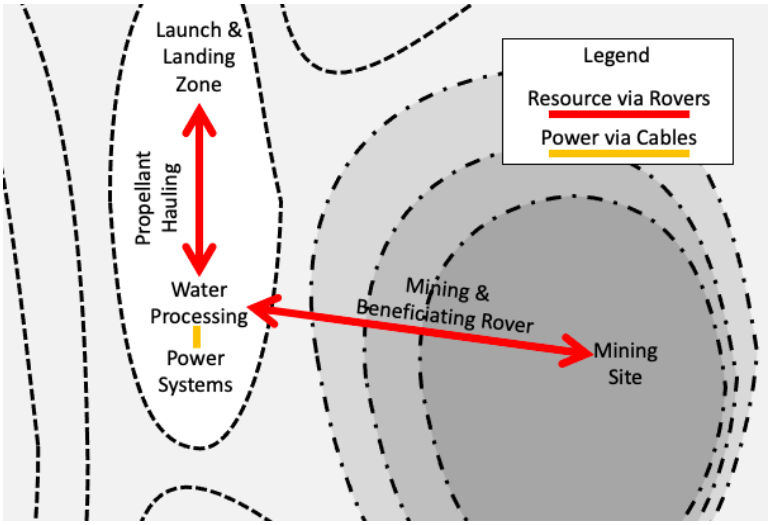

Figure 1: Relationship of Hardware Elements, Option 1

[14] Li, Shuai, and Ralph E. Milliken. "Water on the surface of the Moon as seen by the Moon Mineralogy Mapper: Distribution, abundance, and origins." *Science Advances* 3, no. 9 (2017): e1701471. See Supplementary material for close fits to 70 μm particle size.
[15] Colaprete, Anthony, M. Shirley, J. Heldmann, and D. Wooden. "The Final Minute: Results from the LCROSS Solar Viewing NIR Spectrometer." *LPI* 1608 (2011): 2037.

An enhancement to this basic power system is to move the water cleanup plant partway into the PSR using a superconducting cable to bring the solar power to the plant. This will shorten the driving distance of the mining rovers. A second rover can transport the cleaned water outside the PSR for electrolysis in the sunlit area. This will be beneficial if the beneficiation process is unable to achieve the highest levels of concentration for the water ice.

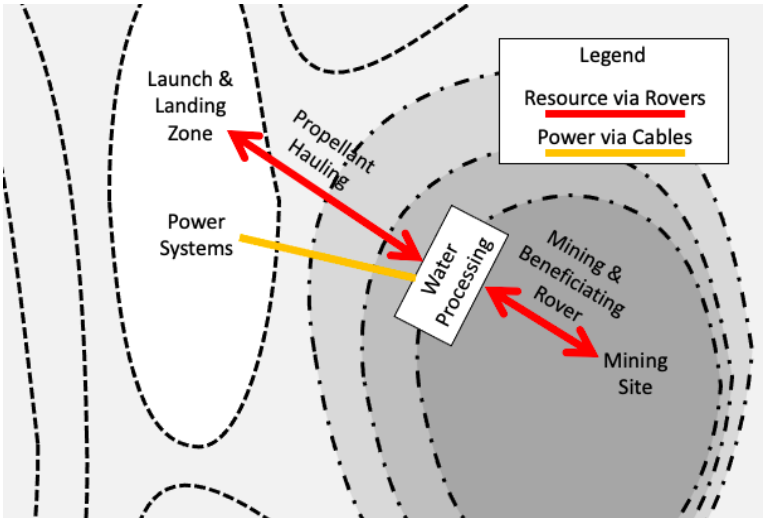

Figure 2: Relationship of Hardware Elements, Option 2

Another possible version is to take the beneficiating systems off the rover and place them in a separate unit that will deploy one time into the PSR near the mining site then remain stationary. Superconducting cables will provide power to the beneficiator from outside the PSR. The mining rover will recharge by plugging into the beneficiating system or by receiving recharged fuel cells that were transported in by the propellant hauling rover(s). The water processing system can be located outside the PSR near the power system.

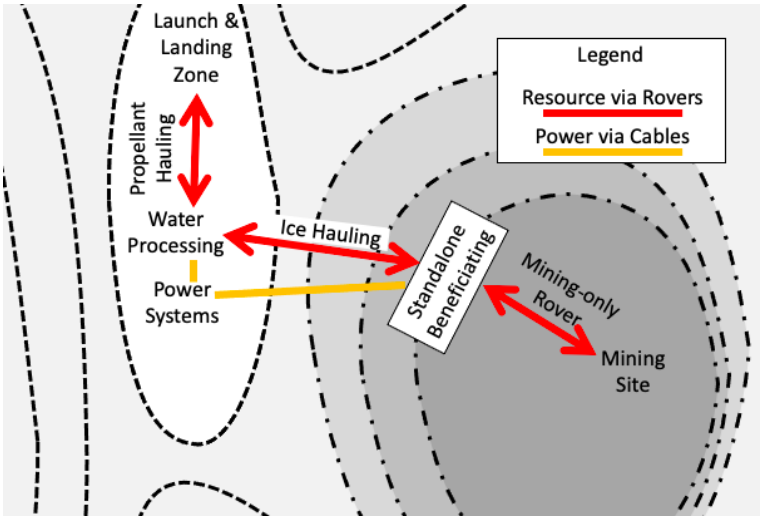

Figure 3: Relationship of Hardware Elements, Option 3

1.3 Physical State of the Resource

There are two concerns about the physical state of the ice. The first is whether the ice exists in solid lenses or in a form that bonds the soil together into a competent solid, which at the cryogenic temperatures of the PSRs would be as hard as rock. If that were the case, then an excavation approach may not be viable. The second concern is whether the ice, although in granular form (either loose grains or only weakly cemented grains and thus excavatable), might exist in polymineralic grains, bonded as a solid icy coating onto the lithic grains. Figure 4 by Doug Rickman of the Marshall Space Flight Center shows several possible relationships between the ice and lithic phases. The Continuous and "Raisins in Pudding" forms would likely not be excavatable, while the Bridging and "Nodules, Fracture Fills, and Lenses" forms might not excavatable depending on the degree of cementation. On the other hand, the Non-Bridging and Non-Filling are excavatable, and the Bridging and "Nodules…" may be excavatable, but the ice may be bonded to lithic grains so a beneficiation approach is brought into question.

If these concerns were realized, then beneficiation would depend very heavily on high-force digging methods (such as the Low Energy Planetary Excavator digging implement developed by Orbitec[16], which uses a cutterhead that is adaptable to digging conditions to minimize energy use) and/or extensive grinding to liberate the ice before beneficiation. That will make the architecture more challenging. While it is true that we need ground-truth to prove the physical state of the ice, this does not appear to be a very high risk to the Aqua Factorem approach. We have assessed the data and found at least four lines of evidence.

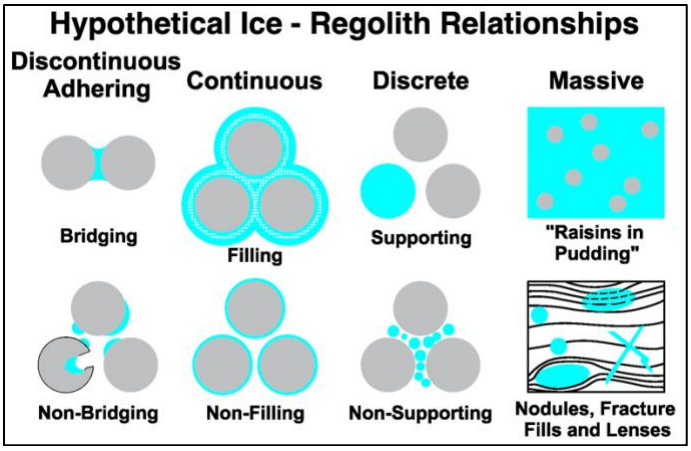

Figure 4: Ice/Lithic Grain Morphologies. Source: Doug Rickman, NASA/MSFC

First, there is no known or proposed mechanism on the Moon to create frozen solid mixtures of ice and soil in the first place. The coldest part of a PSR is either at the surface or very close to the surface, since there is a geothermal gradient pointing upward from below making the subsurface of a PSR generally warmer than the surface. Since vapor during deposition migrates kinetically up a thermal gradient, not down, this will keep most of freezing vapor in the very uppermost

[16] Rostami, Jamal, Leslie S. Gertsch, Robert J. Gustafson, and Chad Swope. "Design and preliminary testing of low-energy planetary excavator." SME Annual Meeting & Exhibit and CMA's 111th National Western Mining Conference (2009: Feb. 22-25, Denver, CO): 830. See also https://techport.nasa.gov/view/5814.

layer. In most parts of the Moon there is a thermal wave in the upper parts of the regolith that could push vapor down. This wave is caused by the moving angle of the Sun and the long lunar night. Therefore, the geothermal gradient is not dominant in the top 30 to 80 cm for most of the Moon and mixing might have occurred in those regions (except that it is too warm for ice to accumulate there). That wave tapers off to a tiny fraction of a degree below about 80 cm at the equator, so the geothermal gradient is dominant below that depth. In a PSR, however, if there is any thermal wave at all, it would exist only because of the weak secondary sunlight reflected off the surrounding terrain and thus it will have extraordinarily tiny amplitude. The tiny amplitude will cause it to have extraordinarily tiny depth in the highly insulating lunar soil. The geothermal gradient will thus dominate at an extremely shallow depth, perhaps only millimeters. When vapor enters a PSR due to a comet impact somewhere on the Moon, or due to the long-term influx of carbonaceous interplanetary dust impacting the Moon and vaporizing over geological timescales, or due to molecules of water that are created by chemical interactions with the space plasma environment hopping one molecule at a time into a PSR, those molecules will all freeze onto the coldest place at very top surface and there will be no physics to make it migrate deeper. In fact, if there is a large enough flux of vapor, such as from a comet or wet asteroid impact, then the freezing vapor will rapidly fill the pore spaces in the top layer, creating a vapor barrier that will prevent any further migration into the subsurface. This view is supported by the observational evidence for thin frost existing on the very top surfaces of some PSRs and by the weak state of the soil at the LCROSS impact. So, if the ice builds up on top of the regolith instead of migrating deeper, it will be pure ice, not a mixture of ice and soil. When subsequent gardening breaks it into fines and mixes it into the soil, they will be pure ice fines mixed with pure lithic fines. This view is supported by the modeling of Hurley et al.[12] These fines will be very easily beneficiated from the lithic fraction of the soil.

Second, we must address the idea that some of the frozen ice is subsequently re-vaporized by micrometeoroid impacts inside the PSR, which also heats the impact site locally so the vapor might migrate to depth and freeze onto the surfaces of grains below the surface. This could create the Bridging or Filling forms of ice in Figure 4, making excavation difficult or impossible when the ice is as hard as granite. However, we already have experimental evidence that this does not happen. Micrometeoroids regularly impact all parts of the Moon and these impacts both heat the surface and vaporize the lithic impactor and a portion of the lithic target material. We see the evidence of the vapor deposition on the soil, including the glass patina on the dust grains and the nanophase iron (npFe) contained in that patina. We see that this vapor deposition, which happens throughout geologic history all over the Moon, does not bond the soil into a soil mass that is hard to excavate. The simple explanation is that the continual bombardment of micrometeorids does vastly more breaking apart than bonding together. Some fragments of broken crusts were identified inside some of the soil cores that were brought back to Earth. They were a rare component of the soil cores, so they did not constitute a significant mass fraction of the soil, but they did exist. They might have formed from the vapor deposition of nearby large impacts so there was a lot of vapor in a short time, enough to overcome the constant refracturing rate. Those fragments were highly friable due to the very weak cementation, and they were already broken into fragments and mixed into the uncemented soil. Thus, they would be no problem for our mining approach. Our calculation shows that the relatively small mass of glass that is deposited by vapor in each micrometeoroid impact event is dwarfed by the mass of regolith that is mechanically disturbed and broken apart by the shockwave of the impact. Our

calculation considered the shock energy of hypervelocity impact spreading over its hemispherical shell in the soil, so the energy density was distributed among the well-known number of grain-to-grain contacts in the soil. We derived the shock energy per grain contact versus radius from impact site. This was compared to experiments by Cole et al.[17] that used micro load cells to measure the frictional and normal forces on individual lunar soil particle grain-to-grain contacts to determine what forcing condition is needed to make grain contacts slide. We found that the radius at which the shock is inadequate to break grains apart encloses a gigantic mass compared to the very tiny mass of the impactor and thus the very tiny mass of resulting vapor. Thus, impacts are a net comminuting process, not a net bonding-via-vapor process, which explains the absence of any significant bonding in the Apollo samples. (We discuss agglutinates that formed as liquid splashes in the next paragraph.) Furthermore, the maturation of soil, which is usually quantified by the accumulation of npFe in the glass patina on the grains is thus is a measure of vapor deposition. It is well known to be a function of how long the soil was lying on the uppermost surface before it was buried by other impact ejecta. Soil buried even less than a centimeter deep is no longer being matured, i.e., no longer receiving vapor deposition. This is in regions where there is a thermal wave so deposition at depth would have been far more likely than in PSRs. This is direct proof that the vapor deposition only occurs in the very top of the soil and does not penetrate to depth where it could cement soil together, and certainly not below the depth that is constantly being broken apart by the shock waves of all the impacts. This provides strong evidence that vapor deposition in the vacuum of the Moon, whether from H_2O molecules or lithic molecules being vaporized, does not bond the soil. We also have observational evidence for this. The LCROSS ejecta found the soil to be extremely weak so the penetrator went in very deeply. It was not a solid mass of soil that would be difficult to excavate. These arguments do not disprove the possibility that the vapor deposition may create a thin coating of ice on the grains (like the Non-Filling form of Figure 4), just like the vaporized lithic minerals all over the Moon freeze as glass patina on the grains. However, the net mass of the patina in lunar soil is tiny compared to the net mass of the solids that never melted via the impact gardening. Thus, by analogy, only a tiny fraction of the lunar ice is expected to exist in Non-Filling (or Non-Bridging) form from vapor coating due to impact gardening. The vast majority of ice will still be in solid form. A patina of ice on the lithic fragments may make electrostatic beneficiation less plausible, but there are options to beneficiate the ice regardless, as we discuss in section 2.0. Also, a minimal surface heating approach (e.g., an infrared lamp, or just the heat of grinding alone) could remove the thin patina from grains prior to electrostatic beneficiation at the cost of slightly higher energy usage in the PSR.

Third, the primary way that ice can freeze onto soil grains to create thick coatings, or bridging, or pore-filling forms is when the liquid water penetrates the soil and then freezes. The community seems to have an incorrect intuition about frozen icy-soil that came from our terrestrial and Mars experiences, not from lunar geology. On Earth, liquid water can exist and flow into soil under gravity before freezing, creating the forms of permafrost that are familiar. Mars' geology is less well understood but shows evidence of liquid flow in the past and perhaps very saline water seapage in the present. On the Moon, these processes cannot occur with water, although they can occur with molten lithic material due to the much slower sublimation rate. Agglutinate particles, which are lithic grains bonded in tiny splashes of glass, form all over the Moon because the small

[17] Cole, David M., and John F. Peters. "Grain-scale mechanics of geologic materials and lunar simulants under normal loading." *Granular Matter* 10, no. 3 (2008): 171.

amount of molten lithic material from micrometeoroid impacts can remain liquid as it falls on the soil before it quench into a glass state. The sublimation rate of liquid water in vacuum, on the other hand, is too fast for this. The flash evaporation rate of water at 19 K (much colder than a PSR) and 100 mbar atmosphere (assuming a vast amount of vaporized water surrounds the droplet, creating the best case for the liquid to survive and mix with soil) is still ~2.7 g/s,[18] so a 100 μm droplet of water would vaporize in 0.2 picoseconds before it got a chance to hit the soil. Thus, liquid water cannot for*m* "water agglutinates." The intuition we have that is based on the liquid form of water in terrestrial experience is incorrect. Of course, we could be wrong, because there may be exotic processes on the Moon that we do not yet know about, and that is why we must get ground truth. It seems likely that if liquid water played any role on the Moon, it must have been at significant depth below large impactors and thus not a significant contributor to surface materials in the gardening zone where excavators will operate. All the evidence suggests Aqua Factorem is a super low-risk approach.

Fourth, even in the worse-case, assuming some weak cementation by vapor deposition has occurred, and therefore if some of the ice is attached to lithic grains, it can be separated by light grinding. Most terrestrial ores are similarly bonded to the surrounding country rock, and it is normative in mining to grind the extracted ore as part of the beneficiation process prior to transportation. Grinding tends to fragment rock along grain boundaries of different minerals, so it would liberate largely ice fragments from largely lithic fragments. We have included light grinding in the Aqua Factorem process for this reason. Grinding requires far less energy than vaporization. Therefore, even in the worst case, we believe Aqua Factorem is a game-changer for the economic viability of startup ice mining.

Finally, we note that mining site selection is another degree of freedom that reduces risk. PI Metzger participated in tests both for icy soil mining[19] and icy soil cone penetrometry[20] with Non-Filling, Filling, and "Raisins…" cases (Figure 4). At cryogenic temperatures, it was found that Filling and "Raisins…" cases are as hard as granite and not appropriate for an excavation-based architecture.[21] The Bridging case should work for lower water concentrations, as long as the 'neck' between the two grains is sufficiently weak. Those types of deposits are unlikely to exist near the surface due to the constant meteoroid gardening. However, if any such deposits do exist, prospecting will identify better candidate deposits with soil more similar to the LCROSS impact site, and that is where Aqua Factorem will begin operations. After scaling up to larger architectures, the operators might choose to go after the non-excavatable deposits using thermal approaches. Our goal here is to define an MVP mining process as a stepping-stone to the larger scale, not to create an architecture that can mine every possible type of deposit.

[18] Saury, Didier, S. Harmand, and M. Siroux. "Experimental study of flash evaporation of a water film." *International Journal of Heat and Mass Transfer* 45, no. 16 (2002): 3447-3457.
[19] Mantovani, James G., Adam Swanger, Ivan I. Townsend III, Laurent Sibille, and Gregory Galloway. "Characterizing the physical and thermal properties of planetary regolith at low temperatures." In *Earth and Space 2014*, pp. 43-51. 2014.
[20] Metzger, P. T., G. M. Galloway, J. G. Mantovani, K. Zacny, Kris Zacny, and Jack Craft. "Low force icy regolith penetration technology." NASA/TM-2011-216302 (July 11, 2011).
[21] Gertsch, Leslie, Richard Gertsch, and Robert Gustafson. "Excavatability of Lunar and Martian Regolith: Initial Laboratory Tests on JSC-1 Simulants." In *Golden Rocks 2006, The 41st US Symposium on Rock Mechanics (USRMS)*. American Rock Mechanics Association, 2006.

1.4 Ice Extraction Method

A particular version of this novel ice extraction method is shown in Figure 5. A robot scoops the regolith with rock-rejection and gravel separation to pass only fines. A grinder fractures the weaker particles, liberating ice fragments from mineral and lithic fragments. This Resource Intake system transfers the regolith into a batch-processing Beneficiation System, with pneumatic separation, magnetic separation, and electrostatic separation combined in a sequence that can handle the exotic lunar geology. The system outputs separated streams of ice grains and slag soil particles. The beneficiation process can be extended to also separate free metal particles and specific mineral grains of high resource value. The soil is 95-98 wt% non-ice ("tailings"), which is dropped in the PSR while the desired 2-5 wt% of ice is transported to sunlight. This kilometers-long transportion is made economically viable by the extreme mass reduction that took place in the PSR. The water cleanup, electrolysis, liquefaction, and storage stages are included in every ice mining architecture but now they are in a location with energy. After hauling the resource to sunlight, the rover recharges or swaps out its batteries or fuel cells then returns to the PSR. In addition to transporting the resource, it also hauls fuel cells into and out of the PSR There are locations in the Moon's poles where driving distances from sunlight to the ice resource are just a few kilometers on gentle slopes.[22,23] Ice concentrations in these "Type 2" locations[24] are expected to have a shallow dry overburden of about 30-50 cm that must be removed.

Variations on this architecture can later be added to extend its reach into the deeper PSRs where ice has higher concentrations and less overburden. For example, additional fuel cells can increase driving distance, or, with solar energy towers as innovated by Sercel,[25] mining and processing could be done entirely inside PSRs (no driving back to sunlight), but still using beneficiation instead of thermal extraction will vastly reduce the energy, the infrastructure, and the cost, improving the economic benefit. To crudely illustrate the benefit, we note the United Launch Alliance (ULA) study[26] calculated that 800 kW thermal energy is needed to extract 2,450 t of water yearly to support the future commercial demand for lunar water. Producing 2,450 t of water yearly at 5% concentration requires processing 49,000 t of regolith yearly or 1.55 kg/s. If we rely on sunlight with a duty cycle of 70% in a polar location and obtain only 2% yield, it must be processed at 5.55 kg/s to make up the difference. Assuming a larger-scale beneficiator processes 3 kg/s (ten times the pilot plant goal), then with a mining/hauling duty cycle of 50% the operation would require 4 of them. With each operating at 5 kW, this is a 97.5% power reduction versus thermal extraction. With subsequent processes taking place in the sunlight, there is potentially >99% reduction of total energy and infrastructure in the PSR.

[22] Austin et al. (2019).
[23] Elliott, J.O., A. Austin, P.T. Metzger, B. Sherwood, and M. Smith, "Operations Modeling of Lunar Base Architectures," poster, *Lunar ISRU 2019 - Developing a New Space Economy through Lunar Resources and Their Utilization*, Columbia, MD, July 15-17, 2019.
[24] Austin et al. (2019).
[25] Sercel, Joel, "Lunar-Polar Propellant Mining Outpost (LPMO): Affordable Exploration and Industrialization," NIAC 2019 Phase I, Phase II, and Phase III Selections, https://www.nasa.gov/directorates/spacetech/niac/2019_Phase_I_Phase_II/Lunar_Polar_Propellant_Mining_Outpost
[26] Kornuta et al. (2018); Kornuta et al. (2019).

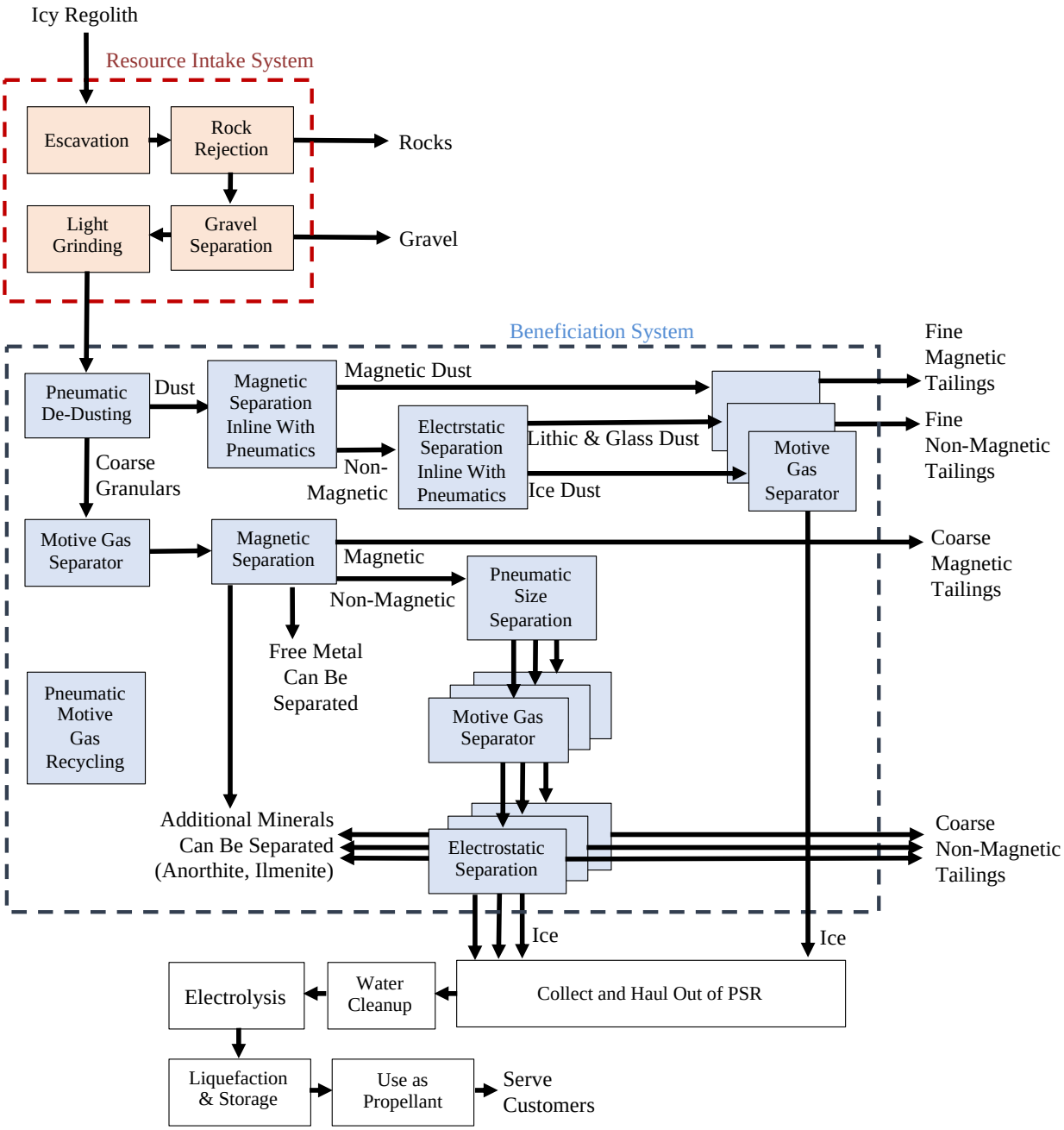

Figure 5. Water Extraction and Propellant Manufacture Method

1.4.1 Excavation Subsystem

The system begins with an excavator that can be a digging bucket or a bucket wheel to break up any weak cementation in the ice/soil mixture. We have strong geological reason to believe the soil is no more than weakly cemented, if at all. More will be written about this in the final report. An example of the type of digging system envisioned is shown in Figure 6.

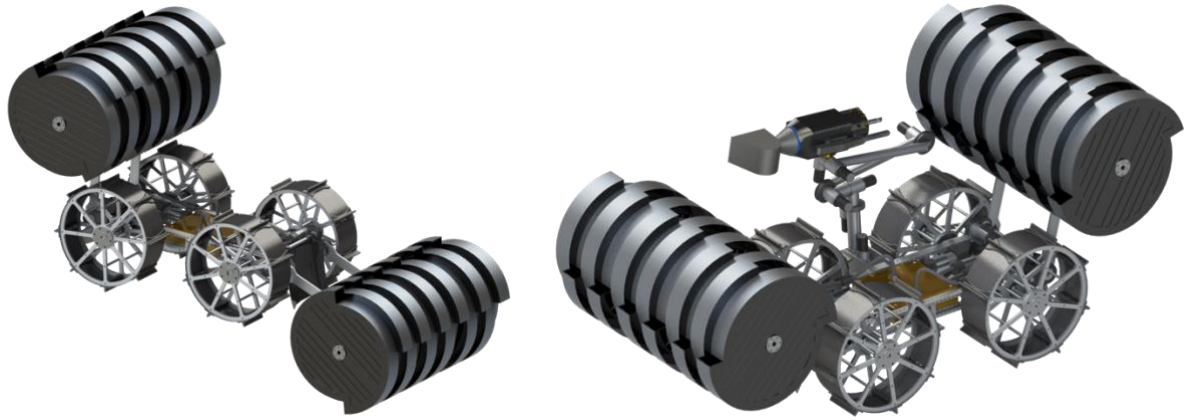

Figure 6. Mining robots for open-pit strip mining following the concept of NASA's Regolith Advanced Surface Systems Operations Robot (RASSOR).

1.4.2 Rock Rejection

Rock rejection in terrestrial excavators is done with "grizzlies", to let soil through while keeping rocks out (Figure 7). Technology advancement is needed to prevent rocks from jamming in the rock rejection process because to be economically viable the mine should have no humans present for most of the time, and there will be nobody there to remove jammed rocks. We have innovated methods to autonomously perform rock-unjamming.

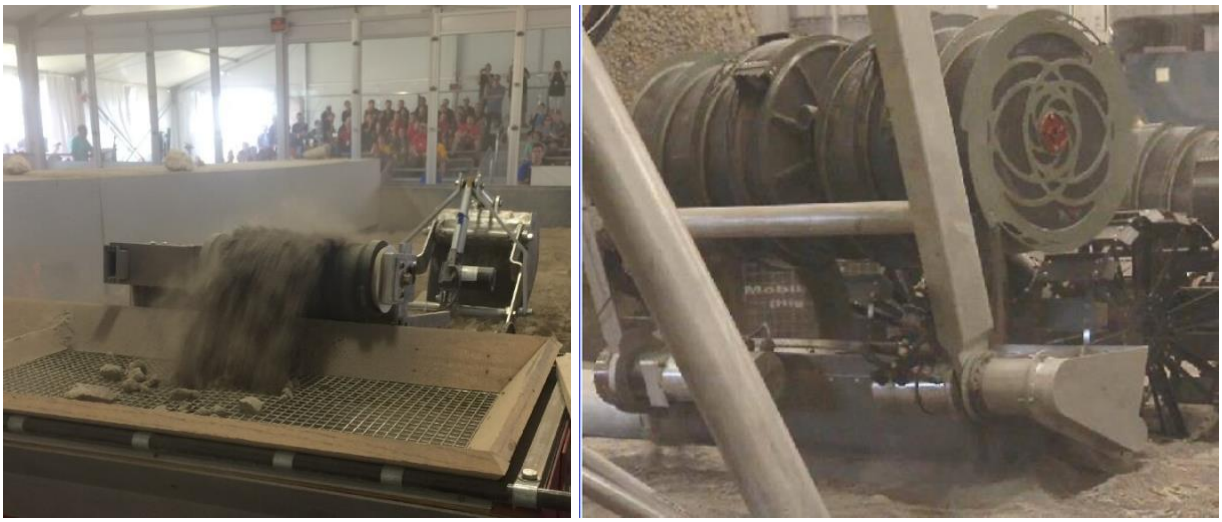

Figure 7. Left: At the 2016 NASA Robotic Mining Competition, a robot depositing regolith through a grizzly to remove rocks. Image: Metzger. Right: NASA's RASSOR bucket drum excavator delivering regolith into a hopper containing an auger to push soil across openings that allow soil through while gravel is rejected out the end.

1.4.3 Gravel Separation Technology

Gravel separation is needed to prevent the next smaller size rocks from proceeding into the Beneficiation System. If we could make the grizzly small enough to reject gravel then and additional gravel separator would be unnecessary, but in lunar gravity the soil will not pass through the smaller gaps due to cohesion. We learned this in reduced gravity flights, showing non-flow of lunar fines through cylindrical openings as wide as 5 cm. Gravel separation needs a

mechanical "wiper" or agitation to move soil through the openings while pushing gravel to a rejection port. This is often done in terrestrial industry with an auger and has been prototyped by NASA (Figure 8), but augers are subject to jamming. In NASA's Robotic Mining Competitions (RMC) with realistic regolith simulant, augurs routinely jam. Jamming can be prevented in most cases by having a gearing system that can increase torque to crush jammed rocks when necessary. Work is needed to develop a jam-proof gravel separator with a release hatch as backup to dump an entire jammed load. The release-hatch idea was innovated by the Embry-Riddle Aeronautical University team at the 2016 NASA RMC.

1.4.4 Grinding and Fracture Subsystem

For beneficiation to extract ice from the Bridging, Non-Bridging, and Non-Filling case of Figure 4, a light grinding stage will be needed to liberate ice fragments from the lithic fragments. Fracture generally occurs along dissimilar material boundaries, so grinding will be effective, and this is why it is commonly used in terrestrial mining. The challenge is that grinding generates heat. At PSR temperatures in vacuum there is no risk of the particles becoming wet and sticky from *melted* ice, but too much heat could cause loss of the resource to sublimation. A 1 μm particle will sublime away in about 12 hours at 200 K, and PSR ice deposits are generally below 100 K. An ice-metal interface fractures with 2 J/m^2,[27] so reasonably assuming equal energy is partitioned into heating the ice phase during fracture, using the heat capacity of water ice at 100 K, a 1 μm particle of ice will be raised from 100 K to 103.4 K by breaking it off the lithic particle. This indicates a margin of 30X to account for grinder inefficiency. Work is needed to compare methods of grinding, rolling, and impact hammering (a review is in Zacny et al., 2009[28]) to maximize liberation of ice fragments without raising their temperature significantly.

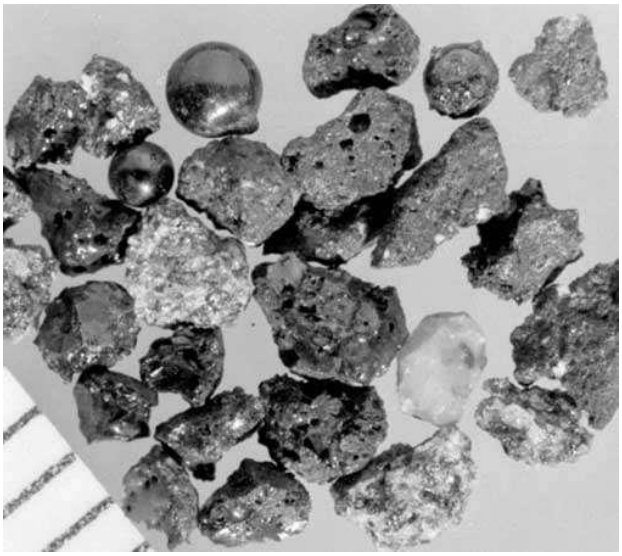

Figure 8. Lunar soil is a mixture of different minerals, rock fragments, volcanic glass beads, agglutinitic glass, etc. Source: NASA.

[27] Wei, Yingchang, Robert M. Adamson, and John P. Dempsey. "Fracture energy of ice/metal interfaces." In *Adhesives Engineering*, vol. 1999, pp. 126-135. International Society for Optics and Photonics, 1993.
[28] Zacny, Kris, Antonio Diaz-Calderon, Paul G. Backes, Kiel Davis, Chris Leger, Erik Mumm, Edward Tunstel, Jason Herman, Gale Paulsen, and Yoseph Bar-Cohen. "Planetary Sample Handling and Processing." In: *Drilling in Extreme Environments: Penetration and Sampling on Earth and other Planets*, Bar-Cohen, Yoseph, and Kris Zacny, eds. John Wiley & Sons, 2009, pp. 559-641.

1.4.5 Beneficiation System

Beneficiation is routinely used in terrestrial mining as the intermediate step between extraction and chemical processing.[29-32] It has been studied for concentration of certain lunar minerals.[33,34] Lunar soil is a mixture of many mineral fragments, rock fragments, glass, agglutinates, and metal in addition to the ice (Figure 8). These could be beneficiated individually using a variety of methods. Our goal is to implement a method that will specifically beneficiate ice.

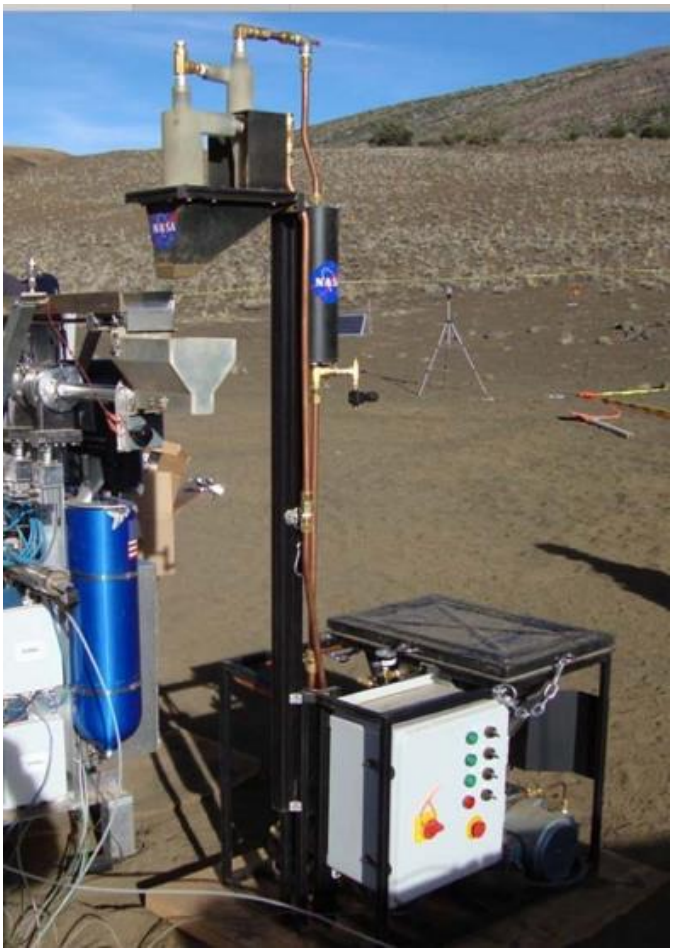

Figure 9. Honeybee Robotics Pneumatic system, 2010 field test.

[29] Svoboda, Jan. *Magnetic Methods for the Treatment of Minerals*. Vol. 692. Amsterdam: Elsevier, 1987.
[30] Oberteuffer, J. "Magnetic separation: A review of principles, devices, and applications." *IEEE Transactions on Magnetics* 10, no. 2 (1974): 223-238.
[31] Cotter-Howells, Janet. "Separation of high density minerals from soil." *Science of the Total Environment* 132, no. 1 (1993): 93-98.
[32] Rickman, D. L., C. Young, D. Stoeser, and J. Edmunson. "Beneficiation of Stillwater Complex Rock for the Production of Lunar Simulants." NASA/TM-2014-217502. NASA Marshall Space Flight Center; Huntsville, AL (2014).
[33] Mason, Larry W., "On the beneficiation and comminution of lunar regolith", In: *Engineering, construction, and operations in space - III: Space '92; Proceedings of the 3rd International Conference*, Denver, CO, May 31-June 4, 1992. Vol. 1 (A93-41976 17-12), p. 1127-1138.
[34] Berggren, Mark, Robert Zubrin, Peter Jonscher, and James Kilgore. "Lunar soil particle separator." In: *49th AIAA Aerospace Sciences Meeting including the New Horizons Forum and Aerospace Exposition*, p. 436. 2010.

1.4.6 Pneumatic Separation

NASA and Honeybee Robotics have developed pneumatic transport and size segregation of lunar soil[35-40] so the technology is already TRL-5/6 (Figure 9). This method separates particles per the ratio of inertial force and aerodynamic drag force, which scales as density times particle diameter, ρd. Since $\rho_{\mathrm{Rock}} \approx 3\ \rho_{\mathrm{Ice}}$, pneumatic separation will separate lithic (rock) particles of d into the same bin as ice particles of $3d$ and thus 9 times larger inertia.

1.4.7 Magnetic Separation

The three pneumatically-separated material streams will each pass through a magnetic separator to remove magnetic particles. This process can be based upon methods commonly used in terrestrial industry.[41-43] Taylor and co-workers[44-46] investigated magnetic separation for lunar soil but concluded it was challenging because paramagnetic susceptibility of minerals is dominated by the superparamagnetic response of npFe contained in the glass coating of the finest particles. Therefore, magnets tend to pull just the fine particles out regardless their composition. However, lunar ice is sufficiently different than regolith particles to enable ice separation from both dust and most of the larger mineral and lithic particles on their magnetic properties. Furthermore, the < 30 μm fines will have been separated pneumatically so the magnetic field in that one stream can be reduced as necessary. (Real lunar soil with npFe can be used in future work.) In highly mature lunar soil, some minerals have lost much of their pristine magnetic character by

[35] Zacny, Kris, Greg Mungas, Chris Mungas, David Fisher, and Magnus Hedlund. "Pneumatic excavator and regolith transport system for lunar ISRU and construction." In *AIAA SPACE 2008 conference & exposition*, p. 7824. 2008.
[36] Mueller, Robert P., Ivan I. Townsend, III, and James G. Mantovani. "Pneumatic regolith transfer systems for in situ resource utilization." In *Earth and Space 2010: Engineering, Science, Construction, and Operations in Challenging Environments*, pp. 1353-1363. 2010.
[37] Zacny, Kris, Jack Craft, Megnus Hedlund, Phil Chu, Greg Galloway, and Robert Mueller. "Investigating the efficiency of pneumatic transfer of JSC-1a lunar regolith simulant in vacuum and lunar gravity during parabolic flights." In: *AIAA SPACE 2010 Conference & Exposition*, p. 8702. 2010.
[38] Craft, Jack, Kris Zacny, Phil Chu, Jack Wilson, Chris Santoro, Lee Carlson, Mike Maksymuk, Ivan Townsend, Robert Mueller, and James Mantovani. "Field Testing of a Pneumatic Regolith Feed System During a 2010 ISRU Field Campaign on Mauna Kea, Hawaii." In: *AIAA SPACE 2010 Conference & Exposition*, p. 8900. 2010.
[39] Mueller, Robert, Ivan Townsend, James Mantonvanni, and Philip Metzger. "Evolution of Regolith Feed Systems for Lunar ISRU O2 Production Plants." In *48th AIAA Aerospace Sciences Meeting Including the New Horizons Forum and Aerospace Exposition*, p. 1547. 2010.
[40] Zacny, Kris, Bruce Betts, Magnus Hedlund, Paul Long, Marc Gramlich, Keith Tura, Phil Chu, Abigail Jacob, and Abel Garcia. "PlanetVac: Pneumatic regolith sampling system." In: *2014 IEEE Aerospace Conference*, pp. 1-8. IEEE, 2014.
[41] Svoboda, Jan. *Magnetic Methods for the Treatment of Minerals*. Vol. 692. Amsterdam: Elsevier, 1987.
[42] Oberteuffer, J. "Magnetic separation: A review of principles, devices, and applications." *IEEE Transactions on Magnetics* 10, no. 2 (1974): 223-238.
[43] Cotter-Howells, Janet. "Separation of high density minerals from soil." *Science of the Total Environment* 132, no. 1 (1993): 93-98
[44] Taylor, L. A., and R. R. Oder. "Magnetic Benefication of Highlands Soils: Concentrations of Anorthite and Agglutinates." In *Lunar and Planetary Science Conference*, vol. 21. 1990.
[45] Oder, R. R. "Beneficiation of lunar soils: Case studies in magnetics." *Mining, Metallurgy & Exploration* 9, no. 3 (1992): 119-130.
[46] Taylor, Lawrence A., and Robin R. Oder. "Magnetic beneficiation of highland and hi-Ti mare soils-Rock, mineral, and glassy components." In *Engineering, construction, and operations in space II*, vol. 1, pp. 143-152. 1990.

incorporation into glass agglutinate particles[47] and will be difficult or impossible to beneficiate from ice by magnetism alone. However, magnetic separation will greatly reduce the material stream prior to electrostatic separation enabling that next stage to keep up with the flow rate and obtain higher yield.

According to the Curie-Weiss law, paramagnetic susceptibility is inversely related to temperature minus the Curie Constant, which is about 11 K for olivine.[48] Comparing olivine's susceptibility in a T=40 K PSR versus at 293K, susceptibility is 6 times stronger in the PSR, making magnetic separation a more efficient process in the PSR.

1.4.8 Tribocharging and Electrostatic Separation

Because tribocharging is a surface phenomenon whereas magnetization is a bulk phenomenon, the magnetic throughput scales better for high processing rate. Therefore, we plan to use magnetic separation first, discarding up to 80% of the lithic material to slag, then use electrostatic separation to achieve more complete separation. NASA has previously developed electrostatic beneficiation and showed it to be highly effective at concentrating ilmenite (for oxygen production) from among the other silicate minerals,[49] producing 50-60% concentration of ilmenite in one pass and 90% in two passes. The method worked by running mixed-mineralogy lunar regolith through a baffle to rub the soil grains across selected materials, causing the various minerals to tribocharge based on their surface chemistry. Ice is known to tribocharge,[50-54] and the properties of ice and silicate grains are so different that electrostatic separation will be highly efficient. Comparing tribocharging against aluminum for silicates[55] versus ice[56] of the same particle diameter, the ice will experience 100 to 10,000 times the acceleration in an electric field as the silicates.

2.0 Viability of the Critical Function

We assessed the viability of the critical function through a combination of laboratory demonstration, theory, and analysis. A low-fidelity (benchtop) prototype for the magnetic and

[47] Oder, R.R. and Jamison, R.E., 1989. *Magnetic Beneficiation of Lunar Soil*. Phase One Final Report, NASA Small Business Innovation Research Program, Contract NAS-9-18092.
[48] Biedermann, Andrea R., Thomas Pettke, Eric Reusser, and Ann M. Hirt. "Anisotropy of magnetic susceptibility in natural olivine single crystals." *Geochemistry, Geophysics, Geosystems* 15, no. 7 (2014): 3051-3065.
[49] Trigwell, Steve, James Captain, Kyle Weis, and Jacqueline Quinn. "Electrostatic Beneficiation of Lunar Regolith: Applications in In Situ Resource Utilization." *Journal of Aerospace Engineering* 26, no. 1 (2012): 30-36.
[50] Akinyemi, M. L., A. O. Boyo, M. E. Emetere, M. R. Usikalu, and F. O. Olawole. "Lightning a fundamental of atmospheric electricity." *IERI Procedia* 9 (2014): 47-52.
[51] Méndez Harper, J., L. M. Courtland, and J. Dufek. "The Effects of Ice on the Frictional Electrification of Plumes." In *AGU Fall Meeting Abstracts*. 2015.
[52] Dunham, Stuart B. "Electrostatic charging by solid precipitation." *Journal of the Atmospheric Sciences* 23, no. 4 (1966): 412-415.
[53] Agosto, William N. "Electrostatic concentration of lunar soil minerals." In: *Lunar Bases and Space activities of the 21st Century*, p. 453. 1985.
[54] Trigwell, Steve, John E. Lane, James G. Captain, Kyle H. Weis, Jacqueline W. Quinn, and Fumiya Watanabe. "Quantification of efficiency of beneficiation of lunar regolith." *Particulate Science and Technology* 31, no. 1 (2013): 45-50.
[55] Agosto, William N. "Lunar beneficiation." In: *Space Resources*, vol. 509, pp. 153-161. 1992.
[56] Dunham (1966).

electrostatic portions of the beneficiation process was developed to support this effort. To meet the full scale propellant production needs of our MVP system (derived in the architectural analysis of transportation requirements, section 3.2), assuming it operates only during daylight hours with 50% downtime between mining cycles and 5% yield of ice from the regolith, it will need to process 88 kg/hr.

2.1 Simulants

For initial laboratory testing, we chose to use ground plastic instead of ice to avoid problems with it melting. Plastic has similar density to water ice and is not significantly magnetic, also similar to ice, so it is an adequate simulant for magnetic, pneumatic, and size sorting processes. The electrostatic properties are still to be determined, so it may not be good for that portion of the Aqua Factorem process, but it will be adequate for preliminary tests to validate the hardware. Final tests will use actual water ice chilled cryogenically.

We have selected the Exolith laboratory's Lunar Mare simulant (LMS-1) and Lunar Highlands Simulant (LHS-1) for the base material for the lithic portion of our simulant. Both mineralogies are relevant. Numerous Lunar South Pole PSRs including Weichert, Weichert E, Weichert J, Kuhn, and Kocher craters are located inside the Pyroxene-Bearing Zone of the South Pole-Aitken Basin and hence have significantly mafic mineralogy.[57,58] The rest of the PSRs are in the Heterogenous Annulus around the SPA Basin and hence have mixtures of mafic and feldspathic mineralogy are found. Localized deposits of mafic minerals, dominantly Mg-pyroxene, are found in that zone. The mineralogy for LMS-1[59] and LHS-1[60] are given in Table 1. The standard densities and typical magnetic susceptibilities from the literature are also provided. Magnetic properties vary considerably, and it was out of scope for the Phase 1 project to do a full analysis, so these values were selected as typical for the sake of this feasibility study.

Table 1: Lunar Soil Simulant Characteristics

Component	**Density (g/cm^3)**	**Typical Magn. Suscept. ($Si \times 10^{-6}$)**	**LMS-1 wt%**	**LHS-1 wt%**
Pyroxene	3.2 – 3.5	130,000	32.8	0.2
Glass-rich basalt	~2.9	7,300	32.0	24.7
Anorthosite	2.62 – 2.82	50	19.8	74.4
Olivine	2.9	400	11.1	0.3
Ilmenite	4.70 – 4.79	8,000	4.3	0.4
Bulk LMS-1	3.02 – 3.16	9E-04	100	–
Bulk LHS-1	2.68 – 2.85	4E-04	–	100

[57] Moriarty Iii, D. P., and C. M. Pieters. "The character of South Pole-Aitken Basin: Patterns of surface and subsurface composition." *Journal of Geophysical Research: Planets* 123, no. 3 (2018): 729-747.
[58] https://www.lpi.usra.edu/lunar/lunar-south-pole-atlas/maps/SPole_80S_LOLA-PSR_v20190515.pdf
[59] Exolith Lab, LMS-1 Lunar Mare Simulant Fact Sheet, University of Central Florida, Jan. 2021, https://cdn.shopify.com/s/files/1/0398/9268/0862/files/lms-1-spec-sheet-2021.pdf?v=1611877987.
[60] Exolith Lab, LMS-1 Lunar Highlands Simulant Fact Sheet, University of Central Florida, Jan. 2021, https://cdn.shopify.com/s/files/1/0398/9268/0862/files/lhs-1-spec-sheet-2021.pdf?v=1611877987.

We used plastic sandblasting material as the ice-simulant additive. Preliminary tests demonstrate that it flows as desired. We noted that the simulated ice easily segregates from the regolith (i.e., it is difficult to keep them mixed), which is supportive of the basic approach of Aqua Factorem.

Figure 10. Plastic particles mixed in lunar soil simulant demonstrating easy segregation by particle size.

After performing each step in the beneficiating process, we needed to measure the concentration of the plastic in the mixture. This could normally be done by immersion in a fluid to measure average density of the mixture using the standard density test for soils. However, plastic may float so that is problematic. Another approach is to use a microscope and an automated procedure to measure grain sizes and numbers for each distinct composition identified in the imagery, but such an effort was out of scope for a Phase 1 project. We chose instead to use a correlation to the bulk density. The method is to fill a graduated cylinder or beaker with the mixture using a standardized filling procedure, measure its mass and volume, then divide to calculate bulk density. The fraction that is plastic has lower specific gravity so the more plastic there is the lower the bulk density will be. This, too, is problematic because granular materials can be packed to have more or less porosity, so the two variables (fraction of plastic, and porosity) create degeneracy in the measurement. However, if a careful filling method can be followed, then the porosity should be repeatable. This does not mean the porosity will be constant for mixtures having different fractions of plastic, though. The plastic has different friction than the mineral grains, so even when identical filling procedures are followed, both the porosity and the bulk density should be functions of the plastic fraction. Therefore, we had to prepare multiple mixtures with known plastic fractions to calibrate the relationship of bulk density vs. plastic fraction for a defined filling procedure. We tried multiple filling procedures. We found that attempting to create a minimum density packing (maximum porosity) did not produce a reliable correlation to plastic fraction. Preparing a maximum density (minimum porosity) packing did prove to be reliable. (Here we defined maximum density as the maximum that is obtained by constant vibration and tapping without overburden in the container.) These results are shown in Figure 11. The linear fits to the data are given by the functions,

$$C_{\mathrm{LMS-1}} = (115.05 \pm 8.11) - (62.763 \pm 4.96)\,\rho_{\mathrm{LMS-1}}$$

$$C_{\mathrm{LHS-1}} = (152.41 \pm 7.15) - (88.762 \pm 4.44)\,\rho_{\mathrm{LHS-1}}$$

where C is concentration of plastic in either simulant and ρ is measured bulk density for either simulant. Using these functions, we can now determine the plastic fraction in a beneficiated sample.

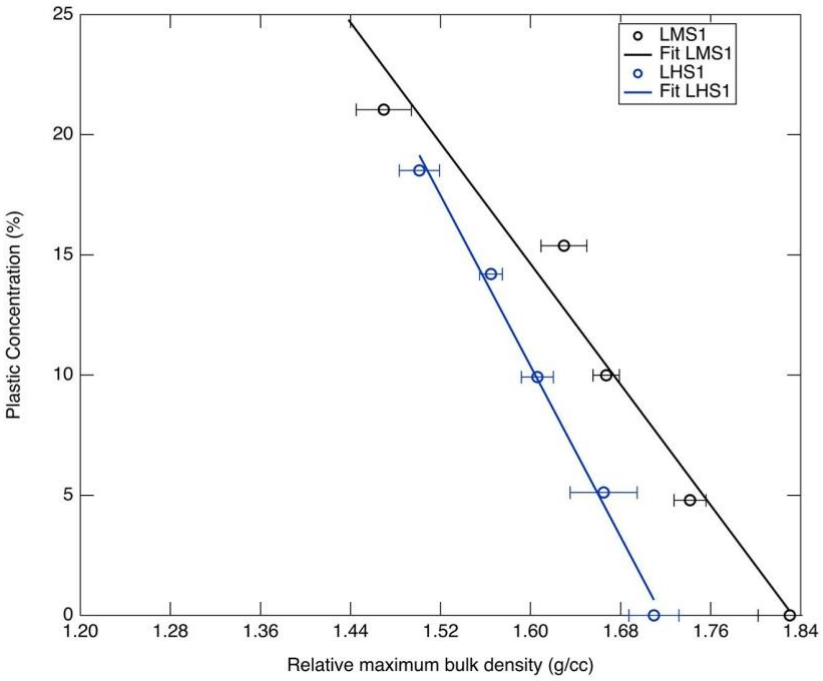

Figure 11. Plastic concentration versus the relative maximum bulk density of lunar simulants.

For comparison with the results that we report below, the magnetic permeability of the lunar simulants and their individual constituent minerals were measured using a Faraday Scale. We also measured the bulk permeability of the magnetic and non-magnetic isolates from the magnetic separation process. These results, including temperature dependence of their permeabilities, will be useful to the lunar community for a wide range of applications. These data are being prepared for publication in a science journal to make them available to the community. The ambient temperature results of mainly the simulants before and after beneficiation are provided below.

The magnetic susceptibility measurement was performed in a Faraday scale. A sample holder hangs under a regular digital scale. An adequate volume of 60 ml was chosen as sample size. For each sample the bulk density and porosity was predetermined for the same compactness. Strong permanent magnets are arranged to sip in and out under the sample holder. The whole system is isolated from unused magnetic substances. Then the excess of force exerted on the samples on a beaker placed on the sample holder with and without the magnets' presence is recorded. The

ratio of the excess magnetic force between experimental samples and reference materials allows to proportionate the magnetic susceptibility.

We used nickel chloride ($NiCl_2$) crystals and aqueous $NiCl_2$(50% by weight) as reference materials. Table 2 shows the summary of the calculations. Apart from LMS-1 and LHS-1, we also include Olivine (which is one of the major constituents to both the simulants). Other samples are magnetic(M) and nonmagnetic (NM) yields of magnetic beneficiation after first and second pass through the system. Five different samples were tested for each experiment. Porosity was calculated by dripping the water to fill the inner granular gap, Olive oil was used for $NiCl_2$ instead of water as it dissolves in the later. The volume susceptibilities χ_1 and χ_2 were calculated by using aqueous $NiCl_2$ and crystalline $NiCl_2$ as reference respectively. The two asterisked values are the standards from which the other values are calculated. The two values in each row are close considering the uncertainties inherent in susceptibility measurements.

Table 2: Volume susceptibilities of lunar simulants and its components. Reference cases indicated by asterisks.

Sample	Bulk density (g/cm^3)	Average magnetic force (g) ± 1 std dev	Poro-sity	Density (g/cm^3)	χ_1 based on aqueous $NiCl_2$ (unitless)	χ_2 based on solid $NiCl_2$ (unitless)
Aqueous $NiCl_2$	1.224	0.644 ± 0.017	0.000	1.2237	2.026E-05*	3.766E-05
$NiCl_2$	0.954	0.92 ± 0.018	0.385	1.5507	2.894E-05	5.379E-05*
Olivine	1.817	6.976 ± 0.237	0.449	3.2937	2.194E-04	4.079E-04
LMS-1	1.897	27.776 ± 1.362	0.328	2.8212	8.737E-04	1.624E-03
LMS-1-M1	1.817	36.672 ± 0.195	0.347	2.7805	1.154E-03	2.144E-03
LMS-1-M2	1.776	32.458 ± 0.797	0.347	2.7180	1.021E-03	1.898E-03
LMS-1-NM1	1.827	5.954 ± 0.218	0.341	2.7716	1.873E-04	3.481E-04
LMS-1-NM2	1.787	3.850 ± 0.137	0.341	2.7105	1.211E-04	2.251E-04
LHS-1	1.703	12.374 ± 0.334	0.378	2.7394	3.892E-04	7.235E-04
LHS-1-M1	1.817	19.872 ± 0.692	0.385	2.9527	6.251E-04	1.162E-03
LHS-1-M2	1.776	18.936 ± 0.373	0.385	2.8863	5.956E-04	1.107E-03
LHS-1-NM1	1.776	3.766 ± 0.273	0.368	2.8087	1.185E-04	2.202E-04
LHS-1-NM2	1.787	3.850 ± 0.137	0.368	2.8266	1.211E-04	2.251E-04

2.2 Lunar Soil and Ice Models

The models of lunar soil and ice particle sizes that we use in this analysis are derived in Appendix A. The particle size distribution for the lithic (non-ice) lunar soil is shown in Figure 12.

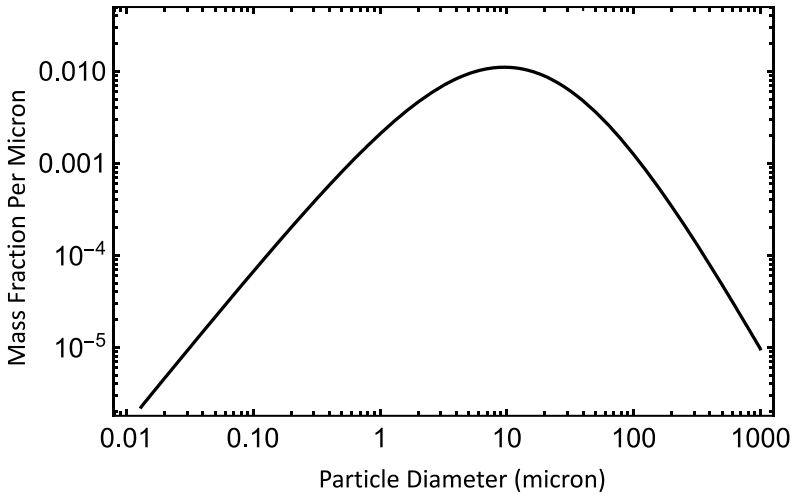

Figure 12. Lunar soil particle size distribution model following Apollo soil 78221,8[61] for the coarser fraction > 1 μm and Apollo soil 10085[62] for the fines fraction < 1 μm.

The equation is:

$$P(D) = A\left[\frac{1}{\left(\frac{1}{0.1\,D^{\varphi}}\right)^{\alpha} + \left(\frac{1}{12{,}500\,D^{\gamma}}\right)^{\alpha}}\right]^{1/\alpha}$$

with $\varphi = +1.70$, $\gamma = -2.50$, $\alpha = 0.19$, and $A = 18.44$ chosen for normalization. This has mass-weighted mean particle size $\widehat{D} = 78.0$ μm. This is close to the D_{50} size for "mean" Apollo soil. The areal-weighted particle size per this equation is $\langle D \rangle = 19.0$ μm. Mass-weighted mean particle size is what is measured by sieving in a laboratory, while areal-weighted mean particle size is what is measured by optical (and some other) remote sensing techniques.

For lithic (non-ice) lunar soil, the particle sizes slowly evolve from coarser to finer as the soil is exposed to the micrometeoroid gardening at the surface. This "maturation" process breaks apart the larger particles but also bonds together the finer particles through micrometeoroid impact melt-glass splashes, creating agglutinate particles. The balance of the fracturing and agglutination processes creates the steady-state size distribution that is characteristic of mature soil. The fracture rate of particles into smaller fragments through micrometeoroid impacts is probably similar for both water ice and lithic particles. However, water ice particles cannot participate in the agglutination process because water will rapidly evaporate at high temperature. The only balancing process to create coarser ice particles might be that ice particles grow larger individually by vapor deposition, with existing particles seeding the accumulation of mass. The differences in geological process suggests the equilibrium mean particle size may be different for ice than for lithic material. The measured mean particle size from the LCROSS impact ejecta

[61] Heiken et al. (1991), Figure 9.1.
[62] Park, Jaesung, Yang Liu, Kenneth D. Kihm, and Lawrence A. Taylor. "Characterization of lunar dust for toxicological studies. I: Particle size distribution." *Journal of Aerospace Engineering* 21, no. 4 (2008): 266-271.

was 8 μm,[63] and the mean size estimated from the M^3 observations of "frost" in some PSRs is 70 μm.[64] Four models of ice particle sizing are derived in Appendix A, using the same equation as the lithic soil but with the constants of Table 3. The models are plotted in Figure 13.

Table 3. Parameters for Soil and Ice Particle Size Distributions.

Model	Assumptions	φ	γ	A	$\langle D \rangle$ (μm)	$\widehat{D}$ (μm)
Lunar Soil	Follow Apollo soils: 78221,8[65] for > 1 μm, or 10085[66] for < 1 μm	+1.70	–2.5	18.44	19.0	78.0
Ice Model 1	Match the Lunar Soil Model	+1.70	–2.5	18.44	19.0	78.0
Ice Model 2	Adjust only φ to match $\langle D \rangle$ from LCROSS	+0.339	–2.5	2.83	8.0	108.2
Ice Model 3	Adjust only γ to match $\langle D \rangle$ from M^3	+1.70	–1.844	173.7	70.0	183.9
Ice Model 4	Use φ from Ice Model 2 and readjust γ to match $\langle D \rangle$ from M^3	+0.339	–1.767	32.66	70.0	144.7

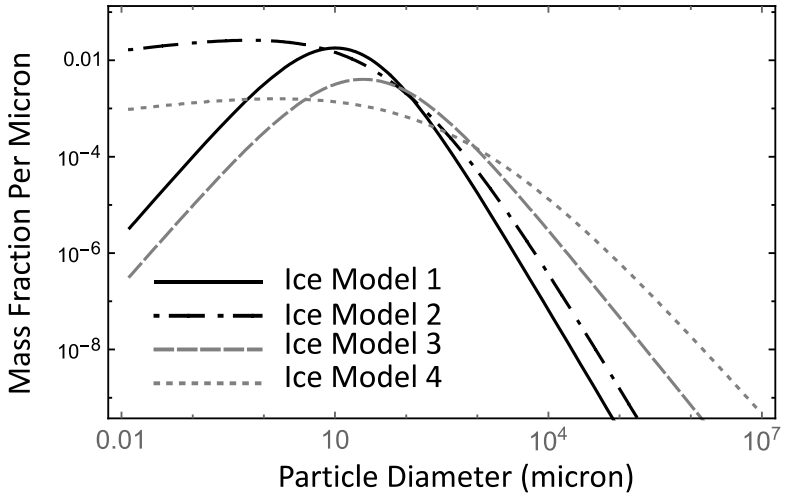

Figure 13. The four models for lunar ice particle size distributions. The lunar soil model for lithic (and glass) fragments is identical to Ice Model 1.

2.3 Grinding

Light grinding will help liberate ice crystals from lithic fragments if they are bound. It will also help liberate other useful resources such as ilmenite, anorthite, and metal grains from lithic fragments. Grinding generates heat, which could cause loss of ice, but an assessment of the

[63] Colaprete, Anthony, M. Shirley, J. Heldmann, and D. Wooden. "The Final Minute: Results from the LCROSS Solar Viewing NIR Spectrometer." *LPI* 1608 (2011): 2037.
[64] Li, Shuai, and Ralph E. Milliken. "Water on the surface of the Moon as seen by the Moon Mineralogy Mapper: Distribution, abundance, and origins." *Science Advances* 3, no. 9 (2017): e1701471; Supplementary Material.
[65] Heiken et al. (1991), Figure 9.1.
[66] Park, Jaesung, Yang Liu, Kenneth D. Kihm, and Lawrence A. Taylor. "Characterization of lunar dust for toxicological studies. I: Particle size distribution." *Journal of Aerospace Engineering* 21, no. 4 (2008): 266-271.

energetics indicates there is a large safety margin. A 1 μm particle will sublime away in about 12 hours at 200 K, and PSR ice deposits are generally below 100 K. An ice-metal interface fractures with 2 J/m^2,[67] so reasonably assuming equal energy is partitioned into heating the ice phase during fracture, using the heat capacity of water ice at 100 K, a 1 μm particle of ice will be raised from 100 K to 103.4 K by breaking it off the lithic particle. This indicates a margin of 30X to account for grinder inefficiency. We assume that, if Bridging, Non-Bridging, and Non-Filling morphologies (Figure 4) existed, then the particle size distributions in the prior section are the outcome of the grinding so no changes to the model distributions occur in this step.

2.4 De-Dusting and Pneumatic Separation

De-dusting is a common first step in terrestrial beneficiation processes for recycling and will be an important first step in lunar gravity due to the poor flowability of the cohesive dust fraction. In order for the downstream separation processes to be efficient, the particles must easily flow and therefore the dust must be removed. Also, lunar dust has high surface area to mass ratio so the superparamagnetic npFe in their glass patina makes their response to magnetic fields more dominant compared to the coarser particles. This can confuse magnetic separation processes. Their large surface areas make them easily adhered to larger particles via the van der waals force. If dust adheres to ice particles then this may cause ice to be misclassified into the magnetic slag. The large shear force of the gas in the entrainment process inside an eductor separates dust from the surfaces of larger particles so the dust can be separated and removed.

De-dusting is ordinarily accomplished in industry via pneumatic separation. Pneumatic separation can be used more generally to separate the material into any arbitrary number of particle size ranges, and this is leveraged in the version of Aqua Factorem shown in Figure 5. That figure shows pneumatic de-dusting as a separate process before the magnetic separation, then separation of the motive gas before magnetic separation, then entrainment in a pneumatic separator a second time to do the pneumatic size sorting. After development we may learn that it is better to sort the material stream into all the size ranges on one step before the magnetic separation instead of the way shown here. The benefit would be that the gas separation need be done only once. There is little benefit in that, however, because gas separation for the non-dusty streams is trivial using a cyclone and requires little hardware mass. The entire beneficiation process (or at least the magnetic part) can be enclosed in the same pressure vessel as the pneumatic processes so there is no need for extensive gas recovery each substep in the process. Instead, the full gas recovery prior to opening the system to vacuum can be done only once at the very end. The possible benefit of doing the pneumatic sorting in two stages before and after magnetic separation, as we have shown here, is that magnetic separation is extremely efficient (as we describe below) and there is no need to do size sorting prior to magnetic separation to make it any more efficient. On the other hand, by doing the magnetic separation first before the pneumatic size sorting the efficiency of the size sorting in the series of cyclones may be more efficient, producing more perfect classification into the desired size ranges in each material stream going into electrostatic separation. It is important for electrostatic separation to have careful control on particle sizes at the inlet. Therefore, it is likely worth having the extra mass of the duplicate gas separation cyclones. More development work in the future is needed to be sure.

[67] Wei, Yingchang, Robert M. Adamson, and John P. Dempsey. "Fracture energy of ice/metal interfaces." In *Adhesives Engineering*, vol. 1999, pp. 126-135. International Society for Optics and Photonics, 1993.

De-dusting and general pneumatic size classification work by entraining the material into an internal gas flow (i.e., gas flow enclosed in a pipe) via an eductor, which is a Venturi that pulls the particles into the gas flow at its throat. Size separation works by passing the particle-laden through a cyclone that spins out the larger particles inertially while the dust-sized ones follow the gas flow out an exit on the top due to their tiny ballistic coefficient. The dust-laden gas then flows through in-line magnetic and electrostatic separators described below. Those processes produce three dusty streams, one that is highly magnetic dust, another that is poorly- or non-magnetic dust with no ice, and the third that is "ice dust" (very small ice fragments).

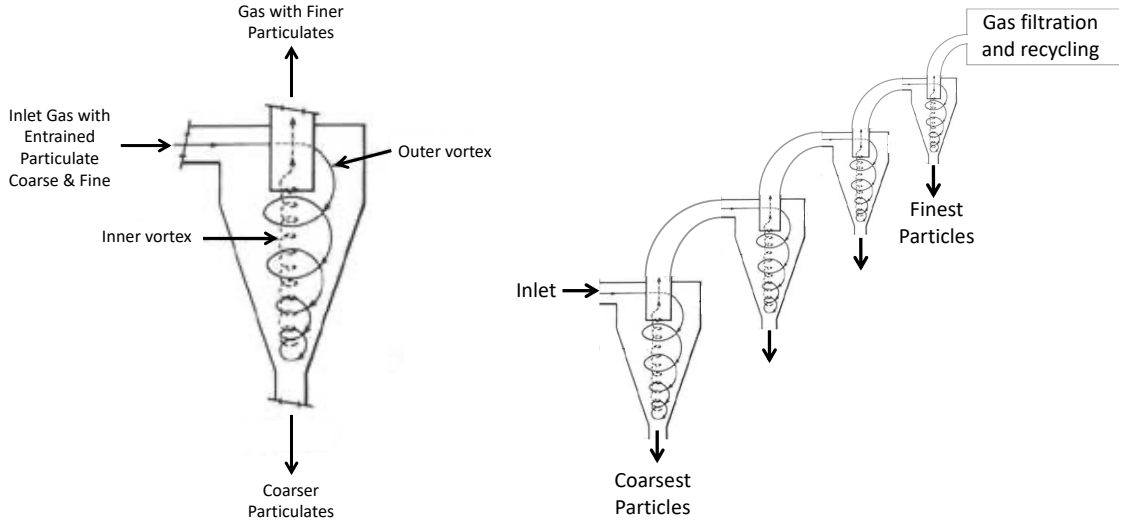

Figure 14. Left: Function of a cyclone for gas separation. Right: Sequential cyclones for size classification. (Adapted from drawing by OSHA/US Dept. of Labor.[68])

Coarse particles are easily separated from the motive gas because they fall via gravity out the bottom of the cyclone into a hopper while the dynamics inside the cylone move the high velocity gas out the top. This assumes the process takes place inside a pressurized container so a pressure difference does not pull the gas out the bottom, too. Fine particles are more difficult to separate from their gas flow, but a wide variety of mature technologies exist for this purpose. The simplest is passing the flow through a material filter (a HEPA filter). NASA has been funding development of regenerable filters so they do not become a consumable, or so their consumption rate can at least be reduced. Other methods use water in a turbulent gas/water flow field to capture dust, which settles in a static water bin then is removed as sludge. In a mining process that produces water, a portion of the mined water could be used for this purpose and the sludge could be at least partially dried by exposure to successively lower pressure by pumping down its chamber (recapturing the evaporated water). If enough water is produced by the mine, simply losing some of the water may be the most economic approach. The benefit of losing a small fraction of the water is that it will clean the beneficiation stream that creates a much larger

[68] Anonymous, "Collecting and Disposting of Dust," chapter 4 in: *Dust Control Handbook* (online), OSHA, https://web.archive.org/web/20050209065324/https://www.osha.gov/SLTC/silicacrystalline/dust/chapter_4.html

quantity of water without extra complexity of machinery to maintain. The ice dust in the third stream could be easily captured by the water filtration method with no water loss.

In more general size sorting, a series of cyclones of decreasing diameter will separate the particulates into successively finer fractions. The exit from the top of one cyclone feeds into the circumferential flow of the next one. The particle sizes for the splits are determined by the diameters of the cyclones for a given flow speed. The output from the top of the last cyclone includes any finer particles that remain entrained in the gas. This is already a mature technology and has been tested by Honeybee Robotics and the NASA Kennedy Space Center using lunar soil simulants.[69-74]

Pneumatic separation uses the same principle as winnowing: separation of particles is determined by the ratio of inertial force and aerodynamic drag force, which is the *ballistic coefficient*. Inertial force scales as density ρ times diameter cubed, ρd^3. Aerodynamic drag force (at typical gas velocities in these systems) scales as particle surface area, or d^2. Thus, the ballistic coefficient scales as ρd. Since the densities are related by $\rho_{\mathrm{Rock}} \approx 3\ \rho_{\mathrm{Ice}}$, pneumatic separation will tend to separate silicate mineral particles of d into the same bin as ice particles of $3d$. Thus, it effects only partial separation of ice from silicates so it is not an adequate process by itself. However, the particles are now contained in bins according to limited size ranges. This is important because tuning of the subsequent separation methods depends on particle size, and if the particles have too broad a range of sizes then the methods would be inefficient, producing too many middlings (particles that are neither kept nor discarded) that would need to be recycled through the system again.

The dust fraction that should be removed to improve soil flow is about 20 μm and finer, which constitutes roughly 29.7 wt% of the mass of the lithic material. This will split the ice at roughly 60 μm, so if ice constitutes only 5 wt% of the bulk soil, then per each of the models the fraction of the resource in each stream, and the fraction of mass in each stream that is the ice resource, are shown in Table 4.

[69] Zacny, Kris, Greg Mungas, Chris Mungas, David Fisher, and Magnus Hedlund. "Pneumatic excavator and regolith transport system for lunar ISRU and construction." In *AIAA SPACE 2008 conference & exposition*, p. 7824. 2008.
[70] Mueller, Robert P., Ivan I. Townsend, III, and James G. Mantovani. "Pneumatic regolith transfer systems for in situ resource utilization." In *Earth and Space 2010: Engineering, Science, Construction, and Operations in Challenging Environments*, pp. 1353-1363. 2010.
[71] Zacny, Kris, Jack Craft, Megnus Hedlund, Phil Chu, Greg Galloway, and Robert Mueller. "Investigating the efficiency of pneumatic transfer of JSC-1a lunar regolith simulant in vacuum and lunar gravity during parabolic flights." In: *AIAA SPACE 2010 Conference & Exposition*, p. 8702. 2010.
[72] Craft, Jack, Kris Zacny, Phil Chu, Jack Wilson, Chris Santoro, Lee Carlson, Mike Maksymuk, Ivan Townsend, Robert Mueller, and James Mantovani. "Field Testing of a Pneumatic Regolith Feed System During a 2010 ISRU Field Campaign on Mauna Kea, Hawaii." In: *AIAA SPACE 2010 Conference & Exposition*, p. 8900. 2010.
[73] Mueller, Robert, Ivan Townsend, James Mantonvanni, and Philip Metzger. "Evolution of Regolith Feed Systems for Lunar ISRU O2 Production Plants." In *48th AIAA Aerospace Sciences Meeting Including the New Horizons Forum and Aerospace Exposition*, p. 1547. 2010.
[74] Zacny, Kris, Bruce Betts, Magnus Hedlund, Paul Long, Marc Gramlich, Keith Tura, Phil Chu, Abigail Jacob, and Abel Garcia. "PlanetVac: Pneumatic regolith sampling system." In: *2014 IEEE Aerospace Conference*, pp. 1-8. IEEE, 2014.

Table 4. Results of model calculations for de-dusting.

Ice Model	Fraction of the Total Ice in the Dust Stream (wt%)	Fraction of the Mass in the Dust Stream That Is Ice (wt%)
1	64.5	10.4
2	54.7	8.9
3	21.2	3.7
4	9.4	1.7

For modeling, we split the lithic basalt dust at 20 μm. Other minerals in the simulant will split at different particle sizes due to their differing specific gravity. The resulting splits for each component of the two simulants are shown in Table 5. For specificity we assumed specific values of each mineral density from the midpoints of their ranges. For simplicity, we approximate the splits as sharp, perfect breaks at the stated sizes. The resulting chemical composition of each mass stream are also given in Table 5. The fraction of ice in each stream, along with the mass flow rate in each stream needed to meet architectural requirements of the MVP system, are given in Table 6.

Table 5. Individual mineral behaviors in model calculations for de-dusting.

Component	**Density (g/cm^3)**	**Split Size (μm)**	**Dust LMS-1 (wt%)**	**Non-Dust LMS-1 (wt%)**	**Dust LHS-1 (wt%)**	**Non-Dust LHS-1 (wt%)**
Using Ice Model 1						
Pyroxene	3.35	17.3	26.54	33.10	0.14	0.21
Glass-rich basalt	2.90	20.0	30.13	30.51	21.28	24.51
Anorthosite	2.72	21.3	19.87	18.37	68.31	71.81
Olivine	2.90	20.0	10.45	10.58	0.26	0.30
Ilmenite	4.745	12.2	2.29	4.84	0.20	0.47
Ice per Model 1	1.00	58.0	10.71	2.60	9.80	2.70
Using Ice Model 2						
Pyroxene	3.35	17.3	27.0	32.9	0.2	0.2
Glass-rich basalt	2.90	20.0	30.6	30.3	21.6	24.3
Anorthosite	2.72	21.3	20.2	18.2	69.3	71.3
Olivine	2.90	20.0	10.6	10.5	0.3	0.3
Ilmenite	4.745	12.2	2.3	4.8	0.2	0.5
Ice per Model 2	1.00	58.0	9.2	3.3	8.5	3.4
Using Ice Model 3						
Pyroxene	3.35	17.3	28.6	32.1	0.2	0.2
Glass-rich basalt	2.90	20.0	32.5	29.6	22.8	23.8
Anorthosite	2.72	21.3	21.4	17.8	73.2	69.6
Olivine	2.90	20.0	11.3	10.3	0.3	0.3
Ilmenite	4.745	12.2	2.5	4.7	0.2	0.5
Ice per Model 3	1.00	58.0	3.7	5.5	3.4	5.7
Using Ice Model 4						

Pyroxene	3.35	17.3	29.2	31.9	0.2	0.2
Glass-rich basalt	2.90	20.0	33.2	29.4	23.2	23.6
Anorthosite	2.72	21.3	21.9	17.7	74.6	69.0
Olivine	2.90	20.0	11.5	10.2	0.3	0.3
Ilmenite	4.745	12.2	2.5	4.7	0.2	0.5
Ice per Model 4	1.00	58.0	1.7	6.2	1.5	6.5

Table 6. Material stream results from model calculations for de-dusting.

Soil Type	Ice Model	wt% of the Total Ice in that is in the Dust Stream	wt% of Dust Stream that is Ice	wt% of Non-Dust Stream that is Ice	Mass Flow Rate of Dust Stream (g/s)	Mass Flow Rate of Non-Dust Stream (g/s)
LMS-1	1	29.6	10.7	2.6	7.24	17.21
	2	29.1	9.2	3.3	7.12	17.32
	3	27.5	3.7	5.5	6.71	17.73
	4	26.9	1.7	6.2	6.58	17.87
LHS-1	1	32.4	9.8	2.7	7.91	16.53
	2	31.9	8.5	3.4	7.79	16.65
	3	30.2	2.4	5.7	7.39	17.06
	4	26.9	1.5	6.5	7.25	17.20

Finding 1: The quantity of ice in the dust stream is so high that a much simpler system could process only the dust stream, leaving the granulars as tailings. This "pneumatics-only" version would be highly appropriate to manifest on a CLPS mission to test the technology.

Finding 2: Generally, ~70% of the resource will be in the granular (non-dust) stream, so the full version should include granular processing, not just dust processing.

2.5 In-line Magnetic Separation

The dust stream output of the De-Dusting stage contains ice that should be recovered. The first step is to remove the magnetic fraction of the dust. Most lithic/glass dust particles are highly magnetic regardless of their chemical composition due to the npFe that builds up in their surfaces through space weathering. A coil of the pneumatic flow in a strong magnetic field can pull magnetic particles to one side of the coil (say, the inner radius). The pipe can be split so a high fraction of the magnetic particles follow path A. The non-magnetic particles will have no preference, so about 50% will follow path A and 50% path B. (This assumes a low concentration of dust in the flow so that particles do not collide often and thus the magnetic concentration does not push the non-magnetic particles out of the magnetic path.) By repeating the process through 10 splits the non-magnetic fraction remaining with the magnetic isolate would be $(0.5)^{10} = 0.1\%$. These 10 splits can fit compactly in a small volume.

For the sake of feasibility modeling, we use typical magnetic susceptibilities from Table 1. We assume the system splits the dust to isolate everything with a magnetic susceptibility greater than that of basalt, and we crudely assume npFe makes 90% of the less magnetic dust as susceptible as basalt for a mature soil, 55% for a submature soil, and 20% for an immature soil. With these assumptions, the dust stream is split as follows. For the sake of brevity, Table 7 shows only the case for Ice Model 1.

Table 7. Results for model calculation of inline pneumatic magnetic separation.

Component	Magnetic Split of Dust Stream for LMS-1 (wt%)	Non-Magnetic Split of Dust Stream for LMS-1 (wt%)	Magnetic Split of Dust Stream for LHS-1 (wt%)	Non-Magnetic Split of Dust Stream for LHS-1 (wt%)
Using Ice Model 1 & Mature Dust				
Pyroxene	30.8	0	0.18	0
Glass-rich basalt	34.9	0	25.5	0
Anorthosite	20.7	14.5	73.8	41.0
Olivine	10.9	7.6	0.28	0.16
Ilmenite	2.7	0	0.23	0
Ice per Model 1	0	77.9	0	58.8
Using Ice Model 1 & Submature Dust				
Pyroxene	35.1	0	0.25	0
Glass-rich basalt	39.8	0	35.9	0
Anorthosite	14.4	36.7	63.3	75.6
Olivine	7.6	19.3	0.24	0.29
Ilmenite	3.0	0	0.33	0
Ice per Model 2	0	44.0	0	24.1
Using Ice Model 1 & Immature Dust				
Pyroxene	40.8	0	0.42	0
Glass-rich basalt	46.3	0	60.2	0
Anorthosite	6.1	45.4	38.7	84.5
Olivine	3.2	23.9	0.15	0.32
Ilmenite	3.5	0	0.55	0
Ice per Model 3	0	30.6	0	15.2

Finding 3: For mature mare soils, the ice in the non-magnetic dust stream will be about 78 wt% pure so it may be possible to do no further processing.

Finding 4: For immature highlands soils, after removing the water from the non-magnetic dust stream, the anorthosite is predicted to be 99.6% pure, making this a valuable byproduct for aluminum extraction.

We note that in the course of doing this research we identified a risk. If ice in lunar PSRs behaves like a mineral, then what is to stop glassy patina with npFe from forming on the ice? If that were the case, then ice dust may be magnetic just as lithic dust is magnetic, so magnetic separation would not be appropriate for the ice dust. In that case, there are be options. There are other separation techniques that are appropriate for fine, cohesive dust, and we have innovated another idea, but that should be the focus of Phase II or another effort. This risk is therefore only a modest issue, but it highlights the need for ground truth of the ice.

2.6 In-line Electrostatic Separation

The non-magnetic material streams contain ice, olivine, and anorthosite. Electrostatic separation is intended to remove the olivine and anorthosite. Electrostatic separation is common in terrestrial industry. Particulates are charged by (1) tribocharging, (2) induction, or (3) ion spray. In pneumatic conveyors developed by NASA at the KSC Swamp Works, the regolith would tribocharge naturally inside the tubes by random collisions with the walls, and personnel standing too close the exterior of the pipes would experience strong static shocks. Experimentation is needed to try intentional tribocharging by running the flow around corners, or inclusion of ion spray inside the flow. For an analogous case, the Fine Particle Analyzer at the KSC Swamp Works used gas to entrain the particles and flow them past a microscope; Metzger modified it by adding a polonium source adjacent to the flow pipe (using a design from the NASA Glenn Research Center) because the polonium decay products ionized the gas in the flow which in turn neutralized the electrostatic charge on the particulates. Even the fast flow past a short segment with polonium decay was adequate to change the flow behaviors of the particulates. By analogy, adding one or more ion sprays inside the flow will easily charge the particles. The pneumatic conveyance pipes can coil between capacitor plates and can use multiple splits (as with the inline magnetic separator) to obtain arbitrarily high separation.

NASA has previously developed electrostatic beneficiation and showed it to be effective at concentrating ilmenite (for oxygen production) from among the other silicate minerals including plagioclase and pyroxene.[75-80] The method worked by running mixed-mineralogy lunar regolith through a baffle to rub the soil grains across selected materials, causing the various minerals to electrically tribocharge based on their surface chemistry. Examples of successful electrostatic separation of minerals include: fine ilmenite particulate beneficiated from fine quartz quartz

[75] Inculet, I. I., and D. R. Criswell. "Electrostatic beneficiation of ores on the moon surface." In: *Electrostatics 1979; 5th Conference on Electrostatic Phenomena,* Oxford, England, April 17-20, 1979, Invited and Contributed Papers (A80-23261 08-70). Bristol, England, Institute of Physics, 1979, p. 45-52.
[76] Inculet, I. I., "Electrostatic Separation of Lunar Soil," *4th Conference on Space Manufacturing*, Princeton, Univ., 14-17 May 1979.
[77] Captain, James, Steve Trigwell, Ellen Arens, Alex Biris, Janine Captain, Jacqueline Quinn, and Carlos Calle. "Tribocharging lunar simulant in vacuum for electrostatic beneficiation." In *AIP Conference Proceedings*, vol. 880, no. 1, pp. 951-956. AIP, 2007.
[78] Trigwell, Steve, James G. Captain, Ellen E. Arens, Jacqueline W. Quinn, and Carlos I. Calle. "The use of tribocharging in the electrostatic beneficiation of lunar simulant." *IEEE Transactions on Industry Applications* 45, no. 3 (2009): 1060-1067.
[79] Trigwell, Steve, James Captain, Kyle Weis, and Jacqueline Quinn. "Electrostatic Beneficiation of Lunar Regolith: Applications in In Situ Resource Utilization." *Journal of Aerospace Engineering* 26, no. 1 (2012): 30-36.
[80]

particulate,[81] muscovite mica separated from feldspathic pegmatites,[82] rutile, ilmenite and zircon separated from heavy mineral sands,[83]

We hypothesized that this process may also be developed for separating ice from the regolith, because ice is known to tribocharge in cumulonimbus cloud updrafts and in volcanic plumes, concentrating electrical charge to cause lighting.[84],[85] Some limited research has been done on tribocharging of snow (ice crystals) as it strikes various materials.[86] The properties of ice and silicate grains should be so different that electrostatic separation will be highly efficient. However, this needs to be measured in the laboratory. We found no papers in the literature investigating the use of electrostatics to separate ice grains from mineral grains. Therefore, this is a low-TRL concept perfect for a NIAC project.

Agosto[87] found that a constant mass of olivine (a common lunar mineral) tribocharged against aluminum with the power law $C \sim \alpha_1 d^{-1.16}$, where C is the developed electrostatic charge, d is average particle size of the sample, and the coefficient is $\alpha_1 \sim -10^{-11}$ for a 1 mm particle (in standard metric units). Since the number of particles N in each sample scales as d^{-3}, the charge per particle scales as $C/N \sim \alpha_1 d^{+1.84}$. Similarly Anorthite's charging scales as $\sim \alpha_2 d^{+1.79}$ with $\alpha_{12} \approx +10^{-11}$and Ilmenite as $\sim \alpha_3 d^{+1.29}$ with $\alpha_3 \approx +10^{-13}$. The value of α for ice charging against aluminum is about $+5 \times 10^{-9}$ for ice grains other than dendritic or needle-shaped crystals.[88]

Triboelectric series have been developed for some lists of minerals but the lists are far from complete. Ferguson (2009)[89] reported a list that includes Pyroxene, Ilmenite, and Feldspar with 21 others. Ferguson repeats a list by Fraas (1961)[90] that includes 28 minerals. The two lists use different measurement scales and they overlap only in Quartz and Ilmenite, but linear interpolation of the two scales enables merging the lists. Together, this provides the triboelectric

[81] Yang, Xing, Haifeng Wang, Zhen Peng, Juan Hao, Guangwen Zhang, Weining Xie, and Yaqun He. "Triboelectric properties of ilmenite and quartz minerals and investigation of triboelectric separation of ilmenite ore." *International Journal of Mining Science and Technology* 28, no. 2 (2018): 223-230.
[82] Iuga, Alexandru, Ioan Cuglesan, Adrian Samuila, Marius Blajan, Dumitru Vadan, and Lucian Dascalescu. "Electrostatic separation of muscovite mica from feldspathic pegmatites." *IEEE Transactions on Industry Applications* 40, no. 2 (2004): 422-429.
[83] Kun, Xiong, Wen Shu-Ming, and Zheng Hai-Lei. "Research on Mineral Processing Status of Ilmenite Resources." *Metal Mine* 39, no. 4 (2010): 93.
[84] Akinyemi, M. L., A. O. Boyo, M. E. Emetere, M. R. Usikalu, and F. O. Olawole. "Lightning a fundamental of atmospheric electricity." *IERI Procedia* 9 (2014): 47-52.
[85] Méndez Harper, J., L. M. Courtland, and J. Dufek. "The Effects of Ice on the Frictional Electrification of Plumes." In *AGU Fall Meeting Abstracts*. 2015.
[86] Dunham, Stuart B. "Electrostatic charging by solid precipitation." *Journal of the Atmospheric Sciences* 23, no. 4 (1966): 412-415.
[87] Agosto, William N. "Lunar beneficiation." In: *Space Resources*, vol. 509, pp. 153-161. 1992.
[88] Dunham, Stuart B. "Electrostatic charging by solid precipitation." *Journal of the Atmospheric Sciences* 23, no. 4 (1966): 412-415.
[89] Ferguson, D.N. "A basic triboelectric series for heavy minerals from inductive electrostatic separation behaviour." The 7th International Heavy Minerals Conference 'What next', The Southern African Institute of Mining and Metallurgy, 2009.
[90] Fraas, Foster. *Electrostatic separation of granular materials.* No. BM-BULL-603. Bureau of Mines, College Park, MD (USA). College Park Metallurgy Research Center, 1961.

series for all the minerals in LMS-1 and LHS-1 except for basalt. Calle et al.[91] provide a short triboelectric series that includes JSC-Mars-1A as slightly more negative on the scale than Quartz. JSC-Mars-1A is a weathered basalt. No better quantitative data on basalt have been located, although many studies report that it charges easily and (for example) produces lightning in volcanic clouds and sparks when Mars wheel rovers rub on basalt. Another approach to quantifying basalt is to linearly mix its components, which are usually plagioclase (a feldspar), pyroxene and olivine as a lesser component. Feldspar and pyroxene are both negative and close to each other on the scale, whereas olivine is extremely positive. Considering this, and the proximity to quartz, basalt is probably close to feldspar and pyroxene on the scale. While this is a crude analysis, it is the best the literature supports at this time. This analysis constructs the triboelectric series in Table 8. Experimental work that is beyond the scope of Phase 1 would be required to quantify this.

Table 8. Estimated triboelectric series for components of the lunar simulants.

Component	Relative Charging
Olivine	Very negative
Ilmenite	About neutral
Pyroxene	Very positive
Anorthosite	Very positive
Basalt	Very positive
Ice	Extremely positive

This triboelectric series indicates that it should be easy to separate the ice from the olivine and anorthosite in the non-magnetic dust stream, and it should be easy to separate the anorthosite from the olivine. The magnetic dust stream contains dust that is coated with glass patina containing npFe, which is what makes much of it so magnetic. The glass patina will interfere with electrostatic separation, so it may not be possible to effectively sort that stream further.

2.7 Granular Magnetic Separation

The De-Dusting process delivers coarse granulars through a motive gas separator (a cyclone) into a hopper to feed into the magnetic separator. The purpose of this stage is to reduce the bulk of material prior to the size classification and electrostatics, to make those processes more efficient. We found granular magnetic processing to be extremely fast and efficient and it reduces the bulk material significantly.

For granular magnetic beneficiation,[92,93] Taylor and co-workers[94] investigated magnetic separation of lunar minerals but concluded it was challenging because paramagnetic

[91] Calle, C. I., J. G. Mantovani, C. R. Buhler, E. E. Groop, M. G. Buehler, and A. W. Nowicki. "Embedded electrostatic sensors for Mars exploration missions." *Journal of Electrostatics* 61, no. 3-4 (2004): 245-257.
[92] Taylor, L. A., and R. R. Oder. "Magnetic Benefication of Highlands Soils: Concentrations of Anorthite and Agglutinates." In *Lunar and Planetary Science Conference*, vol. 21. 1990.
[93] Oder, R. R. "Beneficiation of lunar soils: Case studies in magnetics." *Mining, Metallurgy & Exploration* 9, no. 3 (1992): 119-130.
[94] Taylor, Lawrence A., and Robin R. Oder. "Magnetic beneficiation of highland and hi-Ti mare soils-Rock, mineral, and glassy components." In *Engineering, Construction, and Operations in Space II*, vol. 1, pp. 143-152. 1990.

susceptibility of minerals is dominated by the superparamagnetic response of NpFe contained in the glass coating of the finest particles. Therefore, magnets tend to pull just the fine particles out regardless their composition. However, Aqua Factorem removes the dust fraction prior to magnetic benefiation to reduce the npFe problem. The size split between dust and non-dust can be adjusted to optimize this benefit. Also, the primary goal of Aqua Factorem is not to sort particular lithic minerals, but ice, which has dramatically different magnetic properties. Separation of free lunar metal particles has been done with a magnet and actual lunar soil but has not been developed previously into a high throughput process.[95] It was previously found that after such magnetic removal of the fines, light grinding of the remaining coarse soil and then single-pass electrostatic beneficiation can produce 50-60% concentration Ilmenite,[96] or a multiple-pass system could achieve 90% concentration.[97]

We designed a laboratory experiment using a magnetic separation apparatus with permanent magnets on a roller. The magnets are arranged so north and south poles create maximum stability across the surface of the drum. A clear plastic sleeve moves over the magnets to augment gravity to minimize sticking of dust to the surface. The system is motorized to rotate the plastic sleeve. A funnel assembly with a system of rakes to throttle the flow controls the rate the soil is poured across the drum and falling tangentially. Experiments were performed varying the distance the flow is offset from the magnetics, the rate of flow, and the quantity of ice in the regolith to determine optimum system parameters.

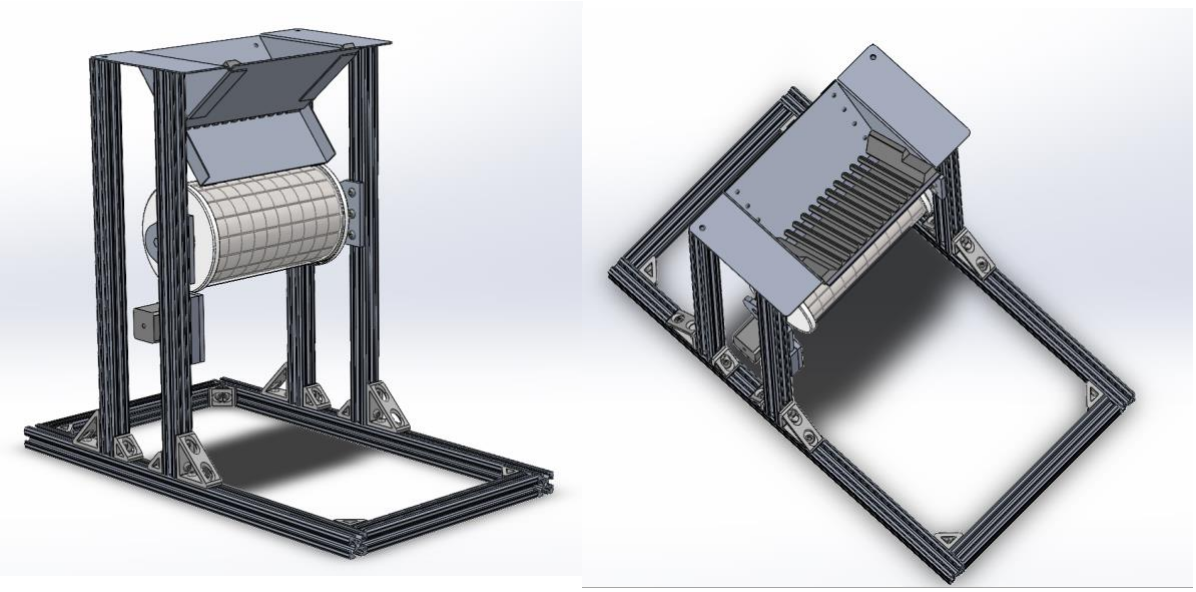

Figure 15. Magnetic Separator Subsystem.

[95] Housley, R. M., R. W. Grant, and M. Abdel-Gawad. "Study of excess Fe metal in the lunar fines by magnetic separation Mössbauer spectroscopy, and microscopic examination." In *Lunar and Planetary Science Conference Proceedings*, vol. 3, p. 1065. 1972.
[96] Mason, Larry W. "Beneficiation and comminution circuit for the production of lunar liquid oxygen (LLOX)." In: *Engineering, Construction, and Operations in Space-III: Space '92*, vol. 1, pp. 1139-1149. 1992.
[97] Agosto, William N. "Electrostatic concentration of lunar soil minerals." In: *Lunar Bases and Space activities of the 21st Century*, p. 453. 1985.

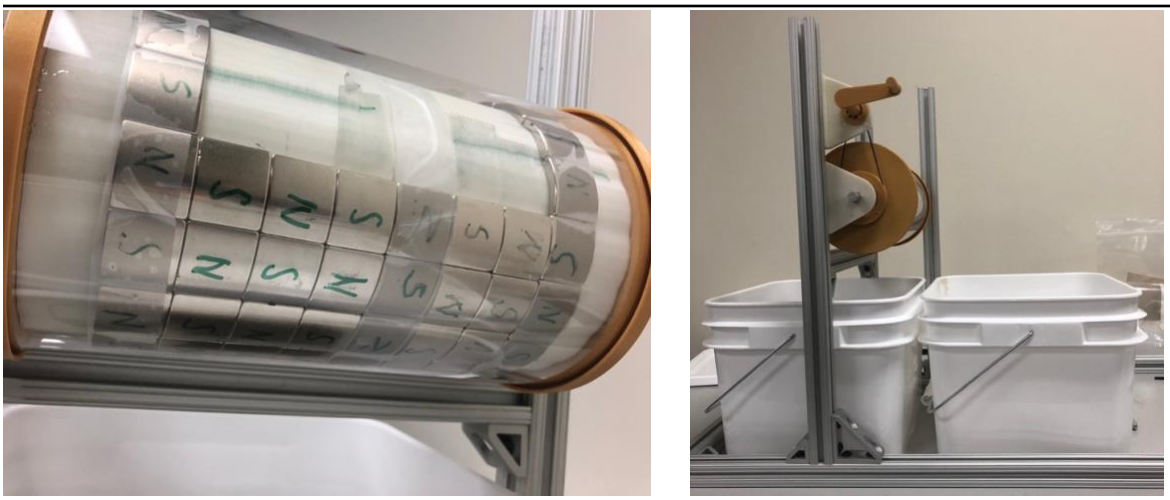

Figure 16. Magnetic Separator Experiment Apparatus.

We found this small-scale system can effectively process magnetic and nonmagnetic isolates at a rate of 11 kg/hr. This can achieve the benchmark rate of 88 kg/hr by scaling it 4 times wider (1 m wide drum) and having only 2 units. For a standalone beneficiation unit with surge capacity to decouple the beneficiation process from the mining cycles, that can be reduced to just one unit. To meet the propellant production rate of the full-scale Kornuta et al. mine, assuming daylight only operation, 5% yield, and surge capacity, we would need to process 3,880 kg/hr, so this would require 88 each 1-m wide drums processing regolith. By then, other technology advances could reasonably increase processing speed a factor of 10 by using more powerful magnetic fields and improved geometry of the regolith falling through the field, so nine units may reasonably be sufficient. For the mine envisioned by Sercel et al. using towers that collect solar energy without downtime, the operation would require fewer units and would have more flexibility where it could operate, enabling access to the highest concentration ice deposits. Thus, by adding units and increasing throughput incrementally as the hardware matures, the risks are bought down, and investor confidence increases, this MVP architecture can scale up smoothly and it can evolve into the larger architectures envisioned by others.

Because the system uses fixed magnets, the only power requirement is to convey the regolith above the magnetic drum and drop it past the magnets, which is miniscule.

The results of our beneficiation test are below. Figure 17 shows the appearance of the simulants before and after magnetic separation, showing evident increase in non-magnetic ice simulant (plastic) in Frame C. Table 9 provides quantitative measurements of these experiments. For the more mafic LMS-1, about 63% of the mass was discarded as tailings after just 1 pass. If soil begins with 5 wt% ice, then discarding 63% of the other 95% produces a mixture in which is now 12.5 wt%, an improvement of 2.5X just by magnetic separation alone. Performing a second pass resulted in 79% of the mass being discarded as tailings, so a resource beginning at 5 wt% will end up 20 wt%, and improvement of 4X. This alone will reduce the amount of mining and the number of mining cycles by a factor of four. We found that a third pass did not produce additional benefit.

For LHS-1, the results are not as dramatic due to the lower magnetic susceptibility of the minerals. One pass magnetic separation would increase ice concentration from 5 wt% to 8.7 wt%, while two passes increases it from 5 wt% to 9.3 wt%. Nevertheless, even with these highlands type soils it will remove about half the silicate minerals as tailings, so the other beneficiation processes need pass only half as much material to produce the desired extraction rate. Even without other processes, magnetic separation alone reduces the mining and hauling requirements by about a factor of two.

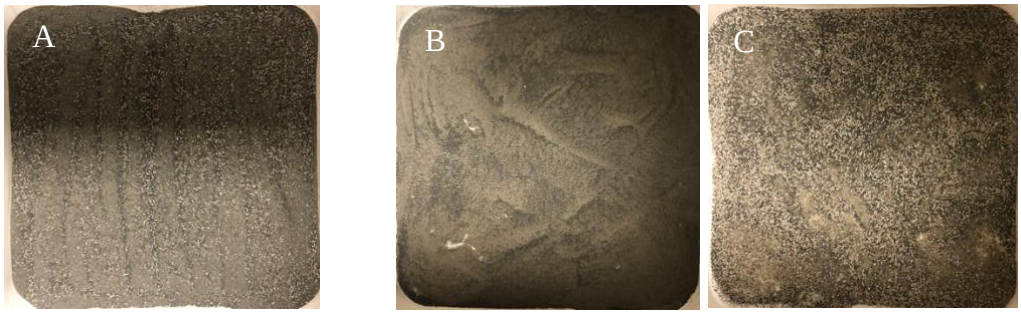

Figure 17. (A) Mixture of Lunar Mare simulant with 5% plastic by weight. (B) After magnetic separation, "rejection" bin consists of mostly regolith. (C) After magnetic separation, "retention" bin contains a high concentration of simulated ice.

Table 9. Experimental magnetic beneficiation of lunar simulants

Size (g)	Magnetic (g)	Non-magnetic (g)	Tailings (wt%)	Mean Tailings ± std error (wt%)
LMS-1, One-Pass Beneficiation				
238.14	152.97	84.11	64.24	63.41 ± 0.25
236.19	149.18	87.01	63.16	
236.10	149.18	85.32	63.19	
234.43	149.29	84.35	63.68	
233.58	146.69	85.99	62.80	
LMS-1, Two-Pass Beneficiation				
570.50	449.57	120.60	78.80	78.97 ± 0.09
570.50	451.23	118.63	79.09	
570.50	451.51	118.21	79.14	
570.50	449.81	119.69	78.84	
LHS-1, One-Pass Beneficiation				
467.03	224.30	242.00	48.03	44.95 ± 0.94
465.38	214.75	250.63	46.15	
465.38	205.84	258.70	44.23	
464.48	201.63	261.97	43.41	
463.57	199.13	263.44	42.96	
LHS-1, Two-Pass Beneficiation				
463.57	218.66	263.44	47.17	48.49 ± 0.55
463.57	219.99	263.08	47.46	
463.57	224.06	262.63	48.33	
463.57	232.14	262.15	50.08	
463.57	229.03	261.92	49.41	

Next, we prepared the mixture 5% plastic with both simulants and passed the mixes through the magnetic beneficiation. We used the above correlation to bulk density to measure the plastic concentration in the non-magnetic isolate. For reliability of the correlation method, we tested it to calculate the concentration ice in the initial 5% mixture and it produced measurements of 4.36 ± 2.18% for LMS-1 and 4.62 ± 2.64% for LHS-1. The reported errors are one sigma. Note that even though plastic is not magnetic a small fraction was found to make it to the magnetic bucket through random systematics of the mechanism. Table 10 shows the measured concentration of plastic in each sample. We can see that one sigma error is quite high, as the name suggests the relative maximum bulk density is not absolute and depends on subjective reproducibility of the compacted volume of the known amount of sample. The systematic error includes the position of the divider that separates the falling flow spread sample into two bins. The predicted concentration of the plastic after the beneficiation agrees with the results listed in Table 2 with systematic rejection of 0 to 2 %. This systematic rejection will be greatly reduced going into the higher TRL designs simply by using a larger magnetic drum diameter.

Table 10. Estimation of plastic concentration after experimental magnetic beneficiation.

Pre-Beneficiation Plastic concentration (wt%)	sample size (g)	Compacted volume (cm^3)	Mean bulk density (g/cm^3)	Measured plastic ± std error (wt %)	Increased concentration
LMS-1 – No Beneficiation					
5	249.53	145.00	1.76	4.36 ± 1.09	N/A
	249.44	140.50			
	249.20	142.00			
	248.85	138.00			
LMS-1 – After Magnetic Beneficiation					
5	61.84	39.00	1.59	15.57 ± 0.04	3.1X
	61.84	39.00			
	61.84	39.00			
	61.74	39.00			
LHS-1 – No Beneficiation					
5	96.81	57.00	1.66	4.62 ± 1.32	N/A
	96.78	59.00			
	96.73	59.00			
	96.70	57.50			
LHS-1 – After Magnetic Beneficiation					
5	45.71	30.00	1.58	12.57 ± 1.96	2.51X
	45.69	28.00			
	45.65	29.00			
	45.60	29.00			

Mineralogical analysis of the beneficiated material was outside of scope for a Phase 1 project so we can only make some inferences. The most magnetic components of these lunar simulants are pyroxene, basalt, and ilmenite. If the beneficiation were pulling out only these three minerals, then the tailings would have been 69.1 wt% for LMS-1 and 25.3 wt% for LHS-1. This is about 10% low for LMS-1 and 23% low for LHS-1. If the magnetic process were also pulling out olivine, then the tailings would have been 80.1 wt% for LMS-1 and 25.6 wt% for LHS-1. This is about right for LMS-1 but still about 23% low for LHS-1. The explanation is the variability of the minerals. Some of the anorthite must be significantly more magnetic than the average, and some of the basalt and ilmenite, perhaps is less magnetic. For the sake of the feasibility modeling we estimate this as follows. The fraction of ilmenite and basalt that were not sufficiently magnetic is X wt%. The fraction of anorthosite that was sufficiently magnetic is Y wt%.

LMS-1: $80.1 - X(32.0 + 4.3) + Y(19.8) = 78.97$ wt%
LHS-1: $25.6 - X(24.7 + 0.4) + Y(74.4) = 48.49$ wt%

Solving simultaneously, X= 24.4% and Y=39.0%. The resulting composition of each granular material stream is given in Table 11.

Table 11. Composition of material streams from model calculations of coarse granular magnetic separation.

Component	LMS-1			LHS-1		
	Before Magn. Separ.	Magnetic Granulars (wt%)	Non-Magnetic Granulars (wt%)	Before Magn. Separ.	Magnetic Granulars (wt%)	Non-Magnetic Granulars (wt%)
Using Ice Model 1						
Pyroxene	33.10	49.4	0	0.21	0.44	0
Glass-rich basalt	30.51	34.4	22.6	24.51	39.3	11.3
Anorthosite	18.37	10.7	33.9	71.81	59.5	82.8
Olivine	10.58	0	32.1	0.30	0	0.56
Ilmenite	4.84	0.05	3.6	0.47	7.5	0.22
Ice per Model 1	2.60	0	7.9	2.70	0	5.1
Using Ice Model 2						
Pyroxene	32.50	49.4	0	0.20	0.45	0
Glass-rich basalt	30.49	34.4	22.0	24.18	39.3	11.1
Anorthosite	18.52	10.7	33.3	71.49	59.4	81.7
Olivine	10.57	0	31.4	0.29	0	0.56
Ilmenite	4.62	5.5	3.5	0.44	0.75	0.22
Ice per Model 2	3.30	0	9.7	3.39	0	6.4
Using Ice Model 3						
Pyroxene	31.65	48.5	0	0.19	0.4	0
Glass-rich basalt	30.52	35.4	21.4	23.75	38.9	10.8
Anorthosite	18.77	11.2	33.0	71.11	60.1	80.6
Olivine	10.59	0	30.5	0.29	0	0.54
Ilmenite	4.24	4.9	3.0	0.40	0.65	0.18
Ice per Model 3	4.23	0	12.2	4.27	0	7.9

Using Ice Model 4						
Pyroxene	31.35	49.4	0	0.19	0.45	0
Glass-rich basalt	30.44	34.4	20.2	23.57	39.3	10.5
Anorthosite	18.79	10.7	30.4	70.83	59.5	77.0
Olivine	10.56	0	28.7	0.29	0	0.52
Ilmenite	4.15	5.5	3.2	0.39	0.75	0.20
Ice per Model 4	4.72	0	17.5	4.74	0	11.8

The increase in concentration of the ice resource for each case is given in Table 12.

Table 12. Increase is ice concentration from magnetic beneficiation in the coarse granular stream.

Ice Model	Increase in Ice Concentration from Before Granular Magnetic Beneficiation to After	
	LMS-1	LHS-1
1	+192%	+89%
2	+194%	+89%
3	+188%	+85%
4	+270%	+149%

The mass throughput rate of the stream containing the ice resource, before and after magnetic separation, is given for each case in Table 13.

Table 13. Mass throughput calculations of magnetic beneficiation in the coarse granular stream.

Ice Model	Mass Flow Rate of the Stream Containing the Ice					
	LMS-1			LHS-1		
	Before Magnetic Separation (g/s)	After Magnetic Separation (g/s)	Flow Rate Reduction	Before Magnetic Separation (g/s)	After Magnetic Separation (g/s)	Flow Rate Reduction
1	17.21	5.68	–67.0%	16.53	8.73	–47.2%
2	17.32	5.80	–66.5%	16.65	8.86	–46.8%
3	17.73	6.20	–65.0%	17.06	9.27	–45.7%
4	17.87	6.34	–64.5%	17.20	9.41	–45.3%

Finding 5: Magnetic Beneficiation of the Non-Dust (Granular) material stream reduces burden on downstream processes by 45 – 67%

2.8 Pneumatic Size Sorting

This stage splits the flow into smaller size ranges so the electrostatic separation in the next stage will be more efficient. Another possibility is that vibrational separation will be used in the next stage instead of electrostatics. Pneumatic sorting followed by vibrational sorting is expected to be highly efficient in isolating the ice as the section 2.10 will show.

For this analysis we split the (granular, non-magnetic) flow into 7 streams. Here we assess whether this many streams are beneficial. There is almost no mass-penalty to having more streams. Cyclones are passive, low mass devices, and if we have more streams then we simply subdivide the electrostatic separator into narrower channels to keep the streams from mixing. The ranges of each stream are chosen for basalt to be 20 – 40, 40 – 80, 80 – 160, 160 – 320, 320 – 640, 640 – 1280, 1280 – 2560, and 2560 – ∞ μm. For each component of the material stream, this puts the splits as listed in Table 14. The numbers listed are the slower size limit of each stream, and the upper size limit is the next column over. For Stream H, the upper size limit was actually determined by the gravel separation stage in the resource intake system. The smallest gravel that was rejected is the largest particle size of Stream H.

Table 14. Particle size splits for 8 material channels in pneumatic size sorting.

Component	Splits (μm) for each stream A-G							
	A	B	C	D	E	F	G	H
Pyroxene	17	35	69	139	277	554	1108	2216
Basalt	20	40	80	160	320	640	1280	2560
Anorthosite	21	43	85	171	341	682	1365	2729
Olivine	20	40	80	160	320	640	1280	2560
Ilmenite	12	24	49	98	196	391	782	1565
Ice	58	116	232	464	928	1856	3712	7424

Finding 6: We can create pneumatic sorting splits such that the smallest size of a water grain in a stream is significantly larger the largest size of a lithic fragments in the same stream, making it easy to do vibrational separation in the next step as an alternative to electrostatic separation.

The composition of each stream is shown in Table 15.

Table 15. Resulting composition in the 8 material flow streams after pneumatic size sorting.

Component	Composition (wt%) for each stream A-G							
	A	B	C	D	E	F	G	H
LMS-1, Using Ice Model 1								
Pyroxene	0	0	0	0	0	0	0	0
Basalt	23.0	23.6	23.8	23.9	23.9	23.9	23.9	23.9
Anorthosite	34.9	34.7	34.2	33.7	33.3	32.9	32.9	32.7
Olivine	32.7	33.5	33.9	34.0	34.0	34.0	34.0	33.9
Ilmenite	3.1	4.1	5.1	6.0	6.7	7.5	7.5	0.8
Ice	6.3	4.1	3.0	2.4	2.1	1.99	1.8	1.7
LMS-1, Using Ice Model 2								
Pyroxene	0	0	0	0	0	0	0	0
Basalt	23.2	23.4	23.4	23.2	23.0	22.8	22.6	22.3
Anorthosite	35.2	34.4	33/5	32.7	32.0	31.4	31.0	30.6
Olivine	33.0	33.3	33.2	33.0	32.7	32.4	32.1	31.7
Ilmenite	3.1	4.1	5.0	5.8	6.4	6.8	7.0	7.2

Ice	5.6	4.9	4.9	5.3	5.9	6.6	7.3	8.2
LMS-1, Using Ice Model 3								
Pyroxene	0	0	0	0	0	0	0	0
Basalt	23.2	23.0	22.5	21.7	20.4	18.7	16.5	11.6
Anorthosite	35.2	33.8	32.3	30.5	28.4	25.8	22.7	15.9
Olivine	33.0	32.7	32.0	30.8	29.0	26.6	23.4	16.5
Ilmenite	3.1	4.0	4.8	5.4	5.7	5.6	5.2	3.7
Ice	5.5	6.5	8.4	11.6	16.4	23.3	32.2	52.3
LMS-1, Using Ice Model 4								
Pyroxene	0	0	0	0	0	0	0	0
Basalt	24.0	23.8	23.1	21.7	19.0	14.9	10.1	3.5
Anorthosite	36.4	35.0	33.2	30.6	26.5	20.6	13.9	0.5
Olivine	34.1	33.8	32.9	30.9	27.0	21.2	14.4	0.5
Ilmenite	3.2	4.1	5.0	5.4	5.3	4.5	3.2	0.1
Ice	2.2	3.3	5.8	11.3	22.1	38.9	58.4	85.8
LHS-1, Using Ice Model 1								
Pyroxene	0	0	0	0	0	0	0	0
Basalt	11.4	11.8	12.4	12.4	12.5	12.6	12.7	12.7
Anorthosite	83.9	84.7	85.0	85.0	85.0	85.0	84.9	84.9
Olivine	0.6	0.6	0.6	0.6	0.6	0.6	0.6	0.6
Ilmenite	0.2	0.2	0.4	0.4	0.4	0.5	0.5	0.5
Ice	4.0	2.7	1.6	1.5	1.3	1.2	1.2	1.2
LHS-1, Using Ice Model 2								
Pyroxene	0	0	0	0	0	0	0	
Basalt	11.4	11.8	12.0	12.1	12.2	12.2	12.2	
Anorthosite	84.3	84.2	83.8	83.3	82.7	82.1	81.4	
Olivine	0.6	5.9	0.6	0.6	0.6	0.6	0.6	
Ilmenite	0.2	2.5	0.3	0.4	0.4	0.4	0.5	
Ice	3.6	3.2	3.3	3.6	4.1	4.6	5.4	
LHS-1, Using Ice Model 3								
Pyroxene	0	0	0	0	0	0	0	0
Basalt	11.4	11.6	11.7	11.6	11.2	10.6	9.7	7.3
Anorthosite	84.3	83.3	81.7	79.5	76.1	71.4	64.9	49.0
Olivine	0.6	0.6	0.6	0.6	0.6	0.5	4.8	0.4
Ilmenite	0.2	0.2	0.3	0.4	0.4	0.4	0.3	0.3
Ice	3.5	4.3	5.7	8.0	11.7	17.1	24.6	43.0
LHS-1, Using Ice Model 4								
Pyroxene	0	0	0	0	0	0	0	0
Basalt	11.7	11.9	11.9	11.6	10.7	8.9	6.6	2.5
Anorthosite	86.1	85.1	83.3	79.6	72.4	60.1	43.9	16.7
Olivine	0.6	0.6	0.6	0.6	0.5	0.4	0.3	0.1
Ilmenite	0.2	0.2	0.3	0.4	0.4	0.3	0.2	0.01
Ice	1.4	2.1	3.9	7.9	16.0	30.2	49.0	80.5

Finding 7: If the model for ice being coarser than lithic soil is correct, then the largest sizes are extremely dominated by ice. A simple excavation and pneumatic separation may be possible. Even though it is a small fraction of the total resource, the simplicity of the mining may make it worthwhile.

The mass flow rates of each stream and the flow rate of ice in each stream are given in Table 16. For brevity we only show Ice Model 1 and 4 for each of the two simulants.

Table 16. Mass flow rate in each fo the 8 material channels after pneumatic size sorting.

Component	Mass Flow Rate for each stream A-G							
	A (g/s)	B (g/s)	C (g/s)	D (g/s)	E (g/s)	F (g/s)	G (g/s)	H (g/s)
LMS-1, Using Ice Model 1								
Overall	1.24	1.13	0.76	0.41	0.19	0.077	.030	0.018
Ice	0.028	0.046	0.023	0.0098	0.0039	0.0015	.00055	0.0003
LMS-1, Using Ice Model 4								
Overall	1.33	1.25	0.87	0.50	0.26	0.14	0.079	0.136
Ice	0.30	0.041	0.051	0.057	0.058	0.054	0.046	0.117
LHS-1, Using Ice Model 1								
Overall	1.94	1.72	1.14	0.61	0.28	0.11	0.044	0.025
Ice	0.078	0.046	0.023	0.0098	0.0039	0.0015	0.00054	0.00031
LHS-1, Using Ice Model 4								
Overall	2.04	1.85	1.26	0.70	0.35	0.17	0.091	0.14
Ice	0.029	0.039	0.049	0.055	0.056	0.052	0.045	0.112

Finding 8: The mass flow rates in these channels are very small and can easily be achieved and scaled up. These are the necessary flow rates to meet system performance, so this indicates overall performance is easily achievable.

2.9 Granular Electrostatic Separation

Experiments are needed to determine if electrostatic separation for the coarse granulars should be in the pneumatic conveyance, just as the fines are, or whether a convential separator should be used. In the recycling and mineral beneficiation industries, a dilute stream of granulars is flowed off a conveyor through a series of charged baffles. Often 5 or more stages is needed to achieve desired concentration. Testing such an apparatus was outside our scope for a phase 1 project, so we focused on a simpler objective: a basic demonstration using a small scale laboratory device An Electrostatic Separator experimental apparatus was designed and fabricated. It uses a variable 20,000 VDC generator to charge the separator plate and a vibrating motor to move icy regolith along a chute to tribocharge the particles according to their individual surface chemistry. The particles are launched between a charged plate and a grounded plate, both 30.48 cm by 30.48 cm, to effect separation. After initial tests the form of the charged plates was changed to short, 30.48 cm across and 7.62 cm down, vertical plates to attempt better separation by preventing the

rebounding of particles within the plates. We can observe the particles are charging and spraying in a wider range of angles with the electric field activated so the basic function is operable. This validated the apparatus to proceed with ice testing.

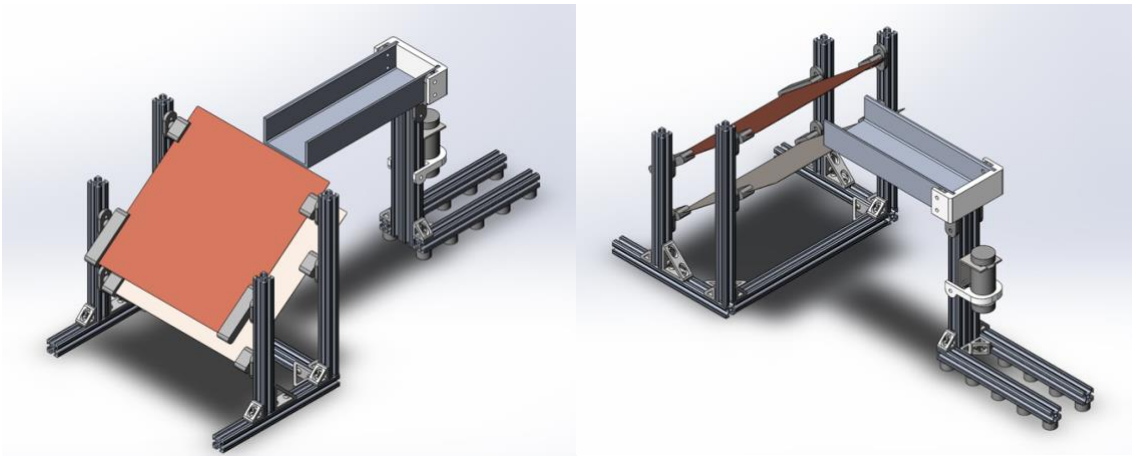

Figure 18. Electrostatic Separator Subsystem.

2.9.1 Electrostatic Experiments with Actual Ice

A method was developed to prepare icy simulants in place of the plastic that had represented ice. Water ice was put through an ice grinder then placed into a mortar and pestle that was in a liquid nitrogen bath while the ice was further ground by hand. This created a fine granular ice that was very dry on its surface even in ambient room conditions. The lunar soil simulant was also chilled in a cup in a liquid nitrogen bath then the two were mixed in the desired ratio. The apparatus was chilled with liquid nitrogen and the icy simulant was place in the inlet. The icy regolith including ice particles was observed to spray through the separator at a higher range of angles when the high voltage as on than when it was off, validating that the mixture was tribocharging. This validated that the ice can be tribocharged just as lithic particles, and that they can be charged in a mixture with lithic particles. Demonstrating enhanced separation is left to future work.

Figure 19. Icy Simulant Preparation.

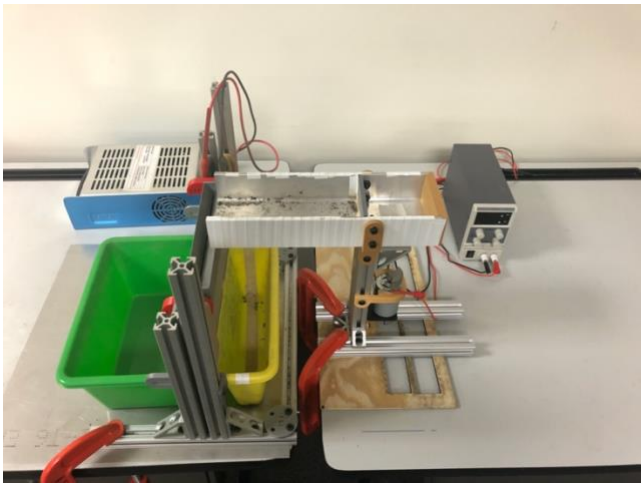

Figure 20. Electrostatic Separation Test Setup with Icy Simulant.

The literature indicates that electrostatic separation is challenging and that it is not possible to predict the achievable concentration. It requires experimental work trying different geometries to perfect the apparatus and to determine the concentration. The triboelectric series shows that ice is a far extreme from the minerals in lunar soil so should be much easier to separate than the other minerals that have been subject of electrostatic separation tests. This is the last step in the process and no problems to success have been identified. To increase confidence in this last step, we also evaluated an alternative in the next section.

2.10 Vibrational Separation

We observed in all our handling of the plastic/lithic mixtures that the plastic component naturally segregates by floating to the top of the mixture. This is a version of the Brazil Nut Effect or an example of buoyancy when granular materials are in a fluid state. The fluid state (unjamming) can be achieved by vibration and is easier in low lunar gravity. In reduced gravity flights where lunar gravity was provided, we observed that lunar soil had much more fluid motion. Significant separation may therefore be possible by shaking or pouring a mixture and then skimming the layer with higher ice concentration off the top.

To quantify this concept, we tested vibrational separation using LMS-1. Many small batches were placed in a square bottomed bin and vibrated with angles between vertically with the container level and at an angle of about 15° from horizontal. The bigger size particles tended to move downward faster and a nominal separation was achieved. The layers were visibly finer or coarser as shown in Figure 21, but multiple strata occurred with we attribute do the depth of the sample containers. The strata were removed and sieved into three size ranges. This confirmed that the isolate that appeared finer was almost entirely finer than 250 μm, while the isolate that appeared coarser contained most of the fraction of the sample coarser than 250 μm. The particle size distribution in each portion is given in Table 17.

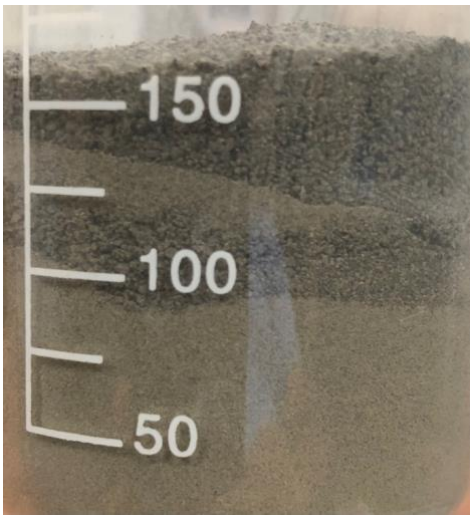

Figure 21. Coarser portion is stacked on top of finer portion after vibrational separation.

Table 17. Particle size distribution in two portions after vibrational separation.

Isolate After Vibration	< 250 μm (wt%)	250-425 μm (wt%)	> 425 μm (wt%)
Visibly Finer	97	2	1
Visibly Coarser	34	31	35

To test whether density separation was also occurring, we repeated the process using LMS-1 that had been pre-sieved to the narrow size range 250 – 425 μm. This did not create the obvious isolates based on particle sizing. The upper and lower halves of the material were fractionated and measured for density. The results are in Table 18. We found the two fractions had very similar bulk densities (1.58 g/ml in the top, 1.55 g/ml in the bottom) and very similar specific gravities, 2.61 vs. 2.77 g/ml. This suggests that vibrational separation segregates primarily by size and is not too sensitive to density.

Table 18. Results from Vibrational Segregation Tests.

Sample Split	Sample Mass (g)	Compacted Volume (cm^3)	Bulk Density (g/cm^3)	Avg. Specific Gravity (g/cm^3)
LMS-1 Pre-Sieved to 250 – 425 μm range				
Top half	54.49	34.50	1.58	2.61
Bottom half	49.51	32.00	1.55	2.77
5 wt% Plastic + LMS-1 Pre-Sieved to 250 – 425 μm range				
Top half	53.16	38.00	1.40	2.29
Bottom half	51.88	39.00	1.33	2.41

Based on these results, dry vibrational separation is plausible as an alternative to electrostatic separation in the final step. The ice fragments in each channel in Table X are significantly larger than the lithic particles in the same channel so they will float to the top during vibration where they can be skimmed into a separate output.

2.11 Summary of Beneficiation Processes

Analysis shows that all the processes in the Aqua Factorem system can easily meet performance requirements for the MVP system. Each element in the system is easily scalable to larger operation. The power requirements are extremely low. Extremely different particle size distributions for the ice were used in the modeling, but the system proved to be not too dependent on that distribution. If the geology of a mining area were known better, the system could be optimized by choosing size splits in the pneumatic system and scaling the flow rate in each channel accordingly. Since this concept clearly meets the requirements, it will be used in the architectural analysis in the next section.

3.0 Architecture Analysis

3.1 Overview

The goal is to mine enough propellant to take a tank of propellant from the Moon and use it to boost a communications satellite from an initial orbit to a final orbit for a fee, enabling the owner of the satellite to begin revenue-making operations much sooner. The mined propellant has to be enough for the entire round-trip journey. Compared to electric thrusters that require 6-12 months to slowly boost a comsat into operational orbit, this fast boost to orbit should save about $100M in lost revenues because the tug can rendezvous with the satellite and move it to its final orbit in just one day. The goal is to design an architecture that will accomplish this for much less than $100M per boost so that all parties may profit. Thus, propellant mining may be rapidly profitable. Then, NASA will become just one of the customers, rather than the only customer that must bear the full cost of maintaining the infrastructure and capability. Creating a method that can be commercially successful without reliance on government funding satisfies NASA's intent to achieve "Sustainable Exploration" because NASA can then purchase propellant at a merely marginal cost of an existing operation, making NASA's funding go much farther and enabling NASA to focus investments on deeper space.

To be more accurate, it is not necessary for this architecture to be profitable from the beginning. Instead, it needs to produce enough optimism to attract commercial investors for subsequent rounds of investment for each stage of development. If the system produces revenue immediately with only modest initial investment, and if it produces results and optimism that promise about a 7-year exit for subsequent rounds of investment, then it can get to the next step. The goal is to do this in a way that enables smooth, incremental scale-up, maturing technologies and operational procedures while buying down risks every step of the way, partially offsetting costs with revenues that are increasing much faster than expenses every step of the way, without reliance on dead-end technologies, until profit and large-scale operations are achieved.

For baseline comparison, the study by Korunata et al.[98] developed an ice mining architecture that would require $4B initial investment to establish operations. The mass of assets would total 30,000 kg. It would sell the propellant for $500/kg on the lunar surface and $3,000/kg in LEO. It would require a 2.8 MW power system. Our architecture is currently estimated at < 2,500 kg mass (8.3% of Kornuta et al.) costing $120M to develop and $83M to land on the Moon, plus $10M to operate on the Moon for a year (half of the Kornuta at al. operating cost, which we think is a deep under-estimate, so our operating cost represents an even greater savings than this comparison suggests). This is achievable with an initial investment of only $213M (5.3% of Kornuta et al.). Like the Kornuta et al. estimate, this is only the lunar surface segment. Our space segment has a baseline Lander & Tug pair totaling 1,322 kg dry mass, so our surface and space segments together are less than 3,822 kg. This architecture will produce 27,900 kg of propellant per year (only 1% of the 2,450,000 kg annually to be produced by Kornuta et al.), but this will be enough to boost one satellite every 4 months. It will require only a 50 kW power system (1.7% of Kornuta et al.). This is enough to produce revenue that significantly offsets costs while buying down the risks leading to optimism for subsequent rounds of funding – which still only need to be modest investment – until the architecture has scaled up to the size of the Kornuta et al. architecture with increasing economics of scale and increasing profit. In other words, it fulfills the purpose of an MVP, making startup feasible, and thus it is a game changer.

The ice mining and propellant manufacturing architecture will consist of four major segments:

1. Mining (Extraction and Beneficiation)
2. Surface Power Systems
3. Water Processing (Chemical Cleanup and Electrolysis)
4. Transportation and Utilization (including storage of manufactured propellant)

We will discuss transportation first, since it determines the requirements for propellant mining and everything else in the architecture.

3.2 Transportation and Utilization of Mined Propellant

3.2.1 Overview of Transportation Architecture

Data on geocentric satellite masses were obtained from the Union of Concerned Scientists (UCS) Satellite Database at https://www.ucsusa.org/resources/satellite-database. Plots of satellite masses are shown in Figure 22 (launch mass) and Figure 23 (dry mass). The data include both satellite using bipropellant boost and electric thrusters undifferentiated, so the dry mass possibly gives a better estimate of the range of masses to move to operational orbit but not of the additional mass of propellant for station keeping.

[98] Kornuta, David, Angel Abbud-Madrid, Jared Atkinson, Jonathan Barr, Gary Barnhard, Dallas Bienhoff, Brad Blair et al. "Commercial lunar propellant architecture: A collaborative study of lunar propellant production." *Reach* 13 (2019): 100026.

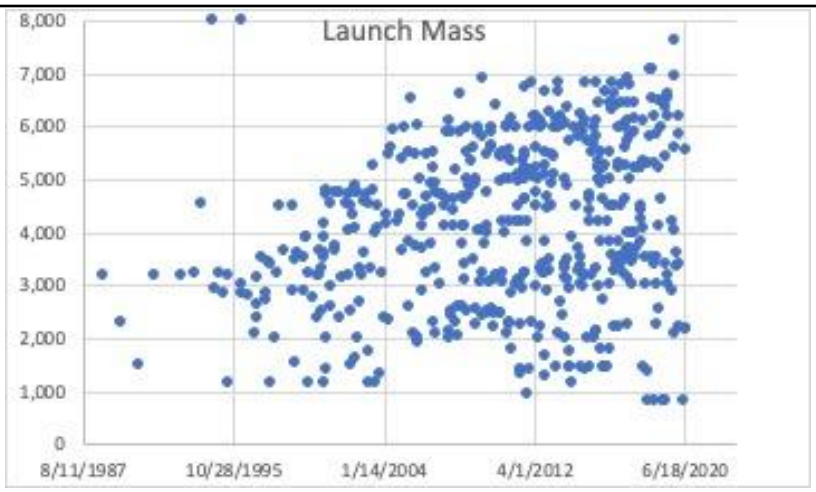

Figure 22. Launch masses of geocentric satellites launched since 1988.

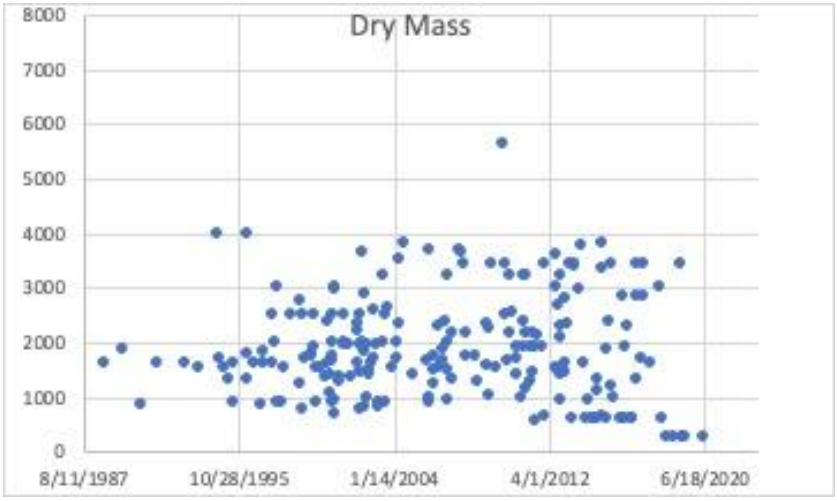

Figure 23. Dry masses of geocentric satellites launched since 1988.

These data demonstrate that a boosting capability for 2,500 kg satellites will enable the architecture to serve most customers as an initial capability. Larger satellites can be boosted by developing a larger tug in the future, or by splitting the boost into two phases. Split boosts may provide additional efficiency advantages so they will be considered in the analysis below. We will use 2,500 kg satelllite mass for the requirement of the initial architecture.

The transportation is based on the following considerations:

1. Refuel Lander and Tug on the lunar surface to remove the dependency on orbital refueling and/or depots. These can be added to the architecture later.
2. The Tug is a combined Tug Tanker in that it takes the propellant to where it can be used but then it immediately uses it to do the job.
3. The Lander just ferries things between the lunar surface and LLO.
4. We provide the lift service in GTO, because that is where the customers are, at least right now, and it appears that the most profit margin will continue to be there for the foreseeable future, as we describe below.

Variants will be considered, such as a case in which the tug is fueled in lunar orbit by taking only the propellant tanks up and down rather than taking the entire lunar tug to the lunar surface each cycle. The basic version of the conops is as follows (refer to Figure 24):

1. Lander with stacked Tug fuels on the lunar surface
2. Lander lifts Tug to Low Lunar Orbit, vehicles unstack
3. Tug Trans-Earth Injection and Ap lowering into the customer GTO
4. Tug grabs the customer GEO bird and lifts it to GEO
5. Tug does a Trans-Lunar Injection from GEO and captures to LLO
6. Tug and Lander rendezvous and stack (Tug grabs the Lander)
7. Lander takes stacked Tug to the lunar surface
8. Repeat

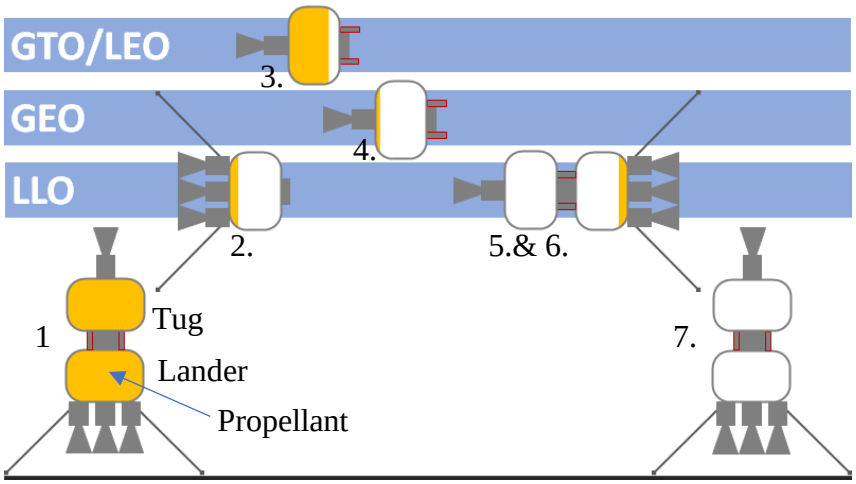

Figure 24. Basic Concept of Operations

We considered variations of the basic architecture that might provide higher efficiencies but at the cost of more complexity and higher capital investment. These could be adopted into the initial architecture or they could be planned for later addition into the architecture after the mining business has proven itself successful, bought-down risks, and proven itself worthy of the additional capital investment. In each of the following, the baseline case is listed as the first sub-bullet:

- Lift the satellite to GEO from different initial orbits:
  - GTO (currently the common practice)
  - LEO (enables the rocket company to launch more payload mass on a single rocket, saving launch costs by shifting boost requirements to the Tug; this is not currently used much since the Tug would need to be launched on the same rocket so there would be no net savings)
  - Split or Distributed Lift (starts in LEO, Tug lifts it to sub-GTO, then a second Tug lifts it to GEO)

- Mass Ratio of Oxidizer to Fuel ratio:
    - Regular 5.6:1 (which provides maximum ISP for the rocket but leaves excess oxygen from the mining process, which could be sold to other customers for another purpose)
    - Stoichiometric 8:1 (which uses the full amount of available oxygen from electrolysis of lunar ice; this provides a higher total delta-v for a given amount of mining despite the lower ISP)

- Aerobraking when dropping into the Earth orbit to rendezvous with the satellite:
    - All propulsive maneuvers (no aerobraking)
    - Use aerobraking in Earth's atmosphere (avoids one propellant burn at the cost of carrying the extra mass of a thermally protective aerobraking shield, so this may or may not require less propellant overall). This is labelled "Aerobraking" or "AB"
    - Slow, multi-pass aerobraking that does not require the mass penalty of extra thermal protection. This is possible only if Zero Boil-Off technology is available to allow for the long travel time. This is labeled "Zero Boil-Off" or "ZBO" on the charts below.

- Ion Propulsion
    - No ion propulsion. Use high-thrust bipropellant engine(s) for all maneuvers.
    - Use ion propulsion when returning from GEO (after boosting a satellite to there) back to LLO. Xe can be provided to the Tug by the satellite for this variation on the boost service. This is a longer return trip to the Moon, so surge storage will be required on the lunar surface so mining can continue while the Tug's propellant tank is away.

- Orbital Tug
    - Tug descends to lunar surface for fueling
    - Tug remains in LLO to act as a Just-In-Time Depot (reduces the mass that must be lowered to the surface then raised again, but the significant mass of a large transfer tank must still be transported up and down, and this requires the additional complexity of orbital cryo-transfer)

The analysis focused first on the baseline scenario and metrics were developed to compare each of the variants: (GTO, LEO, sub-GTO)*(+Stoichiometric)*(+Aerobrake)*(+Ion)*(+Zero Boil-off)*(+Orbital Cryotransfer).

We believe boosting from GTO is very compelling for a business case. As Bennett argued,[99] GEO satellites are currently outfitted with their own electric thrusters to boost themselves from GTO to GEO, so a service can be offered to those satellites at almost no risk, because if the Tug fails to arrive and provide the boost, the satellite can still get to GEO. As comsat companies gain confidence in the Tug service, customer will emerge in LEO to take advantage of the ability to launch larger satellites on a given rocket. Even after that happens, a kg in GTO will be worth 2x

[99] Nicholas J. Bennett, "An Existing Market for Lunar Propellant — GTO Orbit Raising as a Service," Lunar ISRU 2019, Columbia, MD, July 15-17, 2019, abstr. no. 5043.

a kg in LEO, so we will always be able to charge more for a service in a GTO, and it costs us less to provide the service. If we wanted to start today, we would have to start by servicing GTOs, and we would always make higher profits there so that is the baseline CONOP.

This architecture is unusual in that the Tug returns to the Moon each time. One advantage of this is that it can service any inclination. For architectures where the Tug remains in LEO, you need a different Tug in orbit ready to support each launch site: Kennedy, Baikonur, Vostochny, Kourou, etc. The downside is that you must pay the propellant to return to the Moon each time. Having a propellant depot in the Earth-Moon Lagrange Point-1 (EML-1) provides a similar benefit to service multiple inclinations without the cost of descending into the lunar gravity well each time, so that may have greater benefits. Our current architecture is a precursor to that. It will enable an earlier economic water economy that will eventually motivate capital investment in the propellant depot after the risks have been bought-down.

We could model more complex vehicle CONOPs. Tugs could return to their "service start orbits" or to a fueling point after a lift. Propellant could flow from the lunar surface through any of LLO, EML1, or Service Start orbit. We ran a test case to split the function of the Tug into a Tug for boosting and Tanker for long-haul of propellant. The Tug does a lift from GTO-GEO and returns to a GTO to meet the next customer satellite; the Tanker just ferries propellant from LLO to GTO to fill the Tug. The nominal case with the Tug performing both functions took 2,643 kg of propellant. Doing a quick estimate, the Tug performing 1500 m/s lift and a 1500 m/s return to GTO required 1,514 kg propellant. The Tanker was estimated to require a total of 2,702 kg propellant. The net usage is thus +60 kg (+2%) more than the baseline, so it is not beneficial per our quick estimate. Assessing all the many other options is a lot of combinatorics, so this work will be reserved for Phase II or subsequent.

3.2.2 Vehicle Model Methodology

In the basic concept, the transport vehicle has two stages: the Lander and Tug that are autonomously stacking in orbit. Our analysis determined mass estimating relationships for engines, thrust structures, tanks, and insulation. We assumed typical fixed masses for vehicle-generic subsystems including avionics, power, and RCS. We obtained the estimate of a domain experts for the Tug docking hardware and ion propulsion subsystems. We used an aerobrake mass estimator derived from a 1985 crewed GEO servicing vehicle. Landing gear mass was estimated from Apollo and academic studies. Thrust requirements were obtained by scaling from Apollo. The stoichiometric specific impulse (ISP) penalty was modelled using publicly available Rocket Propulsion Analysis software.

3.2.3 Astrodynamics Model Methodology

The delta-v budget was derived from: (1) Simulated trajectories in NASA GMAT; (2) GEO operator domain expertise with 1,500 m/s lift “rule of thumb”; (3) zeroing-out the apoapsis lowering cost for the aerobraking case; (4) vis-viva modifications to the above to account for a distributed/split lift (5) Some margin allocated for lift-off, landing, and proximity maneuvers. We did not perform low thrust modelling for the ion propulsion return from GEO CONOP. We did not perform boil-off tracking and we assumed no zero boil-off mass penalty. We did not

model station keeping for the Orbital Tug remaining in LLO. We accurately modeled the baseline CONOPs, and the others used indicative comparison methods. Our raw deltaV budgets (in m/s) are as follow:

- LS-LLO: 2000 m/s
- LLO-LS: 2100 m/s
- LLO-TEI: 842 m/s
- TEI-GTO: 678 m/s
- GTO-GEO: 1500 m/s
- GTO-LEO: 2500 m/s
- GEO-TLI: 1076 m/s
- LEO-TLI: 3200 m/s
- TLI-LLO: 780 m/s
- 57 LLO-LLO (adjusting orbit to rendezvous)

3.2.4 Baseline Results

The baseline case requires 9,300 kg propellant to perform the conops shown in Figure 24. This uses 5.6:1 OF ratio so 1/3 of the manufactured O_2 will be excess. Electrolysis power dominates the surface plant mass and thus its costs, so there is great incentive to use this excess O_2. It could be sold to other customers if they exist, either on the lunar surface or some location in space, or used for the stoichiometric propulsion as described in the variants. Analysis of the architecture shows this is eminently reasonable so the baseline architecture could operate successfully.

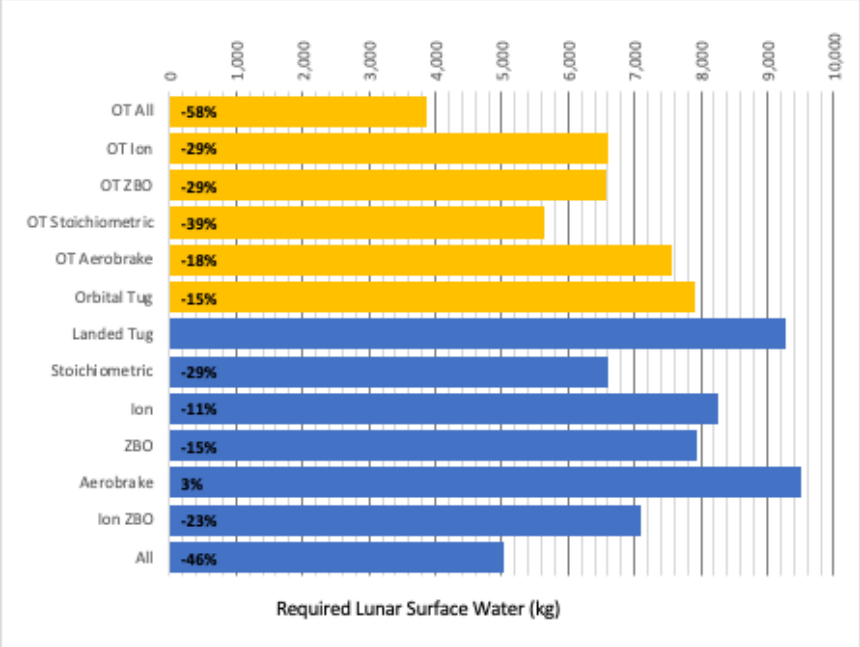

Figure 25. Comparison of Propellant Requirements for GTO-GEO Boosts. Orange: scenarios leaving the Tug in orbit (orbital Tug = OT). “OT all” includes OT stoichiometric and OT Aerobrake. Blue: scenarios landing the Tug on the lunar surface. The baseline scenario is labeled “Landed Tug”. “All” includes stoichiometric, ion, and ZBO (slow aerobraking).

3.2.5 GTO-GEO Variant Results

The variants are summarized in Figure 25 for boosts beginning in GTO.

Adding only aerobraking to the nominal GTO-GEO boost is not beneficial, because the extra propellant used to carry the mass of thermal protection is more than the propellant saved by the aerobraking itself, resulting in a 3% net loss.

Adding only the Orbital Tug capability (cryo-transfer in LLO) results in a 15% reduction of propellant. Adding aerobraking to the Orbital Tug variant produces only 3% additional propellant savings. Therefore, aerobraking is generally not indicated for the GTO-GEO scenarios.

Ion propulsion from GEO-LLO produces (by itself) a modest 11% reduction of propellant. The slow return time to the Moon is therefore probably not worth accepting, at least not for the initial operations, since it will reduce the number of customers that can be served by the Tug during its useful life. However, an 11% savings is significant in the highly competitive telecommunications launch business so this capability would likely be added later after risks have been bought-down and the reliability of all elements of the architecture have been brought up to a sufficiently high level. It should be remembered that the primary cost is energy on the lunar surface, so reducing by even 11% has a large direct impact on capital costs.

"Zero Boil-Off" (ZBO) refers to multi-pass, slow aerobraking such that no extra TPS (mass penalty) is required. This is called ZBO because it is not feasible unless ZBO technology is implemented. This enhancement by itself produces a 15% reduction of propellant demand. Again, this can have a direct impact on capital costs for the mining operation, but at the expense of a more complex and costly Tug. As ZBO technologies develop and improve they can be incorporated into the architecture seamlessly enabling this slow, multi-pass aerobraking for direct savings. We note that a NIAC 2016 project, "Cryogenic Selective Surfaces" (P.I. Robert Youngquist),[100] analyzed the use of special coatings that can passively provide zero boiloff for liquid oxygen even in direct sunlight at Earth's solar distance.

Switching to stoichiometric propulsion produces the single largest improvement in the architecture. It reduces propellant needs by 29%. Another benefit is that it reduces the H_2 more than the O_2, and the H_2 has much lower density requiring larger tanks, and the greater cryocooling requirement, so the dead mass of the spacecraft can be significantly reduced more than proportionally alone. This large benefit will certainly be included in initial operations unless another customer is identified for the extra O_2 at a price equivalent to the savings in comsat boosting. Other customers could include NASA for lunar surface operations or a company like SpaceX that plans to use O_2/CH_4 propulsion, so they could bring their own CH_4 and purchase just the O_2 in space which is most of the mass. However, because of these results we are now planning to include stoichiometric propulsion as the new initial baseline.

[100] https://www.nasa.gov/feature/cryogenic-selective-surfaces-0/

Leaving the Tug in LLO together with using stoichiometric propellant reduces requirements by 39%. Adding aerobraking to these enhancements ("OT All" scenario) can reduce the total propellant needs for GTO-GEO boosts by 46%.

3.2.6 LEO-GEO Variant Results

Boosting comsats from LEO to GEO nominally requires about 57,000 kg of propellant, more than 6X the baseline GTO-GEO case. The benefit of this is that it opens the market for smaller rockets to launch the larger payloads since they only need to throw them into LEO, and it likewise increases the payload capacity of every rocket. It is a larger question whether this will be economically viable as a business in the launch markets or not.

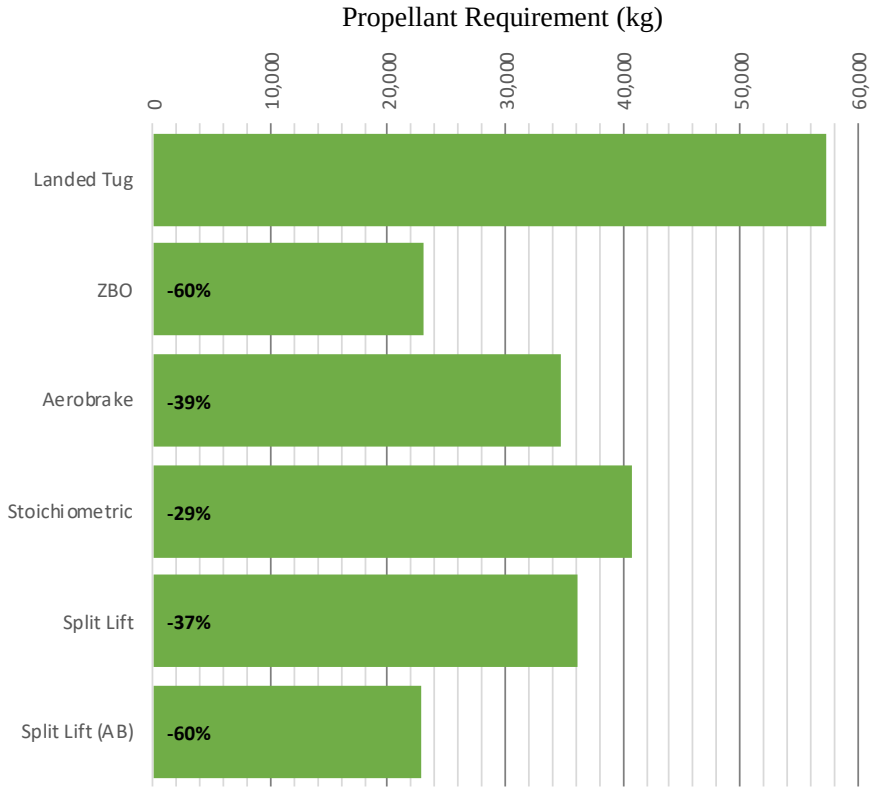

Figure 26. Comparison of Propellant Requirements for LEO-GEO Boosts. The baseline scenario is labeled "Landed Tug."

Variants to the LEO-GEO case are shown in Figure 26. Unlike the GTO-GEO case, adding only aerobraking to the LEO-GEO case is a huge benefit, reducing propellant needs by 39%. Zero Boil-Off, slow, multi-pass aerobraking (i.e., without TPS mass penalty) also has a vastly increased benefit for LEO boosts, reducing propellant needs by 40%. Stoichiometric propellant alone reduces total propellant needs by 29%, the same as for the GTO-GEO scenario. Performing a split boost with aerobraking reduces this by 60%, so two Tugs, each with only slightly more propellant than the baseline case, can boost LEO-GEO. This may be quite viable as a business model for LEO-GEO.

We did not model the LEO cases in high-fidelity because the split lift in spreadsheet methodology requires some "by hand" iteration to converge the two parts to the minimum propellant. A more robust computer program will need to be developed to do all the combinatorics (orbital Tugs, aerobraking fast and slow/ZBO versions, and stoichiometric propellants) with split lifts and more flexible trajectories. GTO is the Phase I focus as the most likely initial business case. We will propose to expand the depth and fidelity of LEO coverage in the Phase II proposal. For now, we expect the LEO Split Lift (AB) with stoichiometric propellant to be about 16,330 kg, and with ion propulsion to be about 14,700 kg. This is about 3X the propellant required just for the GTO-GEO leg because deltaV is 4 km/s vs 1.5 km/s.

3.2.7 Dependence on Vehicle Mass

The resulting vehicle masses needed to execute the various GTO scenarios are shown in Figure 27. The vehicle masses for LEO scenarios are shown in Figure 28 with the GTO cases shown as open circles for reference. There are two versions of the split-lift Tugs and corresponding Landers: in one version the Tug and Lander are optimized to support the LEO-to-subGTO leg, and in the other version the Tug and corresponding Lander are optimized to support the subGTO-to-GTO leg. LEO-subGTO pair are almost identical in mass to the Tug/Lander from the GTO scenarios (open circles). This makes a strong case that there will be a preference for split lifts from LEO because the vehicles will be flexible: the Tug/Lander pair that are optimized for LEO-subGTO can do the GTO-GEO lifts with very little penalty; the Tug/Lander optimized for subGTO-LEO are probably excellent for GTO-GEO with heavier payloads (>2.5 t), and the two pairs together are optimized for LEO split lifts.

We checked the dependence of the calculations upon the "dead"/non-computed vehicle mass. We found that an increase of +1 kg vehicle mass, when we assume optimal O:F ratio, results in vehicle mass changes of:

- Lander: +2.5 kg
- Tug: +8.4 kg

Or, using the stoichiometric O:F ratio of 8:1 with ISP = 433 sec:

- Lander: +1.7 kg
- Tug: +6.0 kg

It may be possible to even-out these sensitivity imbalances by using an elliptical LLO, making the lander do more of the work. Assuming that strategy, $\pm$1 kg dead mass on either vehicle results in O($\pm$5.4 kg) in propellant for both vehicles using optimal O:F, or O($\pm$3.9 kg) in both vehicles using stoichiometric O:F.

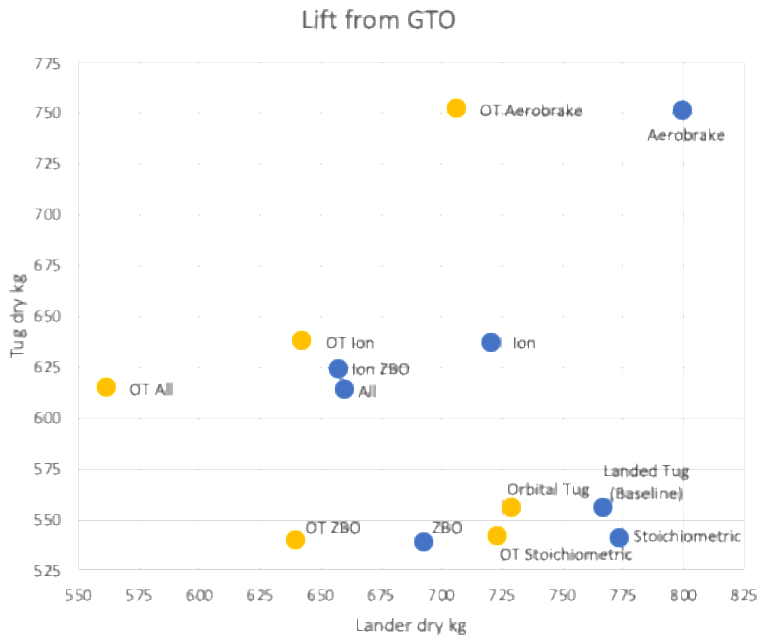

Figure 27. Vehicle Masses for Variant Cases from GTO. Blue: cases where Tug lands on LS. Orange: cases where Tug stays in LLO.

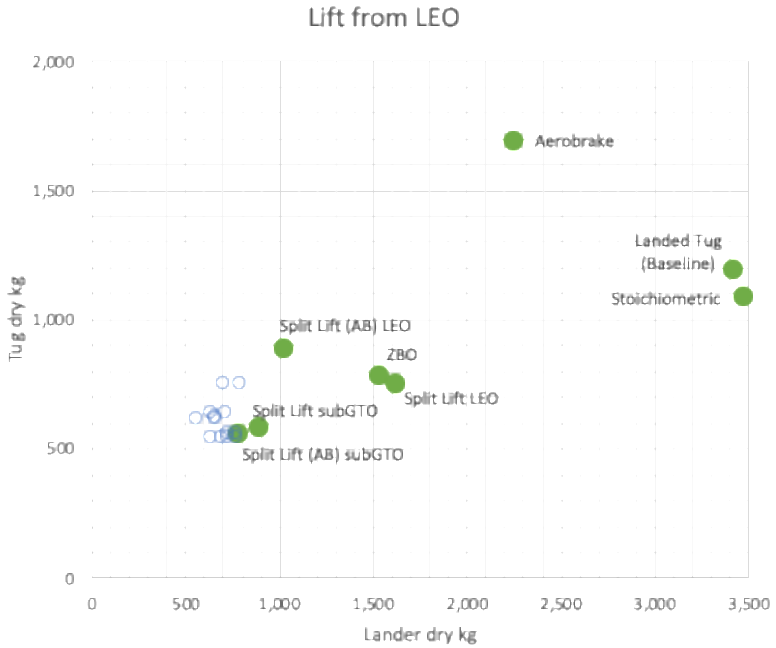

Figure 28. Vehicle Masses for Variant Cases from LEO. Green: cases from LEO. Open circles: cases from GTO for reference. The "split" scenarios (with or without Aerobraking [AB]) have two stacks of Lander+Tug, each optimized for where their lift starts: from LEO or from sub-GTO.

3.2.8 Service Landers to Set Up the Mine

As described in the following sections, we considered two cases for the startup mine. The first is the Minimum Viable Product (MVP) that can produce enough propellant for one satellite boost every 4 months. The total mass of the Surface Segment in that case is <2,500 kg. The second case can support 12 missions per year and its Surface Segment is massed at 8,700 kg. In either case, the Surface Segment must be delivered to the lunar surface (LS). We analyzed the landers from Figs. 21 and 22 for the mass they can deliver to LS. We considered three scenarios of surface asset delivery. Scenario 1 is when the lander brings assets to LS then either ends its life there or awaits refueling from the mine. Scenario 2 is when the lander brings assets to LS but retains enough propellant mass to return to LLO, perhaps to be refueled from Earth to support other operations. Scenario 3 is when the lander begins on LS, ascends to LLO to receive the shipment of cargo, then returns to LS with the cargo. This scenario might occur if the Lander is already supporting a mine then delivers an additional copy of the mining assets to LS to scale-up the operations.

Figure 29 shows the cargo mass that can be landed on the LS for each version of the Lander from Figs. 13 and (does not include dry mass of the Lander). A baseline Lander and Tug mass 1,322 kg, with Aqua Factorem plant of <2,500 kg the total dry mass is 3,822 kg. This means with less than 6 t in LLO we can land and deploy the MVP plant and service vehicles.

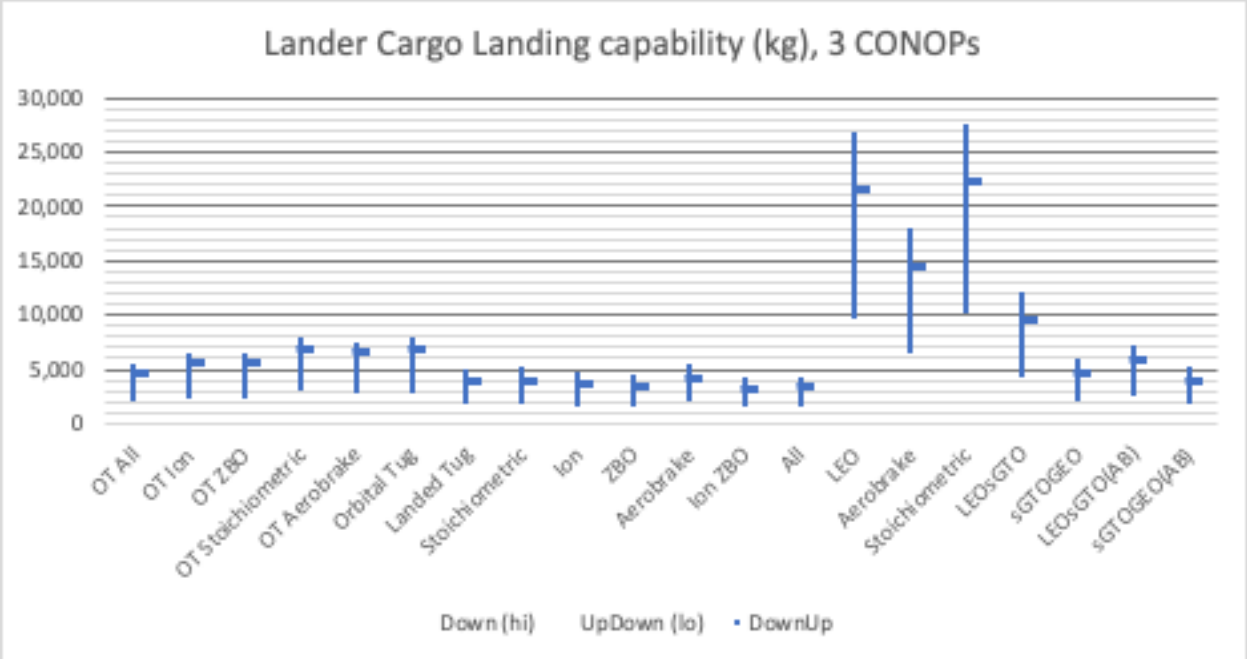

Figure 29. Mass a service Lander can transport to the lunar surface in three scenarios. Top of bar: one-way LLO-LS. Bottom of bar: two-way LS-LLO-LS. Horizontal bar: two-way LLO-LS-LLO.

For the larger version of the mine, rounding its 8,770 kg mass up to 10 t allows contingency growth margin of 15% = 1,300 kg, or alternatively that margin can be allocated to systems to offload and transport some of the equipment to inside the PSR. Going one-way from LLO to LS, the baseline "Service Lander" can land 5 t so two landings will deliver all the surface mass of the

mine. If the Service Lander's mass is 767 kg, it requires 3,542 kg of propellant for 9,309 total mass in LLO. Thus, the entire mine with landers and propellant as-delivered to LLO is just 20 t for the larger startup. Alternatively, if the Blue Moon lander can carry 10 t to LS, then the entire startup mine can be delivered in one landing. For another comparison, the Masten Space Systems / United Launch Alliance Xeus lander was projected to charge $35,000/kg for delivery to the lunar surface with a capacity of 10 t payload.[101]

3.3 Surface Power System

We are estimating 50 We/kg for each "wing" solar PV array based on equivalent systems. The wings we're baselining will provide about 3 kW each, but they can be scaled up or down for different power levels and multiple units can be delivered to the mine. The power systems will be located on a hill that has short lunar nights. The solar array will be on a rotating mast to track the Sun. The power system will be connected by direct cables to the water cleanup and electrolysis system. Progress is being made in superconducting cables and PSRs are cold enough for superconducting, so the water cleanup and electrolysis system could be moved at least partway into the PSR and remain connected. The mining rover will then have shorter driving distances. The power system will regenerate fuel cells or charge batteries that will be hauled in and out of the PSR to power the beneficiating system and the mining rover.

3.4 Water Cleanup and Electrolysis

Lunar water ice may contain the chemicals shown in Table 19[102,103] and the treatment methods are described in Table 20.

Table 19. Potential chemicals in lunar ice.

Vapor-mobilized Volatiles		**Treatment Method(s)**
Nitrogen	N_2	Degasification
Carbon Monoxide	CO	Degasification
Argon	Ar	Degasification
Methane	CH_4	Degasification
Krypton	Kr	Degasification
Argon Clathrate	Ar-$6H_2O$	Activated Catalytic Carbon Filter
Xenon	Xe	Degasification
Hydrogen Sulfide	H_2S	Degasification, Activated Catalytic Carbon Filter
Carbon Dioxide	CO_2	Degasification

[101] Sowers, George, "Creating the Cislunar Economy," Space Studies Colloquium, University of North Dakota, Feb. 26, 2018, https://commons.und.edu/ss-colloquium/76/.
[102] Heiken, G.; Vaniman, D.; French, B.; *Lunar Sourcebook, A User's Guide to the Moon*; Cambridge University Press, 1991.
[103] *The Scientific Context for Exploration of the Moon*, By National Research Council, Division on Engineering and Physical Sciences, Space Studies Board, Committee on the Scientific Context for Exploration of the Moon, 2007, by the National Academy of Sciences.

Sulfur Dioxide	SO_2	Reverse Osmosis, Activated Catalytic Carbon Filter
Ammonia	NH_3	Ion Exchange System
Penthane	C_5H_{12}	Degasification
Hydrogen Cyanide	HCN	Reverse Osmosis, Ion Exchange System
Toluene	C_7H_8	Activated Catalytic Carbon Filter
Ammonium Hydrosulfide	NH_4SH	Reverse Osmosis, Activated Catalytic Carbon Filter
Sulfur	S	Reverse Osmosis, Activated Catalytic Carbon Filter
Copper	Cu	Reverse Osmosis, Ion Exchange System
Zinc	Zn	Reverse Osmosis
Arsenic	As	Reverse Osmosis
Selenium	Se	Ion Exchange System
Silver	Ag	Reverse Osmosis
Bromine	Br	silver (Ag+) impregnated graphene oxide for Catalytic Carbon Filter
Iodine	I	Activated Catalytic Carbon Filter
Solar-Wind-Implanted Volatiles		**Treatment Method(s)**
Hydrogen	H	Degasification
Carbon	C	Degasification
Nitrogen	N	Degasification
Helium	He	Degasification
Neon	Ne	Degasification
Argon	Ar	Degasification
Krypton	Kr	Degasification
Xenon	Xe	Degasification

Table 20. Available Water Treatment Methods.

Water Treatment Methods[104,105]	Description
Micro and ultra-filters[106]	Micro filtration: membranes with pore size < 10 µm to filter nano- and micro-sized particles from liquid. Used in food and pharmaceutical industries, wastewater treatment, filtering oil emulsions, etc. Ultra filtration: filtering particles of 0.001 – 0.1 µm. Used in food industry, metal and textiles. **Micro/Ultra filters would be effective, but the particulates in lunar water will likely clog quickly requiring excessive maintenance.**

[104] https://www.cleanwaterstore.com/technical/water-treatment-guides/definitive-guide-well-water-2016.pdf
[105] https://www.cdc.gov/healthywater/pdf/drinking/Household_Water_Treatment.pdf
[106] https://www.lenntech.com/microfiltration-and-ultrafiltration.htm

Carbon Filters[107]	Removes Volatile organic compounds; Solvents - degreasers, cleaning agents; Used in many industries. Works by a combination of small pore sizes and adsorption of contaminants onto the activated carbon. Three types: carbon block, granular activated carbon (GAC), and radial flow GAC.
Greensand Filter[108]	Removes Arsenic Hydrogen Sulfide, Iron, Manganese, and Radium and Sulfur. May be regenerated with chlorine and life may be extended by pre-loading with chlorine compounds. **Not required since other methods should work well.**
Reverse Osmosis[109]	Often used with pre-and post-filters. Removes metal ions, sodium, chloride, possibly others. **Should be effective.**
Fractional Distillation/ Sublimation[110]	Reduces but does not completely eliminate many chemicals. Does not remove all volatile organic compounds (VOC). **Would be effective, but concerned with energy usage.**
Ion exchange resins[111]	A flow passes across the ion exchange resin, and ions in the flow exchange with ions bonded to the resin. Used to demineralize water and remove other specific chemicals. Can operate in continuous or batch mode. Continuous mode is typically in a column. Resin must be regenerated when exhausted. **Would be effective.**
Electrode-ionisation (EDI)[112]	Ion exchange across a membrane. Removes ammonia, carbon dioxide, other chemicals. Often used as a final stage. **Power and maintenance may be higher than a simpler system.**
Degasifica-tion[113,114,115]	Inducing gases dissolved in liquid to escape via exposure to vacuum, mechanical/ultrasonic perturbation, bubbling another gas, etc. **Heating and spraying into a vacuum vessel should be effective and simple approach.**
Differential Permeation[116]	Permeation media may use zeolites, polymers, glass fibers, etc. Choice of materials maximizes efficiency. Multiple passes to obtain arbitrarily high purity. **Should be very effective.**

[107] https://www.freshwatersystems.com/collections/carbon-filters
[108] https://www.cleanwaterstore.com/resource/frequently-asked-questions/about-greensand-filters/
[109] https://puretecwater.com/reverse-osmosis/what-is-reverse-osmosis
[110] https://extensionpublications.unl.edu/assets/html/g1493/build/g1493.htm
[111] https://www.dupont.com/water/technologies/ion-exchange-ix.html
[112] https://www.dupont.com/water/technologies/electrodeionization-edi.html
[113] https://www.separel.com/en/technology/
[114] https://www.elgalabwater.com/blog/dissolved-gases-purified-water
[115] https://www.sciencedirect.com/science/article/pii/B978178242028600020X
[116] Bastani, Dariush, Nazila Esmaeili, and Mahdieh Asadollahi. "Polymeric mixed matrix membranes containing zeolites as a filler for gas separation applications: A review." *Journal of Industrial and Engineering Chemistry* 19, no. 2 (2013): 375-393.

Our notional water cleanup process therefore consists of the steps in Table 21.

Table 21. Lunar Water Cleanup Process (including pre- and post- processing information)

Step	Description
1	Output from the beneficiation process is first sieved using a 4.0 mm mesh per American National Standard for Industrial Wire Cloth (American Standard ASTM - E11)[16] then undergoes a crushing process.
2	Entrance to the ice melting system has a 35 US Mesh = 500 μm to filter out very large particles. These particles can be returned to the crushing process. Exit of the ice melting system has a 150 US Mesh = 100 μm to filter out large particles prior to entering the water clean-up system. Exit of the ice melting system is not the drain. This allows for gravity to assist in the settling of large particles to minimize them exiting the system. Melting and water cleanup is a continuous flow system. For maintenance, the exit valve is closed and the drain valve is opened. The system is vibrated to allow for large particles that have settled in the bottom to drain out. The drain valve is then closed and the exit valve is opened for water cleanup process to continue.
3	To take advantage of the water already being heated and the natural vacuum environment, the water enters the degassification-1 section. The water is sprayed into the section for optimal surface area exposure to the vacuum environment that allows for gas to come out of solution and vented off. The vent stream is captured and a separation process if performed to collect useful gases for future applications.
4	Gravity-fed water enters the reverse osmosis section of the water cleanup system. The inlet has a 5 μm filter. A pump and an accumulator assure a positive pressure on the membrane. The permeate water continues to the next process. The reject water is returned to the reverse osmosis inlet for another pass. To mitigate inlet side of the membrane becoming blocked, piezoelectric devices agitate the inlet water.
5	Water next flows through the ion exchange resin section of the water cleanup system.
6	Next, water flows through the catalytic carbon filter to remove any remaining heavy metals.
7	The water enters the degassification-2 section that is similar to the degassification-1 section to remove any remaining gases that were formed as a product of the earlier ion exchange resin and catalytic carbon filter processes.
8	The processed water now enters the electrolysis section, which outputs hydrogen and oxygen.
9	The hydrogen and oxygen each enters liquefaction sections to transform into LH2 and LO2.
10	The LH2 and LO2 are transferred into storage vessels.
11	The LH2 and LO2 are then transferred to the Lunar Lander/Tanker.

We assume the output of the water cleanup plant will go into surge storage until the Lander/Tug can return and refuel. This will enable continued operation in parallel with serving customers in Earth orbit. The storage tank will need to store 1 month of production: 258.08 kg LH_2 (3,646.15 liters) and 2,066.93 kg LO_2 (1,812.08 liters). We based the estimate assumed a single-walled

stainless steel tank. The output of the tank is hauled by two robots to load onto the Lander/Tug. These two robots are described in the Site Preparation section.

3.5 Mining (Extraction and Beneficiation)

The mining concept is based on the NASA RASSOR excavation robot.[117] It can haul 20 kg of regolith. It moves 20 cm/s and has a mass of 25 kg. It is powered by two 12 V 19 AH lithium iron phosphate batteries in series. The current draw is 5 A (120 W) while driving, or 10 A (240 W) while positioning, or 2 A (48 W) while excavating loose materials. It must recharge for 8 hours after 16 hours of operation. We estimate 100 m maximum travel between dig site and Aqua Factorem plant inside the PSR. The one way trip takes 8 minutes. Excavating 20 kg takes 4 minutes. Excavation will develop a pit with ramps to enter and exit. The strip-mining strategy needs to be developed in detail. Each hour it performs 3 round trips with 60 kg excavated and moved. At 16 hours/day the operations move 960 kg/day per excavator. To meet requirements of the MVP mining architecture we require two such mining robots.

The inlet to the Aqua Factorem plant includes a crusher to help liberate the bound ice fragments from mineral fragments. The Aqua Factorem beneficiation process is in a standalone unit powered by fuel cells that are regenerable with liquid oxygen and liquid hydrogen hauled into the PSR from the water processing plant. The output of the Aqua Factorem process is hauled by a Transporter rover to the water cleanup plant outside the PSR. We estimate it has the same mass of RASSOR and the same power. It will not have the twin bucket drums of RASSOR, but now an open volume container with cover when ready to transport. Aqua Factorem's output drops directly into the Transporter. The Transporter drops directly into the water processing system with excavator assist. We assume 4 km distance from the Aqua Factorem Plant in the PSR to the sunlit equipment. Roving estimates are in-progress, considering improved wheel speeds and Transporter size. Transfers of ore into the water processing plant take 4 minutes. Each hour: 3 round trips with loads totaling 60 kg. 16 hour/day operation transports maximum 960 kg.

3.6 Site Preparation

It will be necessary to build a landing pad to protect the assets from the repeated landing and launching of the Landers. Notionally (to be improved in on-going work) we specified a polymer-based pad. The water-hauling RASSOR-equivalent robots will perform grading of the site and build berms around it. Two such robots are required. A polymer agent brought from Earth will be applied to the graded surface, based on NASA-funded SBIR development. (More details to follow in on-going work.) The pad will be 100 m^2, which is small due to the modest size of the Landers in this architecture. After constructing the pad, these robots will haul water from the water cleanup plant to the Lander/Tug.

[117] Mueller, Robert & Cox, Rachel & Ebert, Tom & Smith, Jonathan & Schuler, Jason & Nick, Andrew. (2013). Regolith Advanced Surface Systems Operations Robot (RASSOR*). IEEE Aerospace Conference Proceedings*. 1-12. 10.1109/AERO.2013.6497341.

3.7 Mass and Power Estimates

The roll-up of mass estimates is provided in Tables 21 and 22. This work is done in spreadsheet form to enable easy trade studies. On-going work will continue to refine the parameter values based on better estimates of the State-of-the-Art and reasonable expectations of technology advancements. These results currently predict the total mass of the entire Surface Segment will be 2,382.50 kg, or about 2.4 tons.

Table 21. Roll-up of mass estimates for elements inside the PSR.

PSR Element	Mass (kg)
Excavator 1	25.00
Excavator 2	25.00
Beneficiation System	100.00
Crusher	50.00
Transporter	25.00
PSR Element Total	**225.00**

Table 22. Roll-up of mass estimates for elements outside the PSR.

Outside PSR Element	Mass (kg)
Excavator 7	25.00
Excavator 8	25.00
Regolith Binding Agent	10.00
Power/Thermal/Control System	1,500.00
Hopper/Feeder (aluminum)	9.00
Melter	3.50
Degasification-1	3.50
Reverse Osmosis	3.50
Ion Exchange Resin	7.00
Catalytic Carbon Filter	3.50
Degasification-2	3.50
Electrolysis	7.00
Liquefaction	7.00
Storage Vessels	550.00
Sunlit Element Total	**2,157.50**

The system requirements and the roll-up of power requirements are given in Appendix A. They predict the entire power required by the Surface Segment will be 50 kW. ***This is a 98.3% power reduction from the baseline mining system. Reducing power need is the primary objective of our project, so this indicates we are on-track for a successful outcome***.

3.8 Other Business Opportunities in the Architecture

We have begun assessing the other business opportunities of this architecture, which will contribute to its overall success.

- If optimized O:F ratio is used instead of stoichiometric, then as a by-product of the commercial activities there will be 3 ton of oxygen left over every 4 months. NASA has indicated baselining around 10 tons/year of O_2 from regolith to use in lunar operations. NASA could be a customer without having to pay the cost of sustaining this capability.
- NASA (and others) as a transportation customer:
    - Our baseline Lander can fill 3,542 kg of propellant on the surface, go to LLO, get cargo, land 2 tons on the surface. That is small, but we can do 2x the cadence of GEO bird lifts.
    - We could tweak the existing CONOPs spreadsheet to the Gateway (for fetching cargo and "lifting" it to the lunar surface). In Phase II we can assess the propellant requirements to provide this ferry service between GW and LS.
- Other commercial small scale or demonstration opportunities for the baseline vehicles:
    - Disposal of dead GEO satellites into graveyard orbits. The NS station keeping means most of these only potentially intersect the live birds where their orbital planes cross, but over time the "live plane" sweeps through all the dead ones (a 50-year cycle), so eventually, something will come dangerously close or impact. Our baseline CONOP could be tweaked to go to a "dead" GEO bird, grab it, and lift it 300 km (or so) to the disposal orbit. That will be lower dV than our baseline "lift a sat" and thus lower water demand (about 2 km/s less, only 10 m/s to move the corpse to a disposal orbit). Also, the satellite is dead so a very low level of trust is required from the customer. It's a good demonstration mission plan, and best if we can find a government or other customer to pay for it or to pay for a series of such cleanup lifts. Because the deltaV to get to the graveyard is so low it is possible to move a few objects if their inclinations are close.
    - Disposing of upper stages into the atmosphere. Top 20 of the 50 "statistically most concerning" objects are upper stages (https://spacenews.com/upper-stages-top-list-of-most-dangerous-space-debris/) would take less than 100 m/s to bring their perigee into the atmosphere, vs the 1,500 m/s we would do to lift a satellite. This would be another good demo mission. Problems include funding customers/benefactors to pay for this service, the orientation of the orbit is probably not ideal so we'd need astrodynamic modeling to see how expensive it is, and the upper stage is likely spinning and/or may still have residual hazardous propellant.
    - We could use the baseline CONOPs reversed to go to GEO, grab a satellite, and bring its perigee down into the atmosphere. This should require somewhat less deltaV than the lift since we don't care about doing anything to the inclination. This is a low trust demonstration mission that is closer to a full baseline lift. However, everyone seems content to have dead birds in graveyard orbits, so it may be more difficult to find a paying customer/benefactor for this task.

- Even a very partial lift of a fully provisioned satellite translates to life extension and/or a faster lift and sooner beginning of life.
- A rescue of a satellite with a failed apogee motor is an opportunity to demonstrate safety, but it doesn't seem a good mission to plan on.

4.0 Other Products from Lunar Beneficiation

Once a beneficiating operation on the Moon has been established, it can be extended naturally to beneficiate other resource from the regolith. Anorthite is highly valuable to extracting aluminum. In highlands soils, the non-magnetic fraction was highly concentrated in the rock anorthosite (rich in anorthite), and there are deposits of anorthite mineral in lunar soil. Ilmenite can be enhanced in the soil through electrostatic beneficiation. Some free metal exists in the soil and that can be extracted magnetically. In some places it is about 1 wt% of the soil.

5.0 Bringing the Concept to the Aerospace Market

The further implementation path after the successful NIAC project is to develop the beneficiating technology to TRL-6 in laboratory experiments, vacuum chamber tests, and/or analog field demonstrations. That development effort will be low-cost and rapid because equipment for particle separation is inherently scalable to small-size and is low safety risk to personnel, requires low power, can be validated for realistic performance in modest vacuum chambers and in reduced gravity flights, and can be built into inexpensive robotic prototypes for full-scale tests. A fully realistic, yet small-scale experiment can be flown to the lunar surface on a Commercial Lunar Payload Services (CLPS) mission to demonstrate the technology in situ. Then full-scale flight systems can be built for NASA's benefit and for commercial mining. It is our belief this is obviously the correct way to mine lunar regolith so commercial investment will be able to drive this capability forward.

Aqua Factorem will look like technological magic. It will be like pouring a mixture of salt, sugar, and pepper into a box then having three separated material streams come out the other end. As this technology is tested on CLPS missions it will generate excitement as everyone sees that a small-scale system operating on the Moon can easily and with very low power leverage the natural lunar geology to extract rocket fuel and metal. After laboratory demonstrations and the CLPS payload we expect there will be very high enthusiasm to bring the technology to full-scale implementation both to support NASA's operations in cislunar space and beyond, and to support commercial activity. This is especially true because the necessary investment will be quite modest, and yet it is highly leveraged for radical economic benefit.

6.0 Outreach and Public Engagement

In addition to the NIAC Symposium, Metzger presented the Aqua Factorem concept to the Students for the Development of Space, Orlando chapter, the Lunar Surface Innovation Consortium, and to the University of Alabama robotics club. An abstract has been accepted to present it at the International Astronautical Congress, and another abstract has been submitted to

present it at the European Space Agency's Space Resources Week. We plan to present these final results at a conference and include it in additional outreach.

Originally, we planned to involve a high school 4-H team building portions of a prototype to install on a rover for demonstrations, but because of COVID-19, the 4-H policy required that to be cancelled. The 4-H activities can be resumed once the COVID-19 pandemic ends.
Instead, we hired two undergraduate students to work on the project as part of their educational experience: designing and building hardware, performing experiments, and writing portions of this report. The project also contributed to the training of a post doctoral researcher who managed the laboratory activities, prototype design and fabrication, and experimental work.

7.0 Conclusion

The objectives of Phase 1 have been satisfied, demonstrating that the architecture based on Aqua Factorem can meet top level requirements, produces 98.3% reduction of mining energy, can be built for about $213M and only 3,822 kg of hardware delivered to the Moon. This puts it in the range of commercial investment, and it can scale up smoothly to large operations even while it is creating revenue and buy-down the risks.

8.0 Appendices

8.1 Appendix A. Lunar Soil and Ice Particle Size Distributions

Figure A.1 shows the lunar particle size distribution from two sources. The first is derived from the Lunar Sourcebook,[118] from its Figure 9.1, which is cumulative mass fraction[119] vs. particle size. We found the best fit of those data points to a standard fitting function from soil mechanics,

$$C(D) = \left[\mathrm{Ln}\left(e + \left(\frac{a}{D}\right)^n\right)\right]^{-m}\left\{1 - \left[\frac{\mathrm{Ln}\left(1+\frac{d_r}{D}\right)}{\mathrm{Ln}\left(1+\frac{d_r}{0.001}\right)}\right]^7\right\}$$

where the best fit was $a = 30.0984$, $n = 1.15507$, $m = 3.70218$, and $d_r = 35491.2$ with R^2=0.9983. The dashed line in Figure A.1 is the derivative of that function to convert it to a differential rather than cumulative mass fraction.

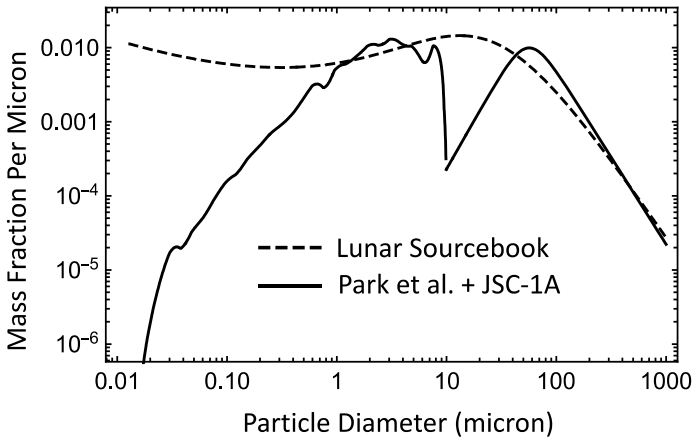

Figure A.1. Lunar soil particle size distributions converted from the Lunar Sourcebook Figure 9.1 and from JSC-1A concatenated with fines from Park et al. scaled relative to each other such that the <10 μm fraction contributes 10 wt%.

The second data source was a concatenation of a measurement of a lunar soil simulant for the fraction >1 μm with a measurement of lunar soil sample 10084 for the <10 μm fraction by Park et al.[120] JSC-1A has relatively miniscule mass content in the 1 to 10 μm range compared to the other dataset so the two datasets can be simply adding together. We scaled their relative amplitudes such that the fraction finer than 10 μm will contribute 10% of the mass, in rough agreement with Figure 9.1 from the Lunar Source Book. This concatenated soil model is the solid line in Figure A.1. The Lunar Sourcebook model is too high in the region < 1 μm, but that

[118] Heiken, et al. (1991).
[119] The axis is labeled as a probability distribution, so we verified by comparing the distribution in the lunar soil 78221 datasheet that it is a cumulative mass distribution. See https://www.lpi.usra.edu/lunar/samples/atlas/compendium/78221.pdf.
[120] Park, Jaesung, Yang Liu, Kenneth D. Kihm, and Lawrence A. Taylor. "Characterization of lunar dust for toxicological studies. I: Particle size distribution." *Journal of Aerospace Engineering*21, no. 4 (2008): 266-271.

is an artefact of extrapolation. The smallest size in the data is ~8 μm, so the fitting function is not constrained in the < 1 μm region. The data by Park et al. are reliable in that region.

There is a second discrepancy in the range $5\ \mu\text{m} \lesssim d \lesssim 50$ where JSC-1A is lower than the data in the Lunar Sourcebook. Comparing JSC-1A to the range of typical Apollo soils, we see it is lower than the Apollo average in the range $10\ \mu\text{m} \lesssim d \lesssim 80$, with the worst deviation in the range $11\ \mu\text{m} \lesssim d \lesssim 50$. JSC-1A has too much of its mass fraction in the extreme ranges $d \lesssim 7\ \mu\text{m}$ and $200 \lesssim d$. Therefore, the discrepancy in the $5\ \mu\text{m} \lesssim d \lesssim 50$ range is the fault of the JSC-1A and the Lunar Sourcebook data are more reliable in that region.

Based on this, we created our soil model to follow the most reliable data in each region. This is shown in Figure A.2 as the dash-dot curve. The functional form is,

$$P(D) = A\left[\frac{1}{\left(\frac{1}{0.1\ D^{1.7}}\right)^{\alpha} + \left(\frac{1}{12{,}500\ D^{-2.5}}\right)^{\alpha}}\right]^{1/\alpha}$$

where $A = 1766$ is for normalization and $\alpha = 0.19$ was chosen to approximately fit the shape of the curve in the transition region between the fines and coarse slopes. This is the soil model we used in the calculations of beneficiation.

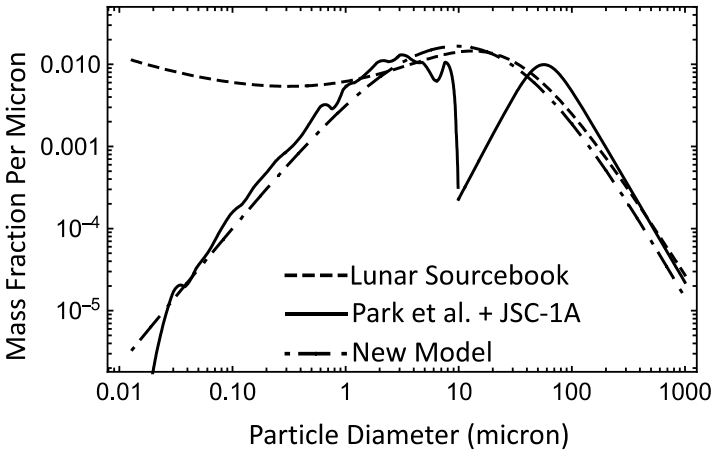

Figure A.2. Lunar soil particle size distributions, the same as Figure A.1 but with an additional new model that follows the most reliable data in each region.

The particle size distribution of the ice particles is informed by only two datapoints. The best modeled fit to the ice grain size in Near Infrared Data from the LCROSS impact is about 8 μm,[121] and the surface frost grain size measured by the Moon Mineralogy Mapper (M^3) is well

[121] Colaprete, Anthony, M. Shirley, J. Heldmann, and D. Wooden. "The Final Minute: Results from the LCROSS Solar Viewing NIR Spectrometer." *LPI* 1608 (2011): 2037

fitted by 70 μm.[122] Both measurements are noisy. They may be from different ice reservoirs and the difference could also be due to surface (M^3 data) versus depth (LCROSS) processes.[123] If the average size is indeed about 70 μm this will make beneficiation easier since that size particle flows more easily.

Since these observational measurements are sensitive to a surface areal-weighted particle size rather than a mass weighted size, we used the new model of Figure A.2 to calculate the areal-weighted mean size of lunar soil and we found it is 19.0 μm. We assess four models of the ice, all following the following equation:

$$P(D) = A\left[\frac{1}{\left(\frac{1}{0.1\,D^{\varphi}}\right)^{\alpha} + \left(\frac{1}{12{,}500\,D^{\gamma}}\right)^{\alpha}}\right]^{1/\alpha}$$

with $\alpha = 0.19$ and A chosen for normalization. Ice Model 1 keeps the two power indices (fines φ and coarse granulars γ) matching the values of the lunar soil model. This assumes the ice has the same size distribution as the lithic soil.

Ice Model 2 modifies only φ to match the LCROSS measurement of 8 μm to the calculated areal-weighted mean particle diameter, $\langle D \rangle$,

$$\langle D \rangle = B\int_{D_{\min}}^{D_{\max}}\left[\frac{1}{\left(\frac{1}{0.1\,D^{\varphi}}\right)^{\alpha} + \left(\frac{1}{12{,}500\,D^{\gamma}}\right)^{\alpha}}\right]^{\frac{1}{\alpha}} \mathrm{d}D$$

where

$$B^{-1} = \int_{D_{\min}}^{D_{\max}}\frac{1}{D}\left[\frac{1}{\left(\frac{1}{0.1\,D^{\varphi}}\right)^{\alpha} + \left(\frac{1}{12{,}500\,D^{\gamma}}\right)^{\alpha}}\right]^{\frac{1}{\alpha}} \mathrm{d}D$$

normalizes the areal-weighted size distribution. The limits of integration are $D_{\min} = 0.013$ μm for the finest particle detected in Park, et al, and $D_{\max} = 1$ m to be so large that no larger value changes the results. The term $1/D$ in the integrand converts the mass-weighted size distribution (scaled by mass-per-particle $= \rho\pi D^3/6$) into an areal-weighted size distribution (scaled by cross sectional area-per-particle $= \pi D^2/4$), with the other constants absorbed into *B.* This Ice Model 2 assumes the LCROSS measurement is correct and that the ice has the same fracture mechanics as the lithic particles in the coarse region but the ice lacks agglutination so there is a greater accumulation of fines than among lithic particles in the fine region.

[122] Li, Shuai, and Ralph E. Milliken. "Water on the surface of the Moon as seen by the Moon Mineralogy Mapper: Distribution, abundance, and origins." *Science Advances* 3, no. 9 (2017): e1701471; and Supplementary Material.
[123] *Ibid.*

Ice Model 3 modifies only γ to match the M^3 areal mean diameter of $\langle D \rangle = 70$ μm. This assumes the LCROSS measurement was not accurate due to noise or that it is not applicable since it represent immature ice at depths too great to mine, but the M^3 measurement was accurate and informs bulk soil in the top half-meter or so that is mineable, not just surficial "frost". This implies the ice is coarser than lithic soil, perhaps due to ongoing growth of grains in the near-surface region by freezing of solar wind or other volatile contributions, which gets mixed into the soil at depths by gardening, and that this ongoing growth compensates partially for the fracturing process in the coarse part of the distribution. This does not seem a likely model due to the lack of an agglutination process to remove fines from the distribution, but we include it to bound the problem.

Ice Model 4 also seeks to bound the problem by combining the fines index φ from Ice Model 2 while adjusting the coarse granulars index γ to match the M^3 measurement as in Ice Model 3. It seems likely the actual size distribution of lunar ice will have values of φ and γ between these extremes, and the four models match the high and low extremes of each index in all four combinations.

In each model, A was recalculated for normalization, and we do not change $\alpha = 0.19$ since we lack any data to inform changes. The five model parameters are summarized in Table A.1.

Table A.1. Model parameters for the particle size distributions.

Model	Assumptions	φ	γ	A	$\langle D \rangle$ (μm)	$\widehat{D}$ (μm)
Lunar Soil	Follow Apollo soils: 78221,8[124] for > 1 μm, or 10085[125] for < 1 μm	+1.70	–2.5	18.44	19.0	78.0
Ice Model 1	Match the Lunar Soil Model	+1.70	–2.5	18.44	19.0	78.0
Ice Model 2	Adjust only φ to match $\langle D \rangle$ from LCROSS	+0.339	–2.5	2.83	8.0	108.2
Ice Model 3	Adjust only γ to match $\langle D \rangle$ from M^3	+1.70	–1.844	173.7	70.0	183.9
Ice Model 4	Use φ from Ice Model 2 and readjust γ to match $\langle D \rangle$ from M^3	+0.339	–1.767	32.66	70.0	144.7

These four Ice Models are plotted in Figure A.3. Using these models, we integrate to find the mass wt% for lithic and ice particles in the < 20 μm range. Assuming ice constitutes 5 wt% of the bulk regolith and lithic particles are 95 wt%, then ice constitutes 5.6 wt% of the < 20 μm fraction. More importantly, 33.2 wt% of the ice is contained in the < 20 μm fraction, so failing to extract ice from the "dust" after de-dusting the material would be a waste of 33.2% of the resource.

If de-dusting only removes the < 10 μm fraction, then 20.8 wt% of the resource is contained in the dust, and the dust stream will be 7.9 wt% ice.

[124] Heiken et al. (1991), Figure 9.1.
[125] Park, Jaesung, Yang Liu, Kenneth D. Kihm, and Lawrence A. Taylor. "Characterization of lunar dust for toxicological studies. I: Particle size distribution." *Journal of Aerospace Engineering* 21, no. 4 (2008): 266-271.

If de-dusting removes the < 30 μm fraction, then 41.9 wt% of the resource is contained in the dust, and the dust stream will be 4.9 wt% ice.

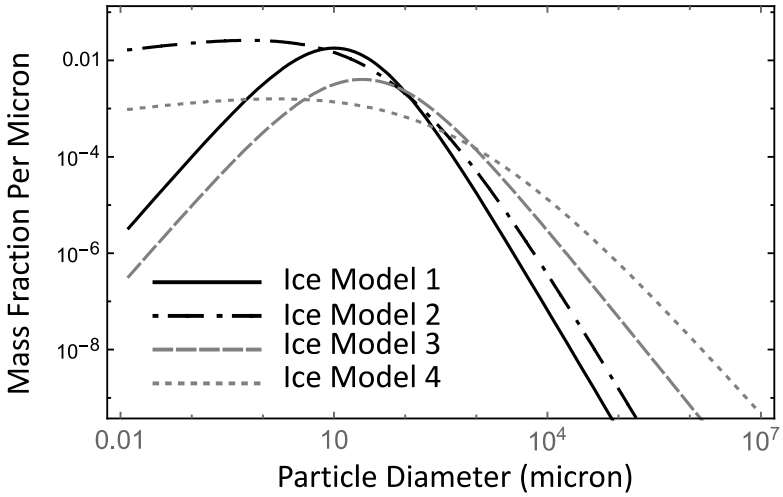

Figure A.3. The four models for lunar ice particle size distributions. The lunar soil model for lithic (and glass) fragments is identical to Ice Model 1.

8.2 Appendix B. Data Tables.

Table B.1. The requirements to meet the MVP requirement of boosting one 2.5 ton satellite every four months.

Requirements	**Daily**		**Monthly**		**Annual**	
Water needs	77.50	kg	2,325.00	kg	27,900.00	kg
Liquid Hydrogen needs	8.6025	kg	258.08	kg	3,096.90	kg
Liquid Oxygen needs	43.0125	kg	1,290.38	kg	15,484.50	kg
Excess Liquid Oxygen	25.89	kg	776.55	kg	9,318.60	kg
Regolith in PSR to excavate	1,550.00	kg	46,500.00	kg	558,000.00	kg
Aqua Factorem removal of waste material	0.75					
Concentrated regolith needed post Aqua Factorem	445.63	kg	13,368.75	kg	160,425.00	kg

Table B.2. Roll-up of MVP power requirements:

Energy Needs	**Inputs**		**Calculated**				Notes
	Daily		**Monthly**		**Annual**		
Water needs			2,325.00	kg			
LH2 needs			258.08	kg			
Mix mass ratio for O with H as 1			5				
LO2 needs			1,290.38	kg			
Excess LO2 produced			776.55	kg			
Energy needs to melt ice	93.18	kWh	2,795.36	kWh	33,544.28	kWh	334 J energy to melt 1 g ice at 0 °C, 1 Megajoules = 0.2778 Kilowatt-hours
Energy needs to raise water temp from 0 to 100 °C	115.05	kWh	3,451.51	kWh	41,418.14	kWh	4124 J to increase 1 kg water 1 °C
Water pump energy needs for reverse osmosis and ion beds	120.00	kWh	3,600.00	kWh	43,200.00	kWh	12 VDC, 5W, 280 liters/hour max flow
Electrolysis energy needs	335.58	kWh	10,067.25	kWh	120,807.00	kWh	100% efficient water electrolysis is 39 kWh/kg H2, 1 kg H2 /9 kg H2O, = 4.33 kWh/kg H2O

LH2 liquefaction energy needs	28.39	kWh	851.65	kWh	10,219.77	kWh	The minimum theoretical energy required to liquify hydrogen is 3.3 kWh/kg.
LO2 liquefaction energy needs	7.74	kWh	232.27	kWh	2,787.21	kWh	The minimum theoretical energy required to liquify oxygen is 0.18 kWh/kg.
LO2 liquefaction energy needs (for excess production)	4.66	kWh	139.78	kWh	1,677.35	kWh	The minimum theoretical energy required to liquify oxygen is 0.18 kWh/kg.
Total energy needs for water processing	**704.59**	**kWh**	**21,137.81**	**kWh**	**253,653.75**	**kWh**	
Other equipment							
Excavator 1	1.791	kWh	53.73	kWh	644.76	kWh	See excavator reference under Mass tab
Excavator 2	1.791	kWh	53.73	kWh	644.76	kWh	See excavator reference under Mass tab
Excavator 3	0	kWh	0	kWh	0	kWh	See excavator reference under Mass tab
Excavator 4	0	kWh	0	kWh	0	kWh	See excavator reference under Mass tab
Excavator 5	0	kWh	0	kWh	0	kWh	See excavator reference under Mass tab
Excavator 6	0	kWh	0	kWh	0	kWh	See excavator reference under Mass tab
Crusher	120.00	kWh	3,600.00	kWh	43,200.00	kWh	Estimated as equivalent to water pump
Aqua Factorem	360.00	kWh	10,800.00	kWh	129,600.00	kWh	Estimated as equivalent to 3 water pumps
Transporter	1.791	kWh	53.73	kWh	644.76	kWh	See transporter reference under Mass tab
Excavator 7	1.791	kWh	53.73	kWh	644.76	kWh	See excavator reference under Mass tab

Excavator 8	1.791	kWh	53.73	kWh	644.76	kWh	See excavator reference under Mass tab
Energy needs for other equipment	**488.96**	**kWh**	**14,668.65**	**kWh**	**176,023.80**	**kWh**	
Total energy needs	**1,193.55**	**kWh**	**35,806.46**	**kWh**	**429,677.55**	**kWh**	

(Daily 1193.55 kWh)/(24 hours) = 49.7 kW